Supplementary Information for

Positional Effects of Second-Sphere Amide Pendants on Electrochemical CO_2 Reduction Catalyzed by Iron Porphyrins

Eva M. Nichols, Jeffrey S. Derrick, Sepand K. Nistanaki, Peter T. Smith, and Christopher J. Chang

Table of Contents

General Synthetic and Physical Methods. Unless noted otherwise, all manipulations were carried out at room temperature under a dinitrogen atmosphere in a VAC glovebox or using high-vacuum Schlenk techniques. THF, DCM, toluene and DMF were dried using a JC Meyer solvent purification system; in addition to desiccant columns, DMF was passed through an isocyanate column to remove dimethylamine impurities. Thionyl chloride was purified by distillation. 2,6-Lutidine was dried over $AlCl_3$ then purified by distillation. All other reagents and solvents were purchased from commercial sources and used without further purification. *Meso*-tetra(4-methoxyphenyl)porphyrin was purchased from Frontier Scientific (Logan, UT). **Fe-*para*-(OMe)$_4$** was prepared according to previously published procedures.[1] NMR spectra were recorded on Bruker spectrometers operating at 300, 400, or 500 MHz as noted. Chemical shifts for ^{1}H and ^{13}C{^{1}H} spectra are reported in ppm relative to residual protiated solvent; those for ^{19}F spectra are reported in ppm relative to an external $CFCl_3$ standard. Coupling constants are reported in Hz.

General Methods for X-Ray Crystallography. Single-crystal X-Ray diffraction was performed at the University of California, Berkeley College of Chemistry X-Ray Crystallography Facility. Crystals were mounted on nylon loops in Paratone-N hydrocarbon oil. Data collection was performed on a Bruker AXS diffractometer using Mo Kα radiation and an APEX II CCD area detector. A low temperature apparatus was used to keep crystals at 100K during data collection. Determination of collection strategy, integration, scaling, and space group was performed using Bruker APEX2 software. Structure solution was performed using SHELXT-2014 and refinement was performed using SHELXL-2014.[2]

General Methods for Electrochemistry. Non-aqueous electrochemical experiments were conducted under Ar or CO_2 atmosphere in 0.1 M NBu_4PF_6 electrolyte in fresh anhydrous DMF that had been purified of dimethylamine by passing through an isocyanate column. Phenol was purified by repeated recrystallization from its melt and stored in the dark in a vacuum desiccator. Cyclic voltammetry and controlled-potential electrolysis experiments were performed using an Epsilon potentiostat from Bioanalytical Systems, Inc. The working electrode for cyclic voltammetry was a 3.0 mm diameter glassy carbon disk (from Bioanalytical Systems, Inc.) and was polished between every scan with 0.05-micron alumina powder on a felt pad. The counter electrode was a platinum wire. A silver wire in porous Vycor tip glass tube filled with 0.1 M NBu_4PF_6 in DMF was used as a pseudo-reference electrode. At the conclusion of a series of experiments, the pseudo-reference potentials were referenced against ferrocene/ferrocenium as an external standard. The scan rate for all cyclic voltammograms was 100 mV/sec unless otherwise noted. All scans were compensated for internal resistance.

Details for CO_2 concentration dependence experiments. The concentration of CO_2 in solution was varied by changing the percentage of CO_2 to N_2 balance using a gas proportioner (G21A2-BA0; Aalborg Instruments; Orangeburg, NY) fitted with sapphire/Viton-A flowtubes (112-02-SA; Aalborg Instruments; Orangeburg, NY). Using metering pressures of 50 psi for N_2 and 15 psi for CO_2, and correlating flow rate with meter reading using calibration curves published at Aalborg.com, the percentage of CO_2 in each gas mixture was calculated. It was assumed that the solution concentration of CO_2 is equal to 0.23 M times the CO_2 percentage in the mixed gas. Cyclic voltammetry experiments were performed by sparging the solution with gas mixtures containing increasing percentages of CO_2 for 10 min, then maintaining the same gas mixture in the headspace for the duration of the scan.

Details for Foot-of-the-Wave Analysis (FOWA) and determination of k_{obs}. Foot-of-the-Wave Analysis was applied to cyclic voltammetry measurements as described by Savéant and coworkers[3] in order to determine k_{obs} = TOF under the specified conditions. At the outset of each experiment, a cyclic

voltammogram was measured of catalyst alone under inert atmosphere in the absence of proton source, from which E^0_{cat} could be determined. The peak height of the formal $Fe^{II/I}$ couple, i^0_p, was determined by taking the difference between peak cathodic current and baseline current before the $Fe^{II/I}$ couple. As described previously,[3, 4] CO_2 reduction with iron porphyrin catalysts may be described as a EC' process

$$Fe(I) + e^- \rightarrow Fe(0)$$

$$Fe(0) + CO_2 + 2H^+ \rightarrow Fe(II)CO + H_2O \quad (RDS)$$

$$Fe(II)CO + Fe(0) \rightarrow 2\ Fe(I) + CO$$

in which the rate-determining step involves pre-equilibrium CO_2 binding to the nucleophilic Fe(0) center and subsequent proton transfer. The following relationship may be derived:

$$\frac{i}{i_p^0} = \frac{2.24\sqrt{\frac{k_{obs}}{fv}}}{1 + e^{[f(E-E^0_{cat})]}}$$

where *i* is the current, *E* is the potential, *v* is the scan rate (V/s), k_{obs} is the observed rate constant, and *f* = F/RT = 38.94 V^{-1}. Thus, a "FOW" plot of $\frac{i}{i_p^0}$ *versus* $\frac{1}{1+e^{[f(E-E^0_{cat})]}}$ yields a straight line with slope $2.24\sqrt{\frac{k_{obs}}{fv}}$, from which k_{obs} may be determined.

Details for controlled-potential electrolysis experiments. Controlled-potential electrolysis experiments were conducted in a homemade PEEK electrolysis cell (Fig. S6). The cell has a working compartment (30 mL liquid volume) and counter compartment (12 mL liquid volume) that are separated by an ultra-fine glass frit. The cell is comprised of five distinct pieces: a main (working compartment) body, a lid, a window covering, a side (counter compartment) cell, and a spacer to hold the glass frit. The cell features quartz windows on both working and counter sides.

The cell windows are made from $^1/_{16}$" thick x 1.5" diameter quartz discs (7500-05; GM Associates; Oakland, CA). A 25 mm diameter x 3-3.5 mm thick ultra-fine glass frit separates the working and counter compartments (7176; Ace Glass; San Francisco, CA). All junctions are sealed with PTFE-coated o-rings (orange with colorless coating) of the appropriate size. The working electrode is attached to 6"-long stainless steel rod ($^1/_{16}$" OD) which passes through the lid and is sealed with a $^1/_{16}$" Tefzel ferrule and flangeless male nut (P-200 and XP-235X, respectively; Upchurch Scientific). The non-aqueous reference electrode consists of a silver wire in a glass tube with a CoralPor frit and is filled with the electrolyte used for the CPE experiment (MW-1085; Bioanalytical Systems, Inc.; West Lafayette, IN). The reference electrode is held in place with a ½-13 UNC plastic bushing and o-ring that makes a gas-tight fitting to the electrode. The gas injection port is constructed using a PEEK union (P-703, Upchurch Scientific) with a Teflon septum cut to size and held in place with a Delrin flat-bottom plug (P-309; Upchurch Scientific). The gas sparging line is made from $^1/_{16}$" OD PEEK tubing (1531, Upchurch Scientific) that is once again sealed to the lid using $^1/_{16}$" Tefzel ferrules and flangeless male nuts (P-200 and XP-235X, respectively; Upchurch Scientific). A Tefzel ETFE shut-off valve (P-782; Upchurch Scientific) was used to seal the gas sparging line. The outlet for GC sampling is constructed from $^1/_8$" OD stainless steel tubing (sealed to the lid with a $^1/_8$" Tefzel ferrule and nut (P-300X and P-335X, respectively; Upchurch Scientific)) that is connected to a Swagelok ball valve (40 series $^1/_8$" tube fitting; Swagelok; Solon, OH). A piece of $^1/_8$" OD stainless steel tubing is used to connect the other end of the ball valve to the stem of a Quick-Connect (SS-QM2-S-200, Swagelok), which is attached directly to the GC inlet that has been modified with a Quick-Connect body (SS-QM2-B-200, Swagelok).

Controlled-potential electrolysis experiments were conducted by preparing a 0.5 mM solution of catalyst in 30 mL of 0.1 M $TBAPF_6$/DMF electrolyte. Phenol was added at a concentration of 0.5 M. The counter electrode chamber was filled with 12 mL of 0.1 M $TBAPF_6$/DMF electrolyte with 20 mM tetrabutylammonium acetate. This soluble source of acetate was sacrificially oxidized *via* the Kolbe reaction to generate CO_2 and ethane, thereby preventing GC detection of solvent oxidation byproducts. Both compartments were sealed to be gas-tight. The working compartment was sparged with CO_2 for 15 min, then closed and injected with 0.5 mL ethylene as a gaseous internal standard. A CV scan was collected to benchmark CPE potential, then the CPE experiment was initiated while stirring the solution at 300 rpm with a 1 cm stirbar. Upon completion, the headspace was injected into a SRI-GC equipped with 6' Hayesep D and 13X Molecular Sieve chromatographic columns, as well as a second Hayesep D guard column which is used to trap solvent volatiles. Two in-line detectors were used: a TCD for H_2 detection, and a FID equipped with a methanizer for $CO/CO_2/C_2H_4$ detection. Temperature and pressure ramping was adjusted so that the analytes of interest eluted separately and not during valve turns. Analytes of interest were quantified by comparing a ratio of analyte:internal standard peak integrals to a calibration curve with known amounts of analyte.

Details for measurement of CO_2 binding constant (K_{CO2}): Equilibrium binding constants were determined electrochemically following methods detailed elsewhere.[5] Cyclic voltammograms were recorded in 0.1 M NBu_4PF_6 in anhydrous DMF (prepared as described in the section "General Methods for Electrochemistry"), first under an atmosphere of argon and then upon saturation with carbon dioxide. Fast scan rates (2-10 V/sec) were necessary to observe a reversible $Fe^{I/0}$ couple under CO_2. Proton sources (other than adventitious water) were omitted to prevent subsequent catalytic turnover. K_{CO2} was calculated based on the difference between the standard potentials under Ar and CO_2, ΔE, using the equation below:

$$K_{CO2} = \frac{e^{(f*\Delta E)} - 1}{[CO_2]}$$

where f = F/RT = 38.94 V^{-1} and $[CO_2]$ (for CO_2-saturated DMF) is 0.23 M.

Details for spectrophotometric pK_a titration experiments. The pK_a values of the amide pendants on the iron porphyrin complexes were determined in DMSO by following slight modifications to a previous literature report.[6] DMSO, base (K-dimsyl), indicator (4-choloro-2-nitroaniline; Sigma Aldrich), and porphyrin stock solutions were freshly prepared (as detailed below) before the spectrophotometric titration experiments were performed. Amounts of indicator, porphyrin, and DMSO, as well as amounts of indicator and porphyrin solutions, were determined gravimetrically using a microbalance.

DMSO. Rigorously dry and degassed DMSO was required for accurate determination of pK_a values. DMSO was dried following a previous report.[7] A commercial source of DMSO was dried over freshly activated alumina (Al_2O_3) overnight. The DMSO was filtered with a Schlenk-frit into a clean, flame-dried Schlenk flask equipped with a stir bar and dried over calcium hydride (CaH_2) overnight. Subsequent distillation under reduced pressure and degassing *via* three freeze-pump-thaw cycles afforded the dry DMSO, which was brought into a nitrogen filled glovebox and stored over 4 Å molecular sieves overnight before use. The fresh solvent was used within a two-day period.

K-dimsyl base. A clean Schlenk tube equipped with a glass stir bar was pre-weighed and flame dried. To this tube was added approximately 100 mg of potassium hydride (KH; Alfa Aesar) (30–35 w%

dispersion in mineral oil) under N_2 atmosphere and was washed with pentane (1 mL x3). The solvent was removed with a syringe, and the remaining solid was dried under vacuum for at least 1 hr. Once dry, the Schlenk tube was again weighed under N_2 atmosphere so that the amount of KH could be determined. With vigorous stirring, 20 mL of freshly dried DMSO was added to the Schlenk tube and allowed to stir until the KH was fully dissolved and no more H_2 was released. The K-dimsyl stock solution was then sealed and brought into a nitrogen filled glovebox and used within a two-day period. The concentration of the K-dimsyl base stock solution was calculated and was used to prepare an approximately 5 mM K-dimsyl solution. The 5 mM K-dimsyl base solution was protected from the light and used for the spectrophotometric titration experiments.

Indicator solution. 4-chloro-2-nitroaniline (pK_a in DMSO = 18.9; λ_{max} of deprotonated indicator = 520 nm; Sigma Aldrich)[6] was selected as the appropriate indicator due to its pK_a and lack of spectral overlap with Fe-amide porphyrins. The indicator was recrystallized from hot ethanol and dried under vacuum overnight prior to use. To a pre-weighed, oven-dried vial was added approximately 4.5 mg of 4-chloro-2-nitroaniline, with the exact amount determined gravimetrically using a microbalance. The vial was then brought into the glovebox and approximately 5 mL of dry DMSO was added. The vial was tightly sealed and taken out of the glovebox, quickly weighed using a microbalance, and brought back into the glovebox where it was stored in the absence of light. The exact concentration of the indicator solution was determined gravimetrically, assuming that the dilute stock solutions had the same density as pure DMSO (1.1 g/mL). A 2.59 mM indicator solution was utilized in these studies (*i.e.*, 4.40 mg of 4-chloro-2-nitroaniline in 9.71 mL dry DMSO). The indicator solution was used within a two-day period.

Fe porphyrin solutions. Approximately 1.10–2.50 mg of each iron porphyrin complex was added to pre-weighed, oven-dried vials, with the exact amount determined gravimetrically using a microbalance. The vials were then brought into the glovebox and 2.5–5.0 mL of dry DMSO was added. The vials were then tightly sealed and taken out of the glovebox, quickly weighed using a microbalance, and brought back into the glovebox where they were stored in the absence of light. The exact concentrations of the iron porphyrin solutions were determined gravimetrically, assuming that the dilute stock solutions had the same density as pure DMSO. The following concentrations were utilized for the iron porphyrin complexes reported in these studies: **Fe-*para*-1-amide** (0.46 mM; 2.30 mg in 4.89 mL DMSO); **Fe-*para*-2-amide** (0.43 mM; 2.30 mg in 4.97 mL DMSO); **Fe-*ortho*-1-amide** (0.49 mM; 2.50 mg in 4.97 mL DMSO); **Fe-*ortho*-2-amide** (0.44 mM; 1.1 mg in 2.48 mL DMSO).

Titration experiment. In the first phase of each experiment, a solution of indicator was titrated into a K-dimsyl solution, allowing for determination of the extinction coefficient of the deprotonated indicator. This phase of the titration was repeated separately for each porphyrin measured.

An oven-dried semi-micro rectangular quartz cuvette with a screw cap and septum (*d* = 1 cm) (Starna Scientific; Atascadero, CA) was pre-weighed and brought into the glovebox. The cell was charged with 1 mL of freshly distilled DMSO, tightly sealed shut, and brought outside of the glovebox and weighed again to determine the amount of DMSO used. The cell was brought back into the glovebox, where 70 μL of the 5 mM K-dimsyl solution was carefully added to the cuvette with an oven-dried Hamilton syringe. The cuvette was sealed tightly with the screw septum cap and re-weighed outside the glovebox. The first UV-visible (UV-vis) spectrum was then recorded to determine the base line, and the titration was started. An oven-dried 100 μl Hamilton syringe was loaded with the indicator

solution in the glovebox and then plugged with a rubber gasket. Approximately a 10 μl aliquot of the indicator stock solution was then added to the air-free cuvette and vigorously shaken to ensure proper mixing. The solution in the cuvette should turn pink in color. After addition of indicator, the cuvette was weighed and the UV-vis spectrum was recorded. The Hamilton syringe was quickly re-plugged with the rubber gasket and stored in the small antechamber of the glovebox under vacuum between each measurement. The addition of 10 μl aliquots of the indicator solution, weighing the cuvette, and recording UV-visible spectra was repeated until no further increase in the absorption spectrum at 520 nm was observed (see Figure S49).

These data were used to determine the extinction coefficient (ε) of the indicator anion by plotting the concentration of the indicator in the cuvette *vs*. the absorbance at 520 nm (Figure S48). Dilution effects were taken into account through the volume increase upon sample addition. At the conclusion of this phase of the experiment, all K-dimsyl base (B^-) has been protonated (BH), and the cuvette contains only the two species of 4-chloro-2-nitroaniline indicator (HInd and Ind^-), with the maximum concentration of the deprotonated indicator (Ind^-). It is extremely important that all K-dimsyl base has been consumed before addition of iron porphyrin solutions, as direct protonation of K-dimsyl by the porphyrin amide will lead to significant error in determining the pK_a.

Once no further spectral change at 520 nm is observed, the second phase of the titration is initiated. An oven-dried Hamilton syringe (25 μl–200 μL) was loaded with the iron porphyrin solution inside the glovebox and then plugged with a rubber gasket. Small aliquots (10–25 μL) of the porphyrin solution were added to the air-free cuvette, which was vigorously shaken, weighed, and the UV-vis spectrum recorded. The syringe loaded with the porphyrin solution was re-plugged with the rubber gasket and stored in the small antechamber of the glovebox between titrations. With each addition of porphyrin solution to the cuvette, a new acid-base equilibrium is established, causing a loss in the absorbance of the deprotonated indicator (Ind^-) at 520 nm as the indicator anion is re-protonated (HInd). At least five titration points were collected for each iron porphyrin complex.

pK_a calculation. The first and second phases of the titration experiment involve the equilibria shown in Equations 1 and 2, where BH/B^-, HInd/Ind^-, and HA/A^- are the protonated and deprotonated K-dimsyl base, 4-chloro-2-nitroaniline indicator, and iron porphyrin complexes, respectively. The pK_a value of the iron porphyrin complex was determined using the equilibrium constant (K_{eq}) for Equation 2 and the known pK_a of the indicator. A value for K_{eq} was determined for each titration point; thus, the reported pK_a values represent the average over at least 5 measurements.

Equation 1: $B^- + HInd \rightarrow BH + Ind^-$

Equation 2: $Ind^- + HA \rightarrow HInd + A^-$

The equilibrium constant can be determined by measuring the exact concentrations of HInd/Ind^- and HA/A^- (Equation 3) in the cuvette at each titration point. Once the equilibrium constants have been measured, the pK_a of the iron porphyrin complex can be calculated from Equation 4. In order for the pK_a of the unknown to be determined accurately, the indicator pK_a must be within 2 pK_a units of the unknown porphyrin complex.

Equation 3: $K_{eq} = \frac{[HInd][A^-]}{[HA][Ind^-]}$

Equation 4: $pK_a = pK_{a\ indicator} - logK_{eq}$

The concentration of the deprotonated indicator, [Ind⁻], was determined by the Beer-Lambert Law, Equation 5, using the absorbance of the indicator anion at 520 nm. The extinction coefficient (ε) was determined during each experiment from the gradual addition of the indicator solution to the cuvette as described above.

Equation 5: $[Ind^-] = \frac{Abs\ @520\ nm}{\varepsilon * l}$

The concentration of the protonated indicator, [HInd], was determined by subtracting the concentration of [Ind⁻] from the total concentration of indicator that was added to the cell, [Ind_{total}] (Equation 6).

Equation 6: $[IH] = [Ind_{total}] - [Ind^-]$

Because Ind⁻ is stoichiometrically protonated by HA, the change in concentration of Ind⁻ and A⁻ are equal in magnitude (Equation 7). The concentration of deprotonated iron porphyrin complex, [A⁻], was therefore determined from the change in absorption at 520 nm upon addition of the porphyrin.

Equation 7: $-\Delta[Ind^-] = \Delta[A^-]$

Finally, [HA] was determined by subtracting the concentration of deprotonated porphyrin, [A⁻], from the concentration of the total amount of porphyrin complex added to the cuvette, [$porphyrin_{total}$] according to Equation 8.

Equation 8: $[HA] = [porphyrin_{total}] - [A^-]$

Details for measurement of KIE. Kinetic isotope effect (KIE) values were measured for each Fe porphyrin bearing a pendant amide group. Water (H_2O or D_2O) was used as the proton source for these studies. Observed rate constants, k_{obs}, were determined using FOWA for various concentrations of H_2O or D_2O as described above. The reported KIE is an average of $k_{obs}(H)/k_{obs}(D)$ over several water concentrations.

Computational details. Calculations were performed using Gaussian 16.[8] Calculations were run using the B3LYP functional and LAN12DZ basis set. Minimum energy structures were fully optimized.

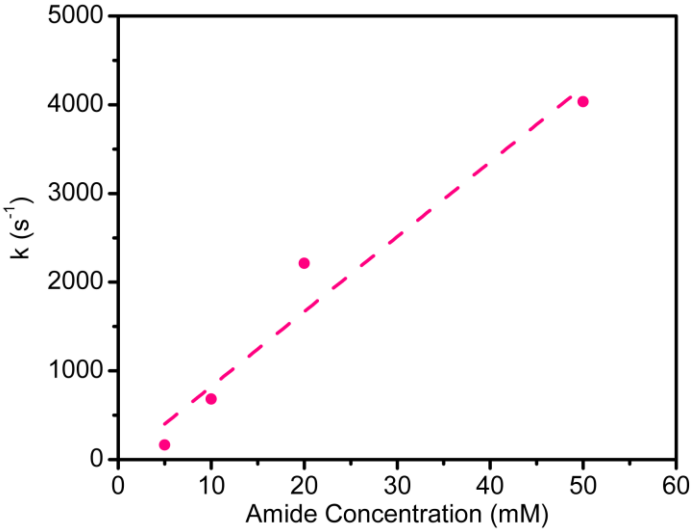

Figure S1. Intramolecular addition of amide additive to **Fe-TPP** shows that CO_2 reduction rate exhibits first-order dependence on amide concentration. Cyclic voltammograms recorded for 1 mM **Fe-TPP** in 0.1 M $TBAPF_6$ in DMF under 1 atm of CO_2. Rates were determined using Foot-of-the-Wave analysis.

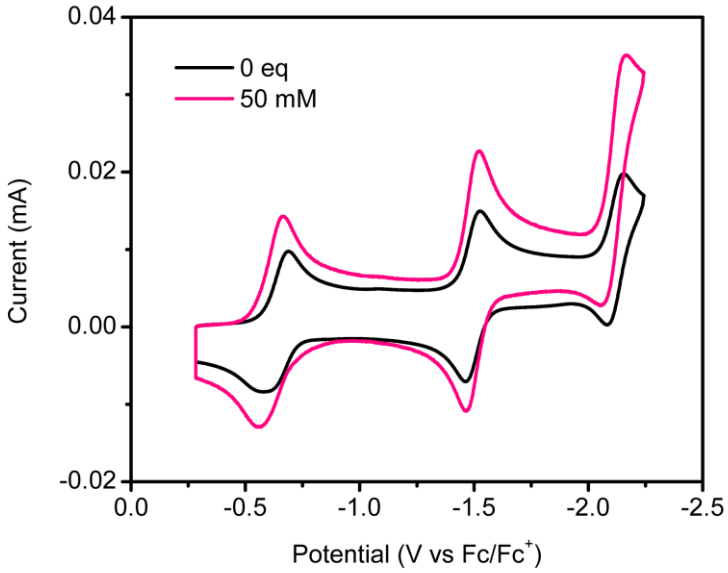

Figure S2. Cyclic voltammograms of **Fe-TPP** (1 mM) in 0.1 M $TBAPF_6$ under Ar atmosphere in the absence (black) or presence (pink) of 50 mM of amide additive.

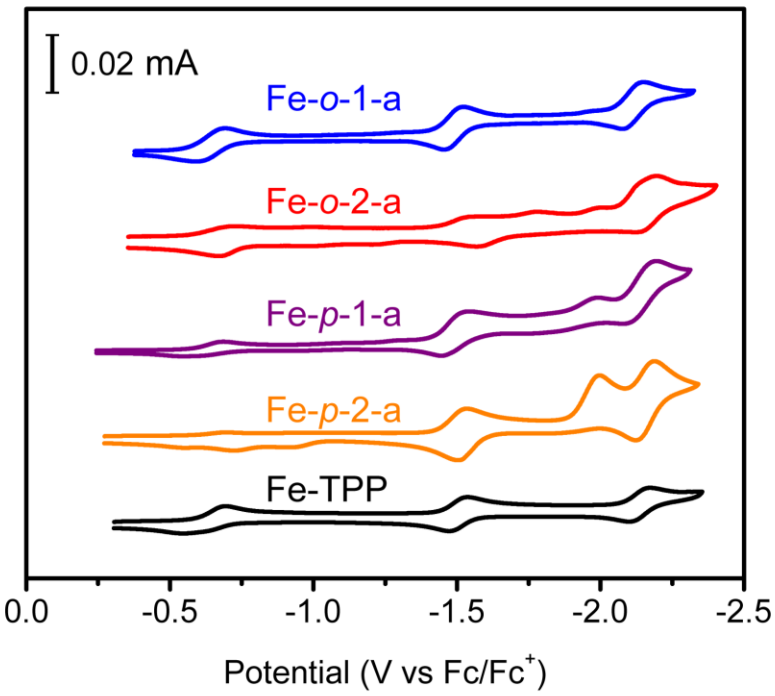

Figure S3. Cyclic voltammograms of the pendant amide Fe porphyrin complexes compared to unfunctionalized **Fe-TPP**, [Fe] = 1 mM. Voltammograms were recorded in 0.1 M $TBAPF_6$ in DMF under Ar atmosphere at 100 mV/sec.

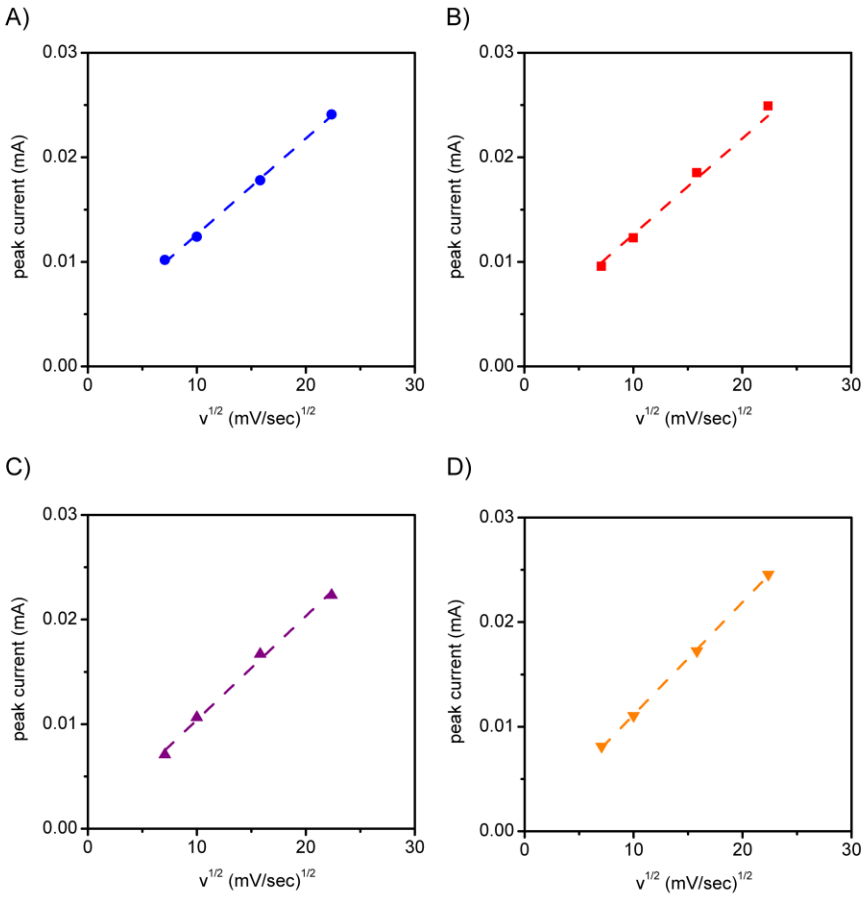

Figure S4. Scan rate dependence for A) **Fe-*ortho*-1-amide**, B) **Fe-*ortho*-2-amide**, C) **Fe-*para*-1-amide**, and D) **Fe-*para*-2-amide** measured under Ar atmosphere in 0.1 M $TBAPF_6$ in DMF. Peak currents for the $Fe^{II/I}$ couple were used.

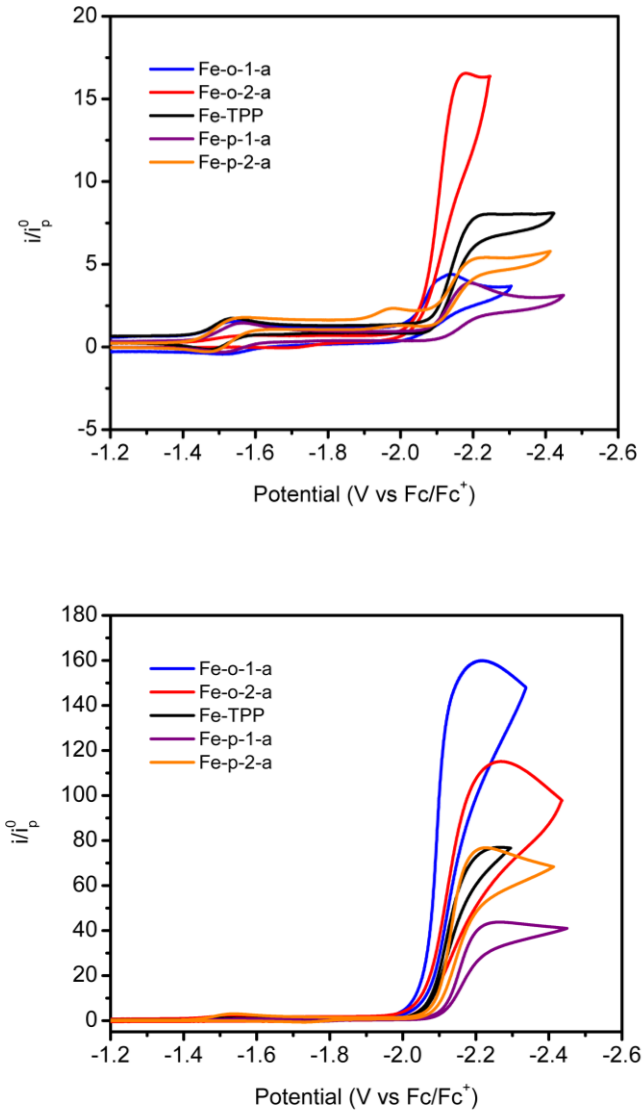

Figure S5. Cyclic voltammograms of amide-functionalized porphyrins and unfunctionalized **Fe-TPP** under CO_2 atmosphere in the presence of 5 mM phenol (top) and 250 mM phenol (bottom). Conditions: 0.1 M $TBAPF_6$ in DMF, saturated with CO_2 (0.23 M); scan rate 100 mV/sec.

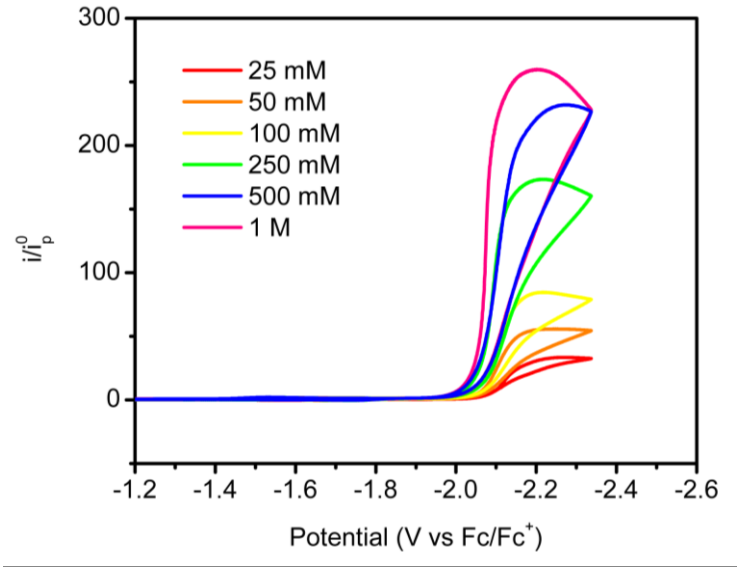

Figure S6. Cyclic voltammograms of **Fe-*ortho*-1-amide** (1 mM) in the presence of 25-1000 mM phenol under CO_2 atmosphere (0.23 M) in 0.1 M $TBAPF_6$ in DMF at a scan rate of 100 mV/sec.

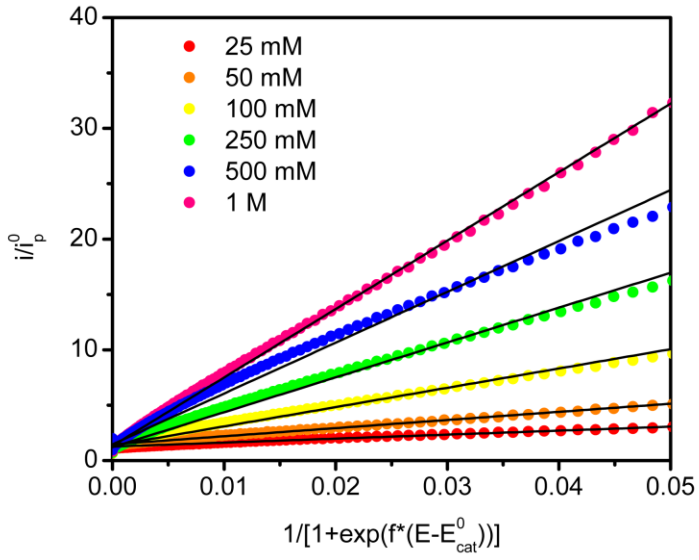

Figure S7. FOW plots for **Fe-*ortho*-1-amide** (1 mM) as a function of phenol concentration. Black lines denote linear fits used to obtain k_{obs}.

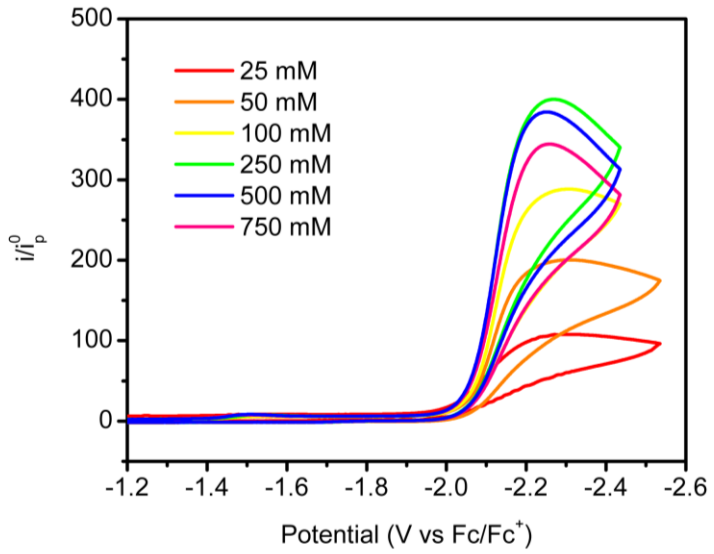

Figure S8. Cyclic voltammograms of **Fe-*ortho*-2-amide** (1 mM) in the presence of 25-1000 mM phenol under CO_2 atmosphere (0.23 M) in 0.1 M $TBAPF_6$ in DMF at a scan rate of 100 mV/sec.

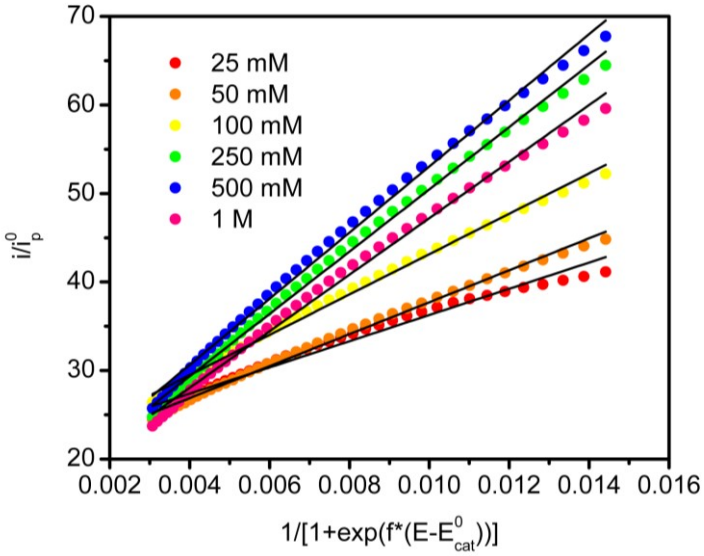

Figure S9. FOW plots for **Fe-*ortho*-2-amide** (1 mM) as a function of phenol concentration. Black lines denote linear fits used to obtain k_{obs}.

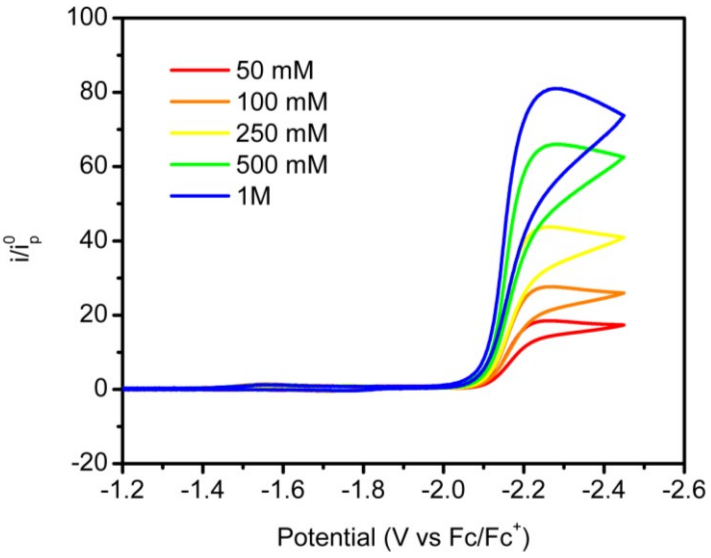

Figure S10. Cyclic voltammograms of **Fe-*para*-1-amide** (1 mM) in the presence of 50-1000 mM phenol under CO_2 atmosphere (0.23 M) in 0.1 M $TBAPF_6$ in DMF at a scan rate of 100 mV/sec.

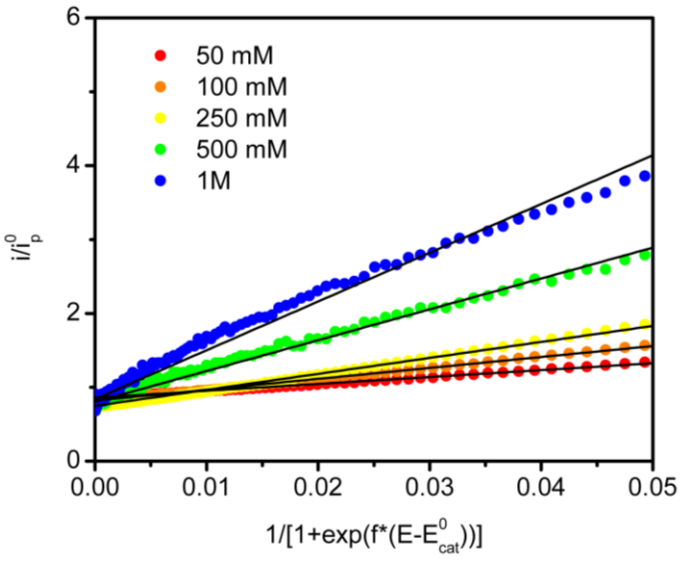

Figure S11. FOW plots for **Fe-*para*-1-amide** (1 mM) as a function of phenol concentration. Black lines denote linear fits used to obtain k_{obs}.

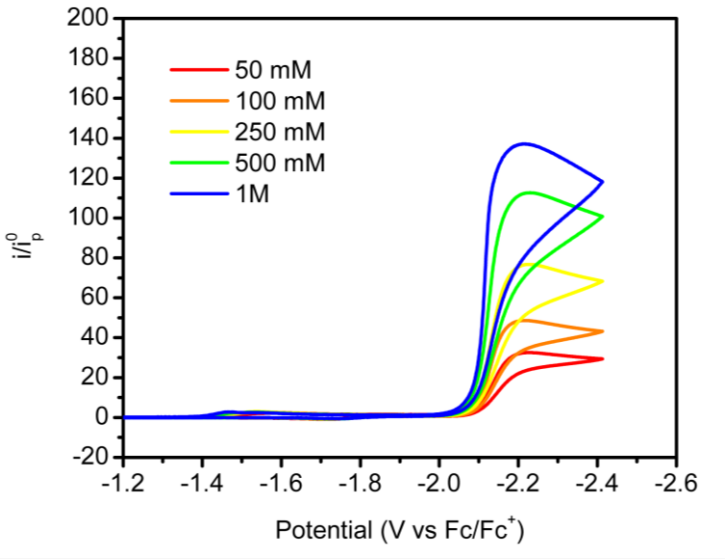

Figure S12. Cyclic voltammograms of **Fe-*para*-2-amide** (1 mM) in the presence of 50-1000 mM phenol under CO_2 atmosphere (0.23 M) in 0.1 M $TBAPF_6$ in DMF at a scan rate of 100 mV/sec.

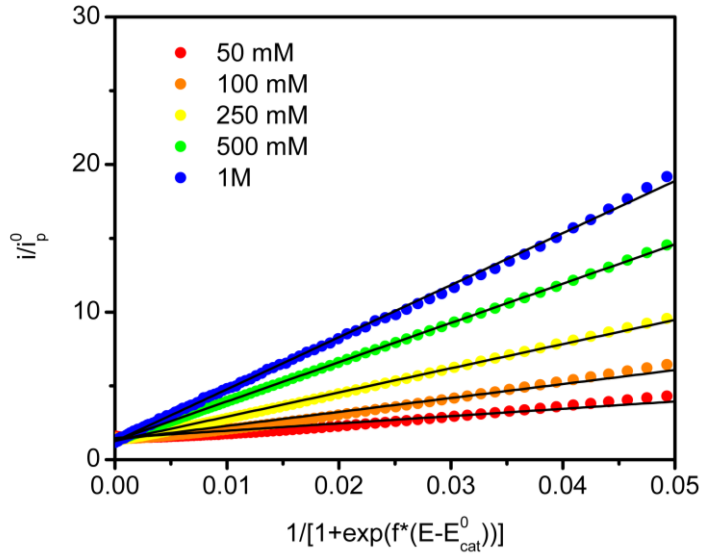

Figure S13. FOW plots for **Fe-*para*-2-amide** (1 mM) as a function of phenol concentration. Black lines denote linear fits used to obtain k_{obs}.

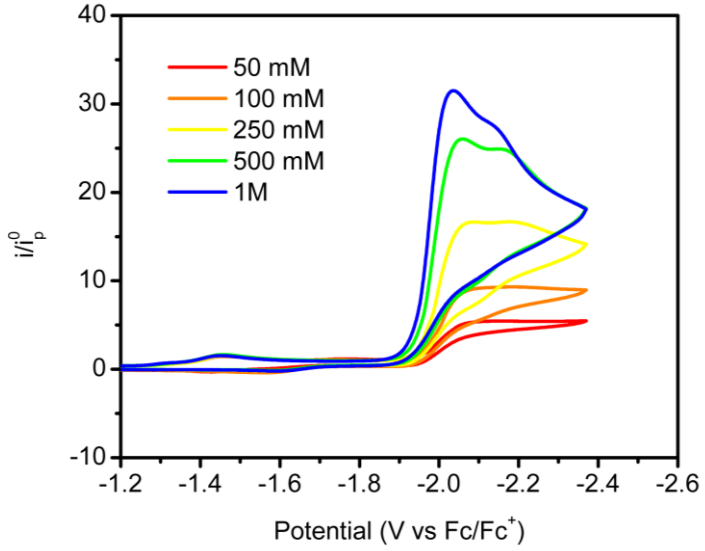

Figure S14. Cyclic voltammograms of **Fe-*para*-$(CF_3)_4$** (1 mM) in the presence of 50-1000 mM phenol under CO_2 atmosphere (0.23 M) in 0.1 M $TBAPF_6$ in DMF at a scan rate of 100 mV/sec.

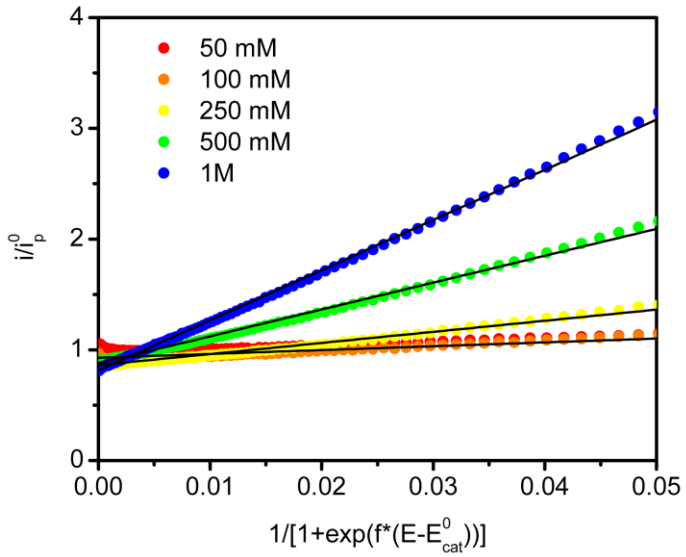

Figure S15. FOW plots for **Fe-*para*-$(CF_3)_4$** (1 mM) as a function of phenol concentration. Black lines denote linear fits used to obtain k_{obs}.

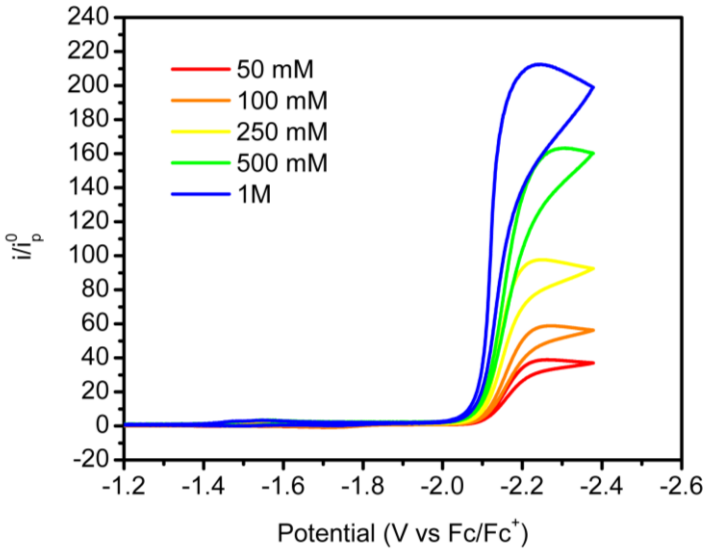

Figure S16. Cyclic voltammograms of **Fe-TPP** (1 mM) in the presence of 50-1000 mM phenol under CO_2 atmosphere (0.23 M) in 0.1 M $TBAPF_6$ in DMF at a scan rate of 100 mV/sec.

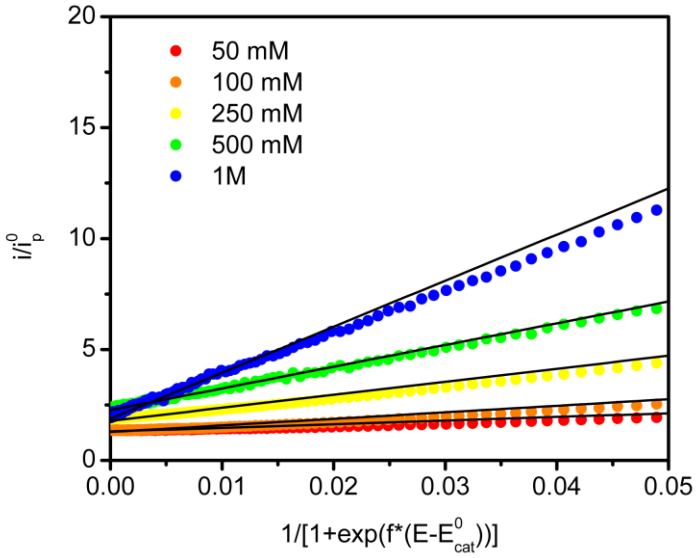

Figure S17. FOW plots for **Fe-TPP** (1 mM) as a function of phenol concentration. Black lines denote linear fits used to obtain k_{obs}.

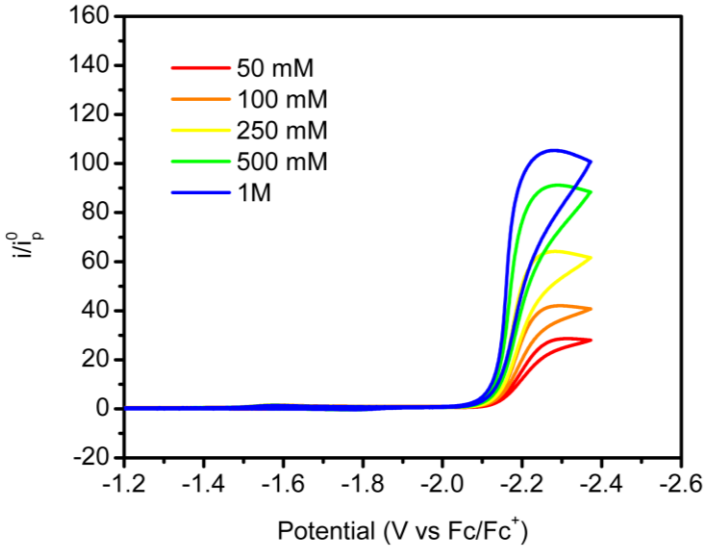

Figure S18. Cyclic voltammograms of **Fe-*para*-(OMe)$_4$** (1 mM) in the presence of 50-1000 mM phenol under CO_2 atmosphere (0.23 M) in 0.1 M $TBAPF_6$ in DMF at a scan rate of 100 mV/sec.

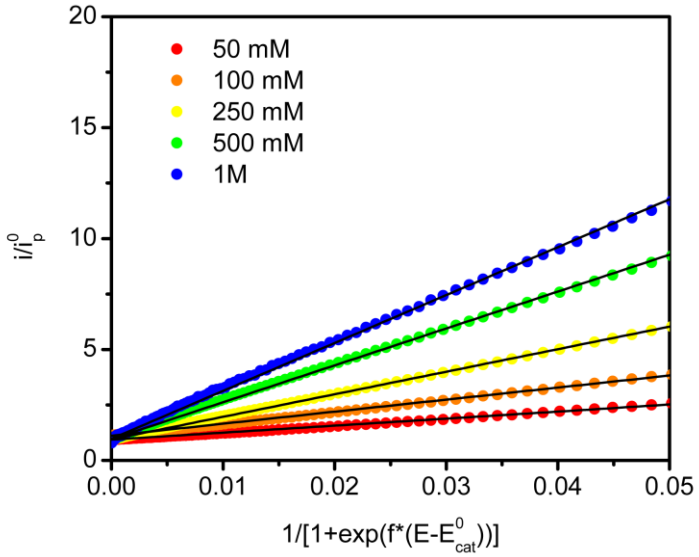

Figure S19. FOW plots for **Fe-*para*-(OMe)$_4$** (1 mM) as a function of phenol concentration. Black lines denote linear fits used to obtain k_{obs}.

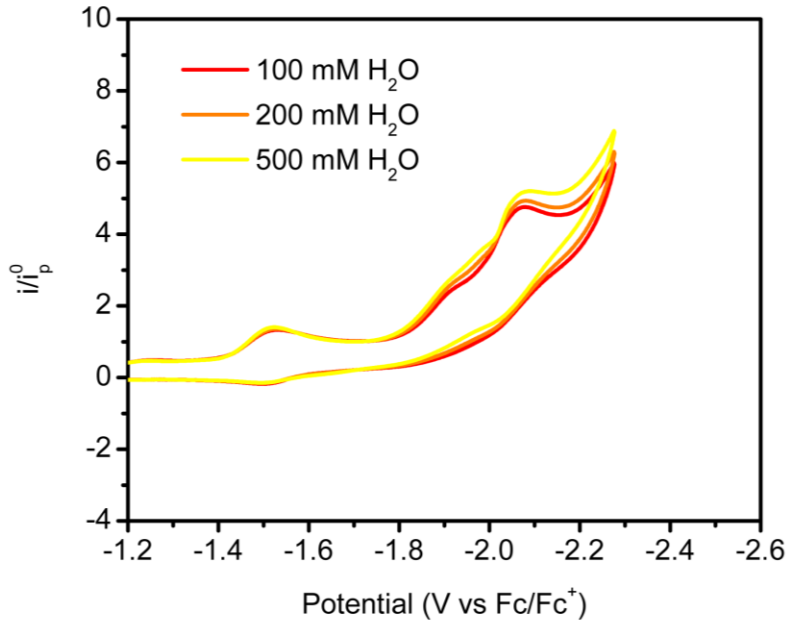

Figure S20. Cyclic voltammograms of **Fe-*ortho*-1-amide** (1 mM) in the presence of 100-500 mM H_2O under CO_2 atmosphere (0.23 M) in 0.1 M $TBAPF_6$ in DMF at a scan rate of 100 mV/sec.

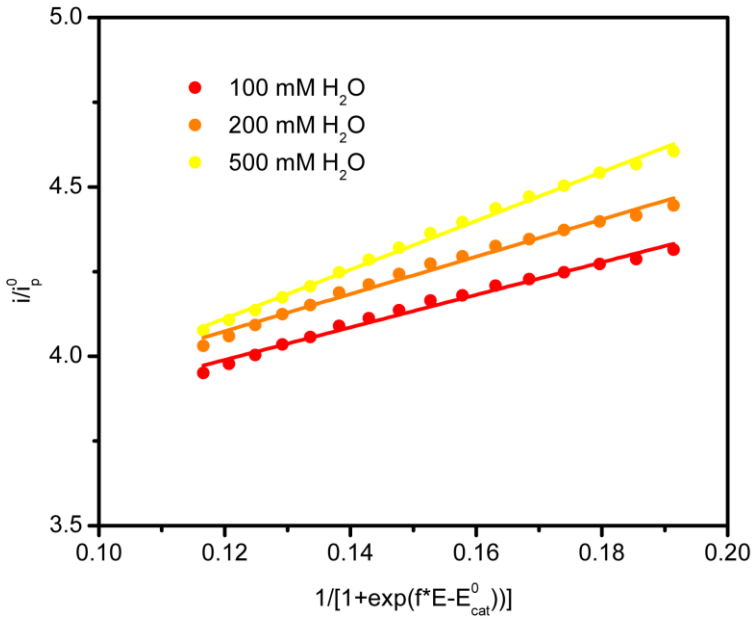

Figure S21. FOW plots for **Fe-*ortho*-1-amide** (1 mM) as a function of H_2O concentration. Lines denote linear fits used to obtain k_{obs}.

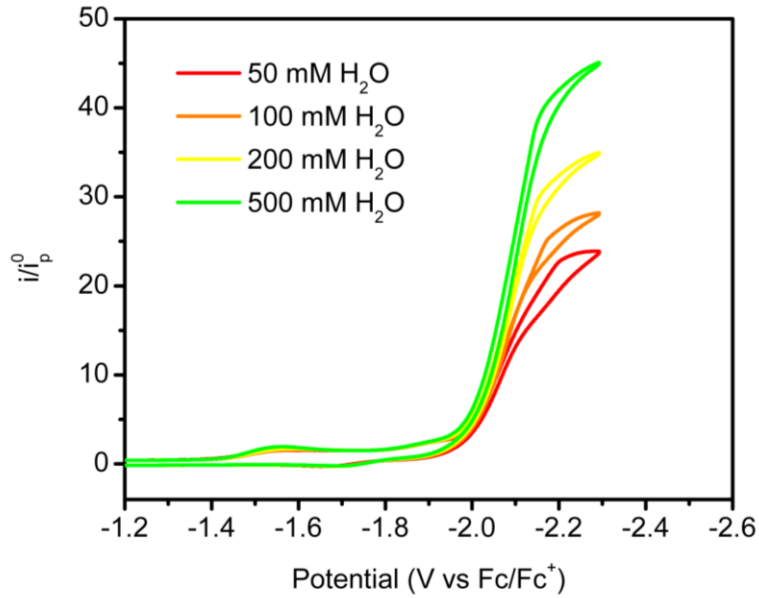

Figure S22. Cyclic voltammograms of **Fe-*ortho*-2-amide** (1 mM) in the presence of 50-500 mM H_2O under CO_2 atmosphere (0.23 M) in 0.1 M $TBAPF_6$ in DMF at a scan rate of 100 mV/sec.

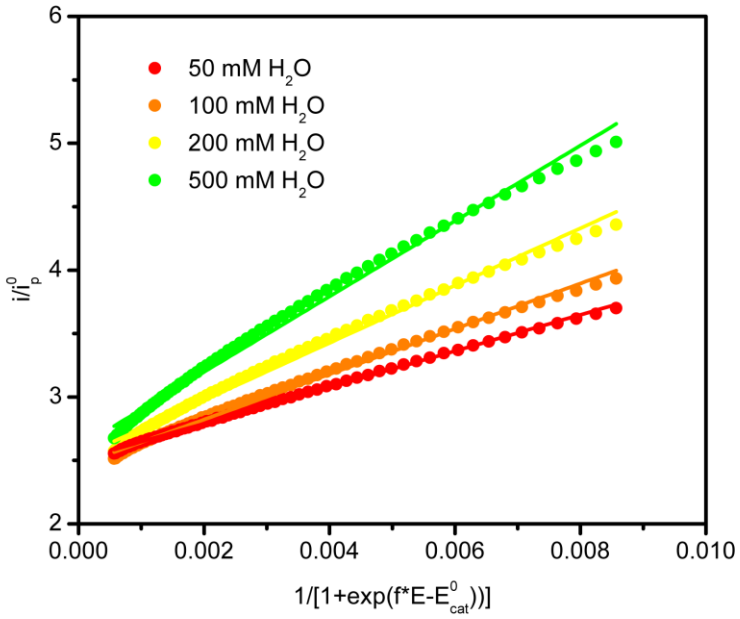

Figure S23. FOW plots for **Fe-*ortho*-2-amide** (1 mM) as a function of H_2O concentration. Lines denote linear fits used to obtain k_{obs}.

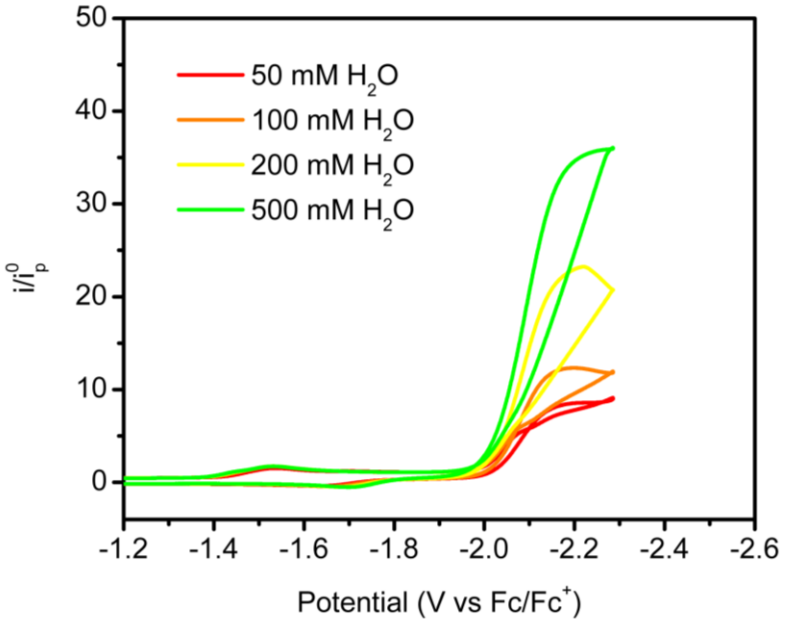

Figure S24. Cyclic voltammograms of **Fe-*para*-1-amide** (1 mM) in the presence of 50-500 mM H_2O under CO_2 atmosphere (0.23 M) in 0.1 M $TBAPF_6$ in DMF at a scan rate of 100 mV/sec.

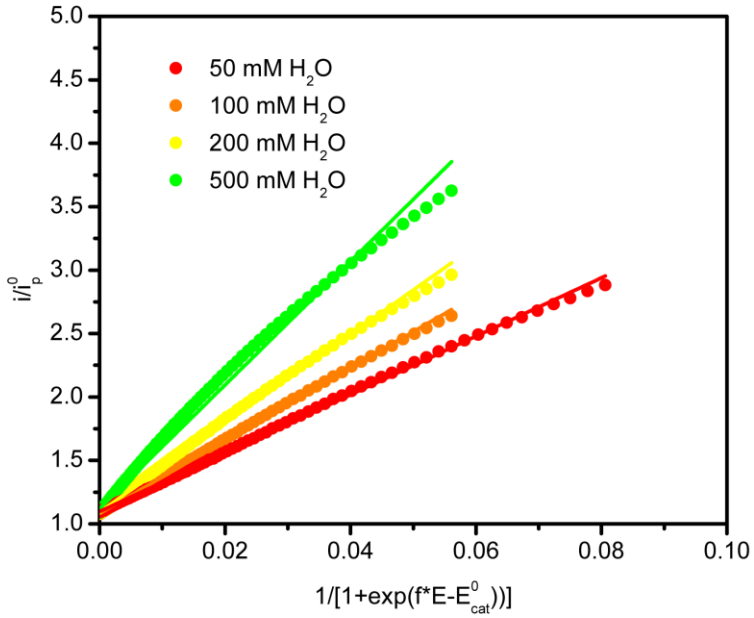

Figure S25. FOW plots for **Fe-para-1-amide** (1 mM) as a function of H_2O concentration. Lines denote linear fits used to obtain k_{obs}.

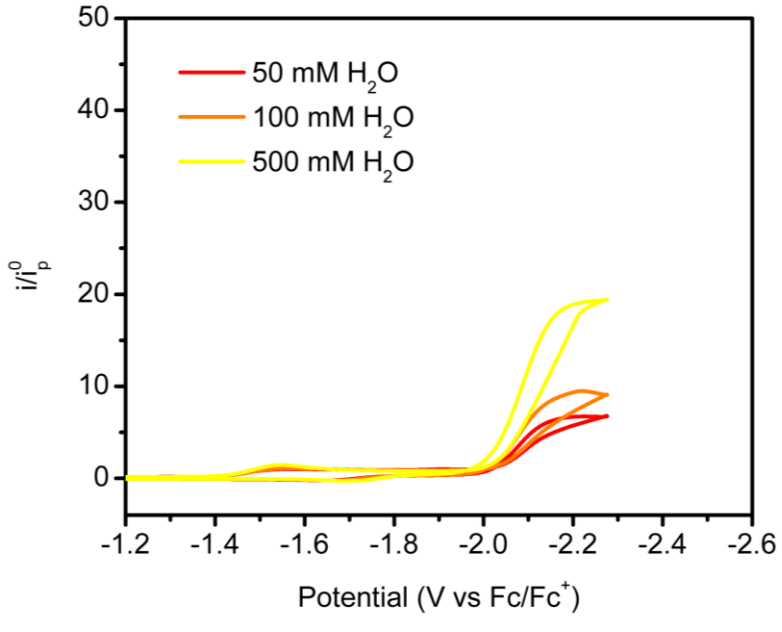

Figure S26. Cyclic voltammograms of **Fe-*para*-2-amide** (1 mM) in the presence of 50-500 mM H_2O under CO_2 atmosphere (0.23 M) in 0.1 M $TBAPF_6$ in DMF at a scan rate of 100 mV/sec.

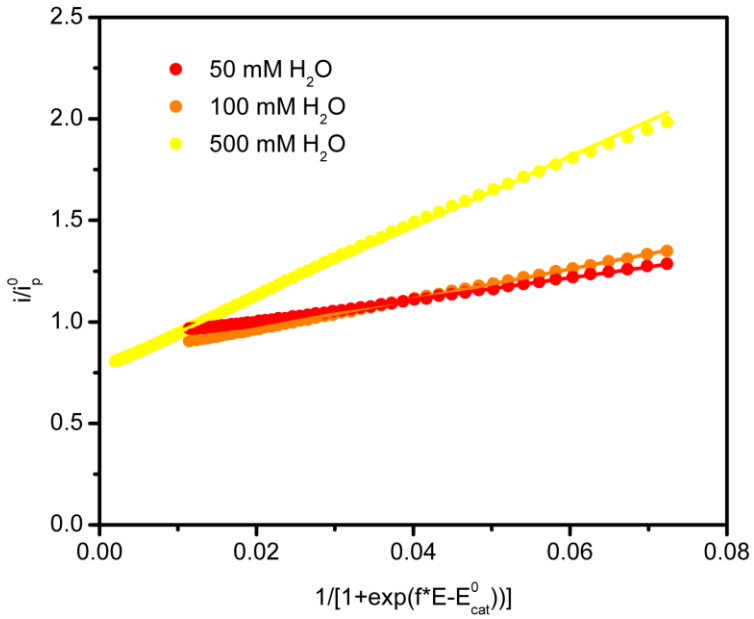

Figure S27. FOW plots for **Fe-*para*-2-amide** (1 mM) as a function of H_2O concentration. Lines denote linear fits used to obtain k_{obs}.

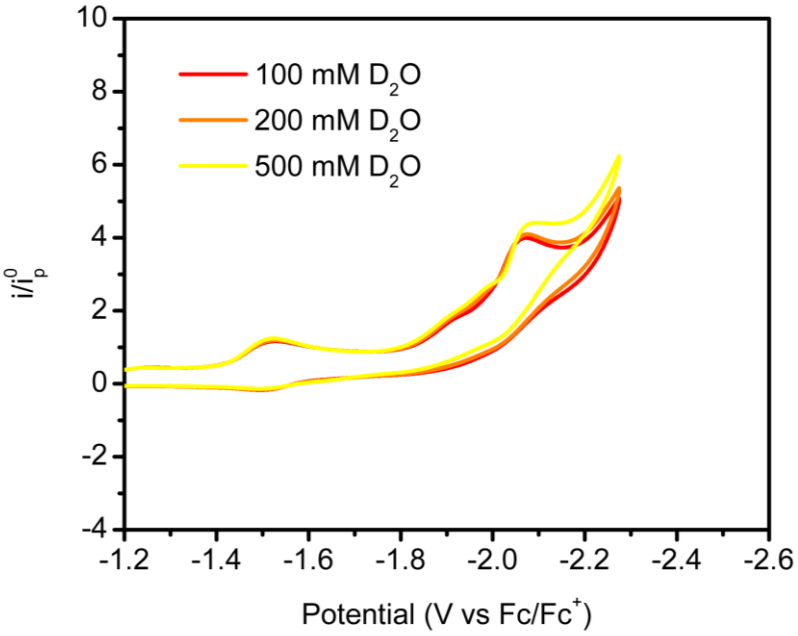

Figure S28. Cyclic voltammograms of **Fe-*ortho*-1-amide** (1 mM) in the presence of 100-500 mM D_2O under CO_2 atmosphere (0.23 M) in 0.1 M $TBAPF_6$ in DMF at a scan rate of 100 mV/sec.

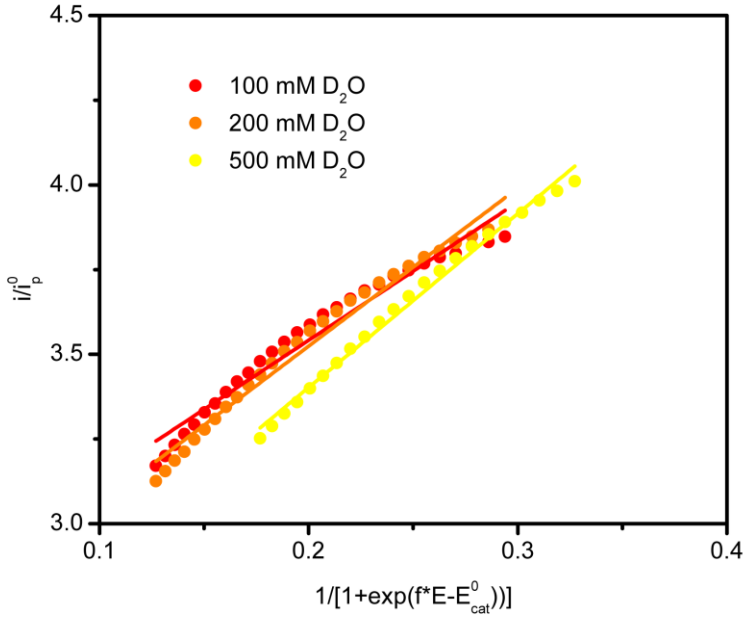

Figure S29. FOW plots for **Fe-*ortho*-1-amide** (1 mM) as a function of D_2O concentration. Lines denote linear fits used to obtain k_{obs}.

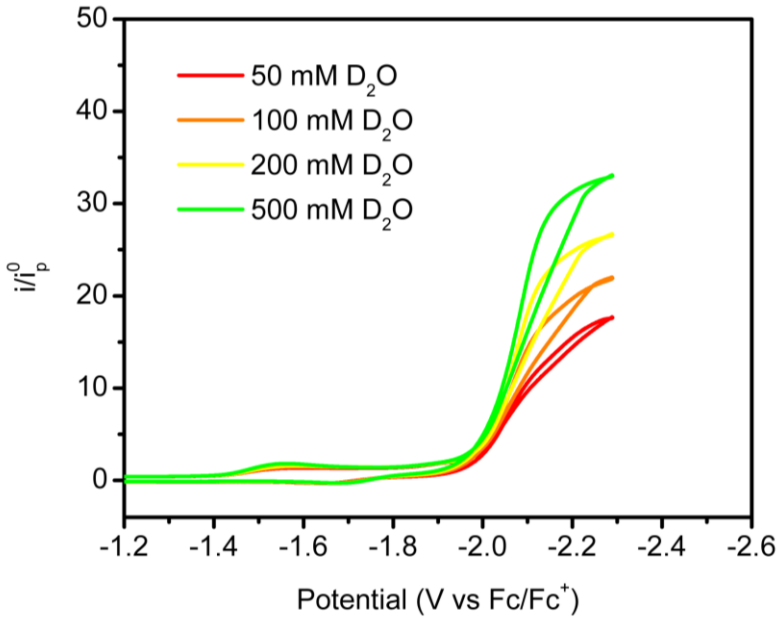

Figure S30. Cyclic voltammograms of **Fe-*ortho*-2-amide** (1 mM) in the presence of 50-500 mM D_2O under CO_2 atmosphere (0.23 M) in 0.1 M $TBAPF_6$ in DMF at a scan rate of 100 mV/sec.

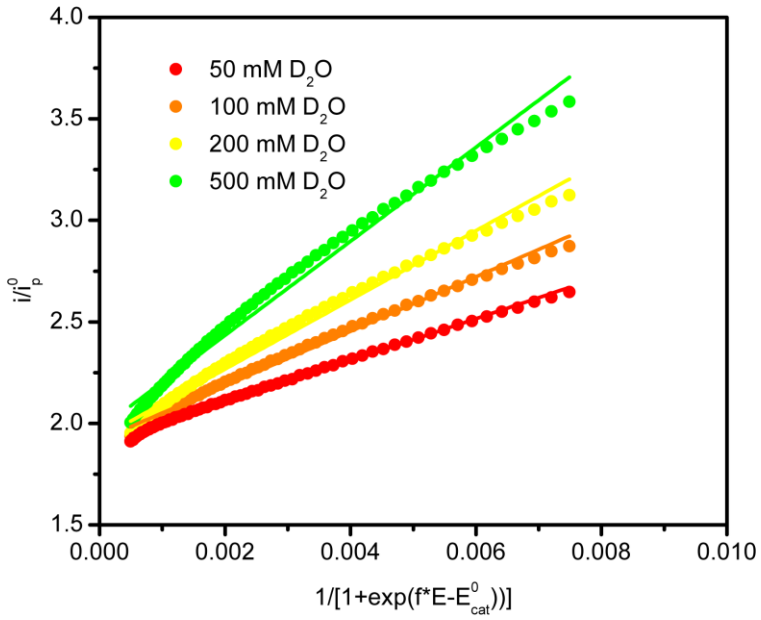

Figure S31. FOW plots for **Fe-*ortho*-2-amide** (1 mM) as a function of D_2O concentration. Lines denote linear fits used to obtain k_{obs}.

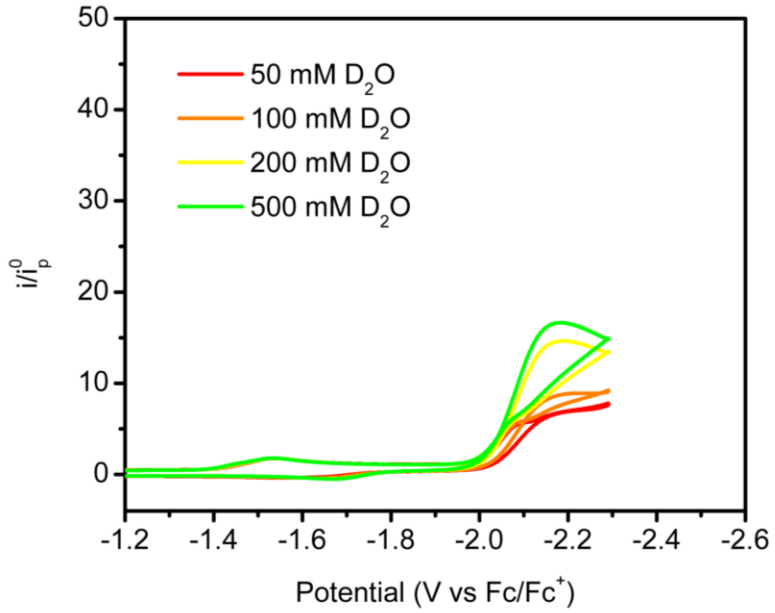

Figure S32. Cyclic voltammograms of **Fe-*para*-1-amide** (1 mM) in the presence of 50-500 mM D_2O under CO_2 atmosphere (0.23 M) in 0.1 M $TBAPF_6$ in DMF at a scan rate of 100 mV/sec.

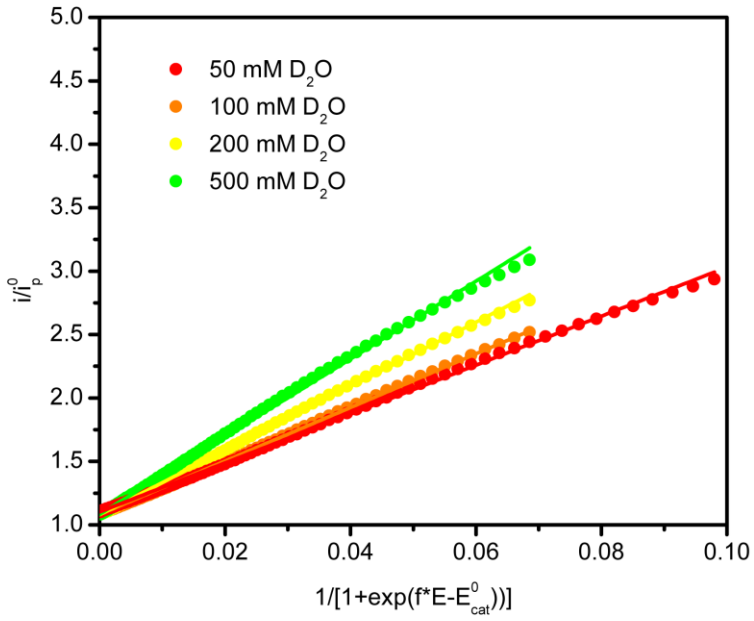

Figure S33. FOW plots for **Fe-*para*-1-amide** (1 mM) as a function of D_2O concentration. Lines denote linear fits used to obtain k_{obs}.

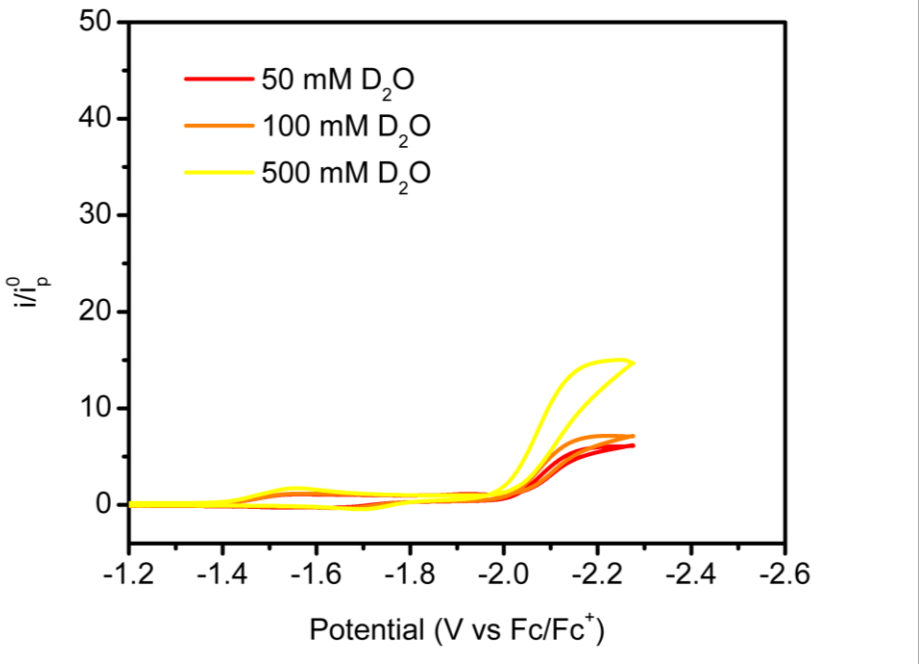

Figure S34. Cyclic voltammograms of **Fe-*para*-2-amide** (1 mM) in the presence of 50-500 mM D_2O under CO_2 atmosphere (0.23 M) in 0.1 M $TBAPF_6$ in DMF at a scan rate of 100 mV/sec.

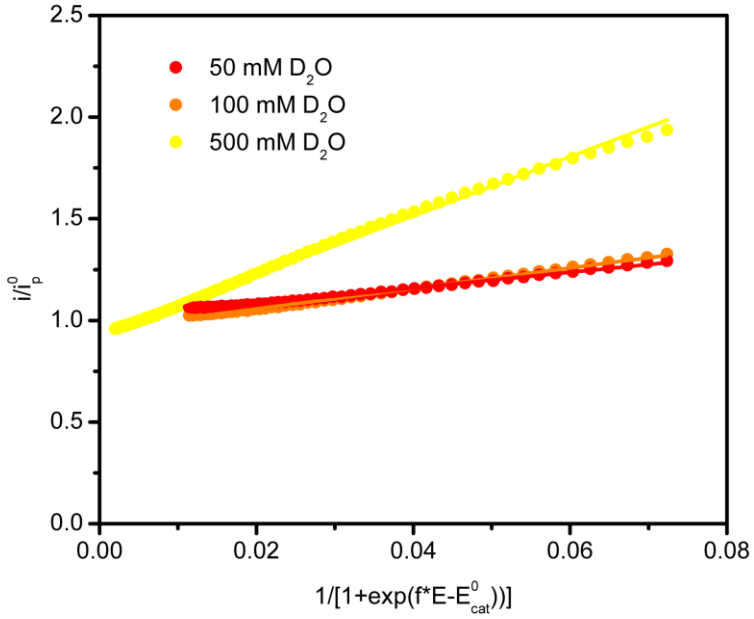

Figure S35. FOW plots for **Fe-*para*-2-amide** (1 mM) as a function of D_2O concentration. Lines denote linear fits used to obtain k_{obs}.

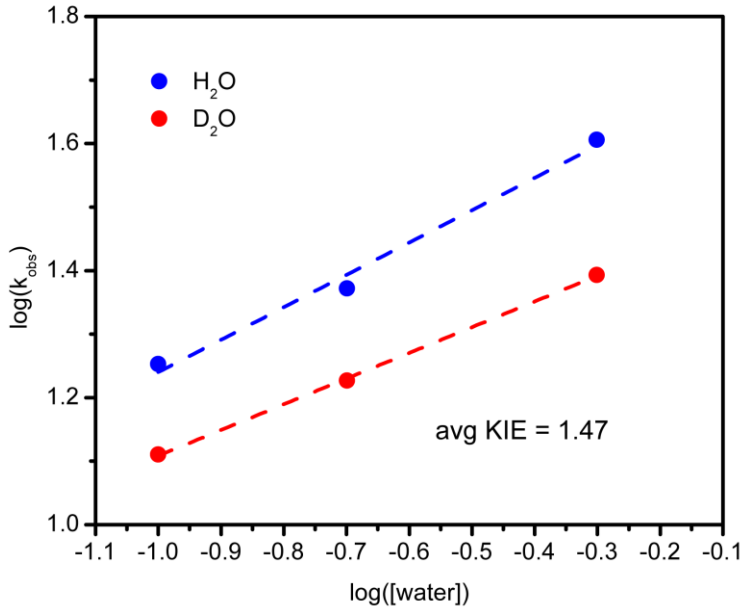

Figure S36. Variation of k_{obs} as a function of water concentration for **Fe-*ortho*-1-amide**. KIE was determined as an average of $k_{obs}(H_2O)/ k_{obs}(D_2O)$ for the three concentration points.

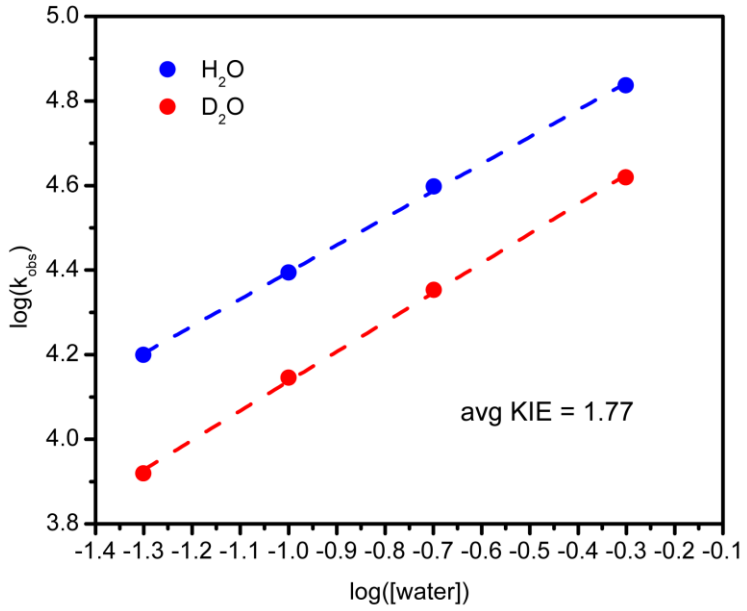

Figure S37. Variation of k_{obs} as a function of water concentration for **Fe-*ortho*-2-amide**. KIE was determined as an average of $k_{obs}(H_2O)/ k_{obs}(D_2O)$ for the four concentration points.

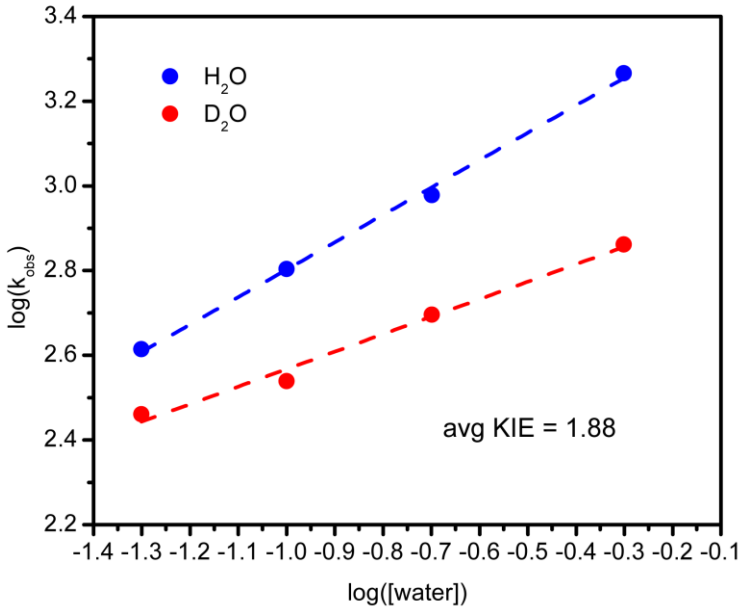

Figure S38. Variation of k_{obs} as a function of water concentration for **Fe-*para*-1-amide**. KIE was determined as an average of $k_{obs}(H_2O)/ k_{obs}(D_2O)$ for the four concentration points.

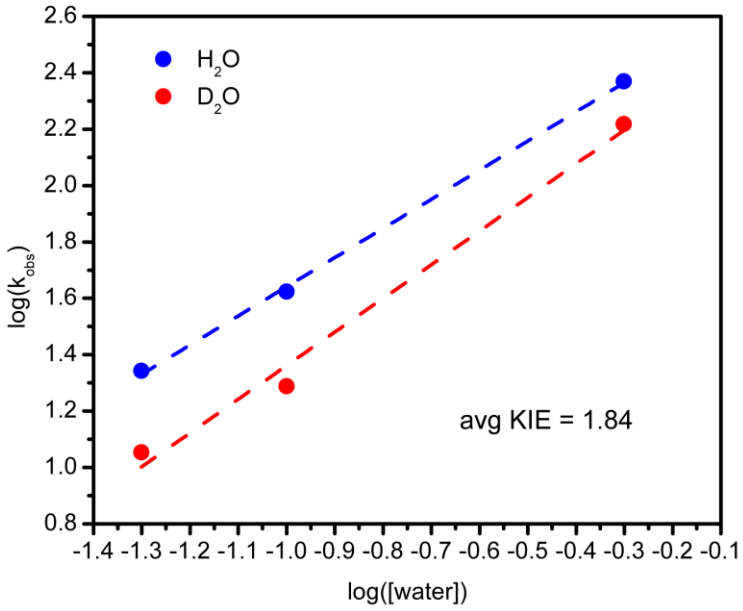

Figure S39. Variation of k_{obs} as a function of water concentration for **Fe-*para*-2-amide**. KIE was determined as an average of $k_{obs}(H_2O)/ k_{obs}(D_2O)$ for the three concentration points.

Table S1. Summary of electrochemical properties of iron porphyrin catalysts. [a]The standard reduction potential for the formal $Fe^{I/0}$ couple, E^0_{cat}, is reported as an average over three independent experiments. [b]TOF_{max} values are reported as an average over three sets of experimental conditions (different [PhOH], 0.23 M CO_2, in the regime where rate is linearly dependent on [PhOH]). [c]FE for CO is reported as an average over three CPE experiments,

Catalyst	E^0_{cat} (V vs Fc/Fc^+)[a]	TOF_{max} (s^{-1})[b]	$\log(TOF_{max})$	k_{cat} (M^{-2} s^{-1})	FE_{CO} (%)[c]
Fe-*para*-$(CF_3)_4$	-2.00	9.33×10^0	0.97	1.01×10^6	74 ± 5
Fe-TPP	-2.15	6.76×10^2	2.83	2.13×10^5	90 ± 6
Fe-*para*-$(OMe)_4$	-2.19	2.75×10^3	3.44	3.33×10^8	70 ± 6

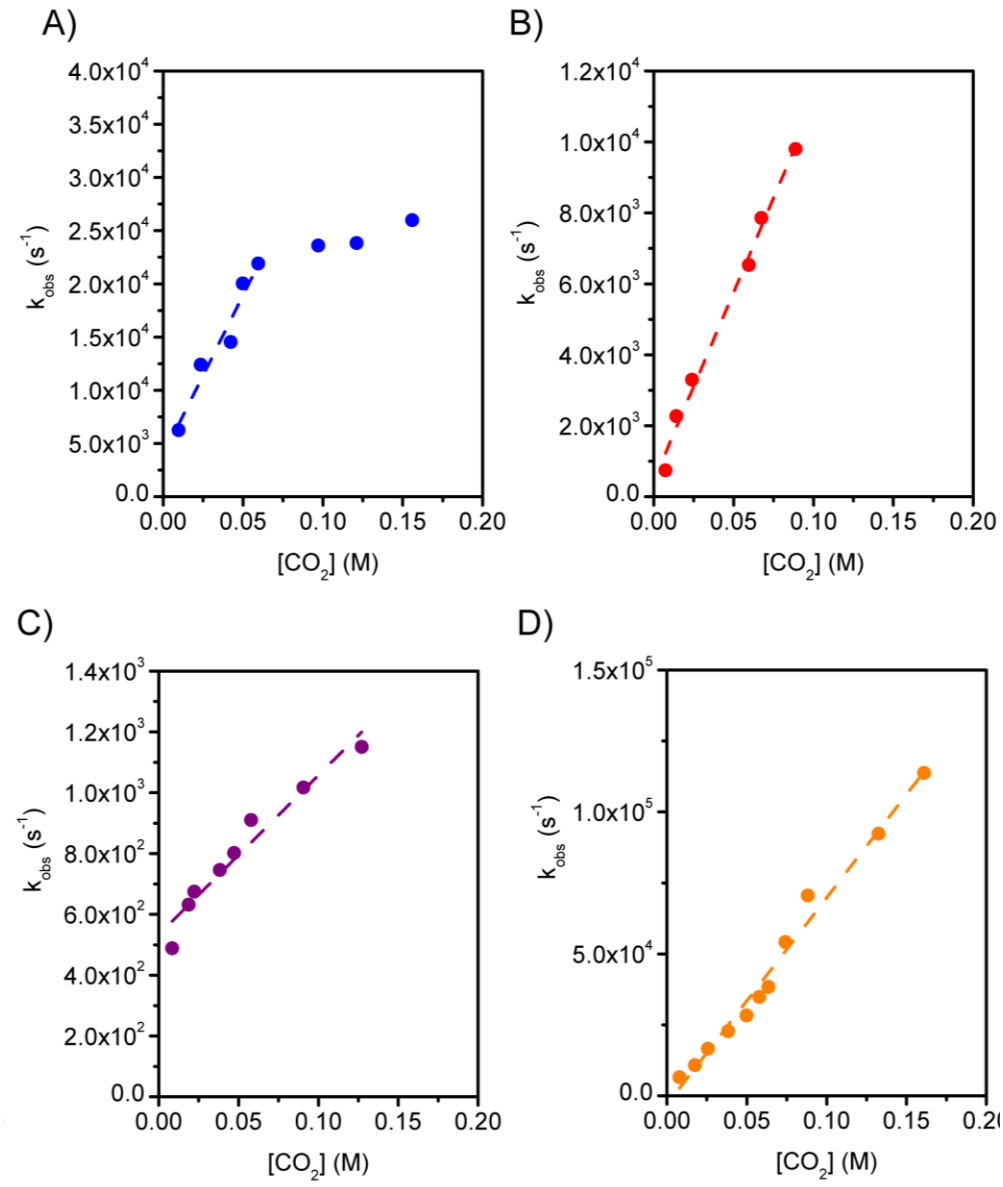

Figure S40. Observed rate constants (s^{-1}) as a function of CO_2 concentration for A) **Fe-ortho-1-amide**, B) **Fe-ortho-2-amide**, C) **Fe-para-1-amide**, and D) **Fe-para-2-amide**. Conditions: 1 mM catalyst, 0.1 M $TBAPF_6$ in DMF; 0.5 M PhOH; scan rate is 100 mV/sec. k_{obs} values were determined by Foot-of-the-Wave analysis.

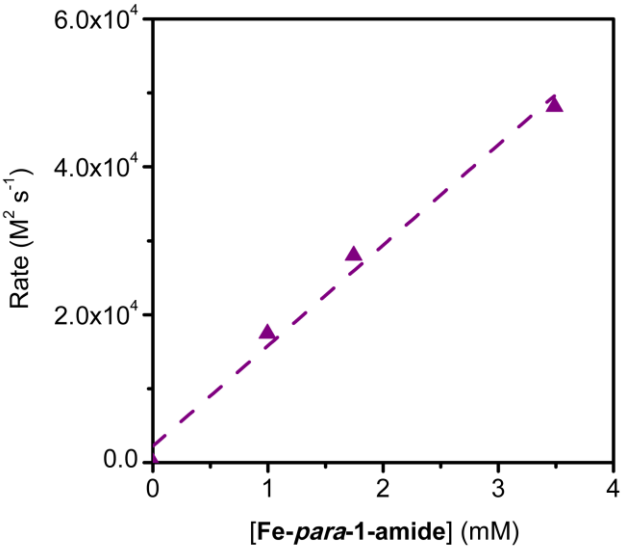

Figure S41. Observed rate constant, k_{obs} (s^{-1}), as a function of catalyst concentration for **Fe-*para*-1-amide**, indicating first-order dependence on catalyst concentration. Experiments performed in the presence of 0.5 M PhOH and 0.23 M CO_2; rates determined by Foot-of-the-Wave analysis.

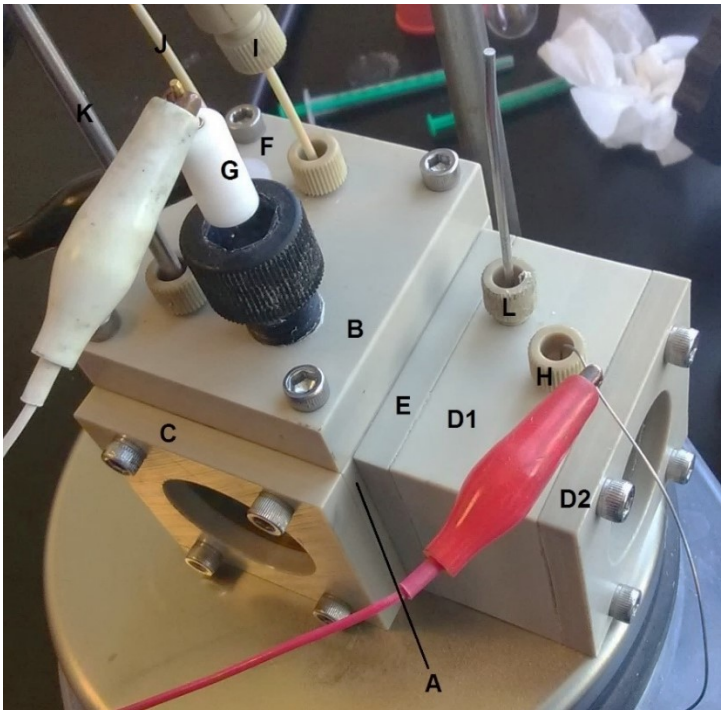

Figure S42. Photograph of the PEEK two-compartment cell. Important design features are A) main body/working electrode compartment, B) lid, C) quartz window covering, D1) counter electrode compartment, D2) counter electrode window covering, E) spacer for glass frit, F) working electrode feedthrough, G) non-aqueous reference electrode, H) counter electrode, I) gas injection port, J) gas sparging line, K) gas sampling line to GC, L) opening to counter electrode compartment.

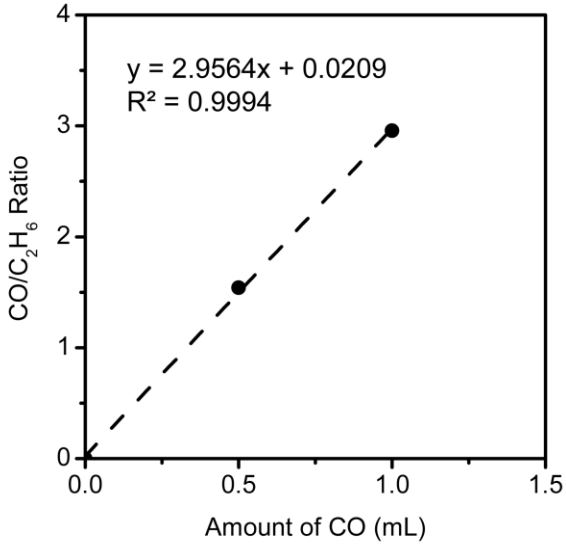

Figure S43. GC calibration curve for CO, using 0.5 mL C_2H_6 as internal standard. CO/C_2H_6 ratio is defined as the ratio of peak integrals measured by flame ionization detector.

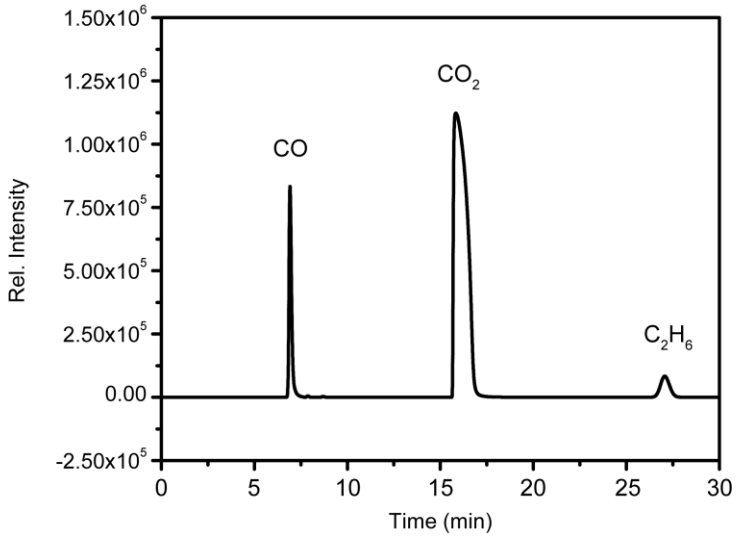

Figure S44. Representative GC trace (FID channel) showing CO, CO_2, and C_2H_6 internal standard.

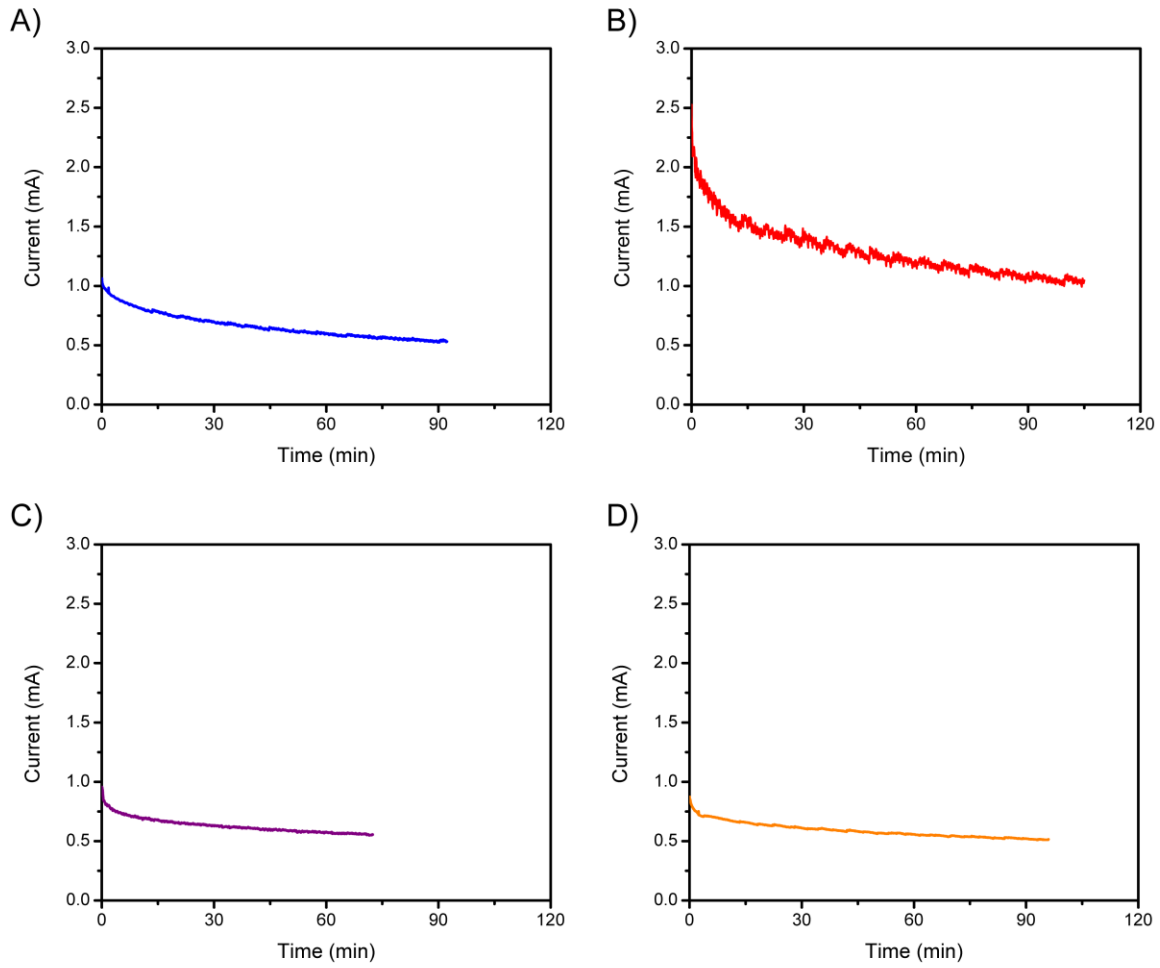

Figure S45. Representative CPE traces for A) **Fe-*ortho*-1-amide** held at -2.15 V vs Fc/Fc^+, B) **Fe-*ortho*-2-amide** held at -2.15 V vs Fc/Fc^+, C) **Fe-*para*-1-amide** held at -2.27 V vs Fc/Fc^+, and D) **Fe-*para*-2-amide** held at -2.16 V vs Fc/Fc^+.

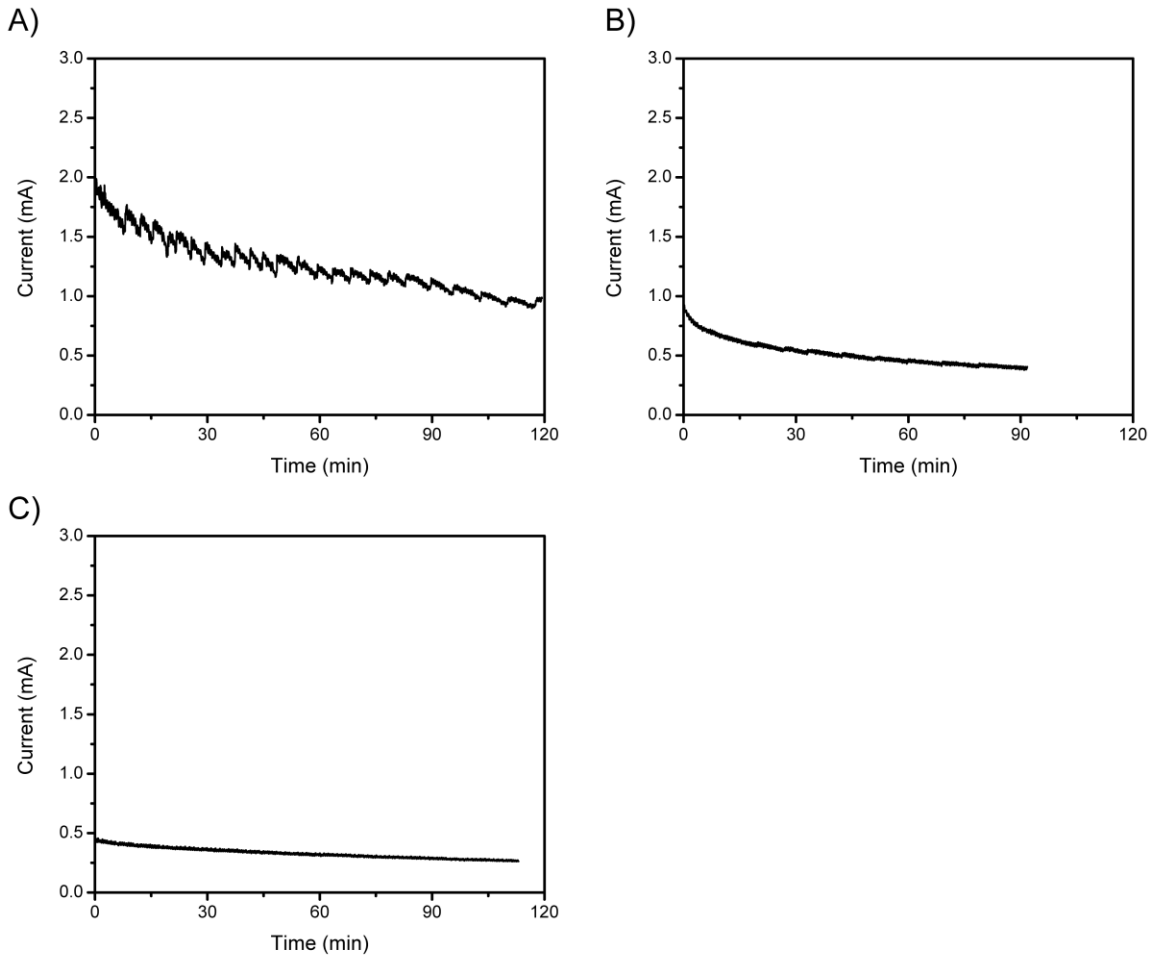

Figure S46. Representative CPE traces for A) **Fe-TPP** held at -2.22 V vs Fc/Fc^+, B) **Fe-*para*-$(OMe)_4$** held at -2.20 V vs Fc/Fc^+, and C) **Fe-*para*-$(CF_3)_4$** held at -2.09 V vs Fc/Fc^+.

Table S2. Raw results for controlled potential electrolysis replicates for all iron porphyrin complexes including electrolysis potential E, the charge passed Q, amount of CO measured by headspace GC versus expected based on charge (mL), and the resulting Faradaic Efficiency (%). No H_2 gas was detected in any case.

Catalyst	E (V vs Fc/Fc^+)	Charge (Q)	Amount CO measured (mL)	Amount CO expected (mL)	FE_{CO} (%)
Fe-*ortho*-1-amide	-2.12	2.22	0.224	0.281	80
	-2.15	3.67	0.399	0.465	86
	-2.14	3.04	0.316	0.385	82
Fe-*ortho*-2-amide	-2.19	8.78	1.030	1.113	93
	-2.15	8.15	0.964	1.034	93
	-2.17	8.55	0.978	1.084	90
Fe-*para*-1-amide	-2.19	1.76	0.184	0.223	82
	-2.22	1.67	0.153	0.212	72
	-2.27	2.74	0.229	0.348	66
Fe-*para*-2-amide	-2.16	3.01	0.329	0.381	86
	-2.16	1.99	0.180	0.253	71
	-2.16	3.40	0.343	0.431	80
Fe-*para*-$(CF_3)_4$	-2.06	2.75	0.246	0.349	71
	-2.10	4.40	0.408	0.558	73
	-2.09	5.04	0.508	0.639	80
Fe-TPP	-2.15	10.00	1.066	1.268	84
	-2.14	9.00	1.102	1.141	97
	-2.22	9.00	1.019	1.141	89
Fe-*para*-$(OMe)_4$	-2.18	2.51	0.200	0.318	63
	-2.21	2.71	0.253	0.344	74
	-2.20	2.86	0.269	0.363	74

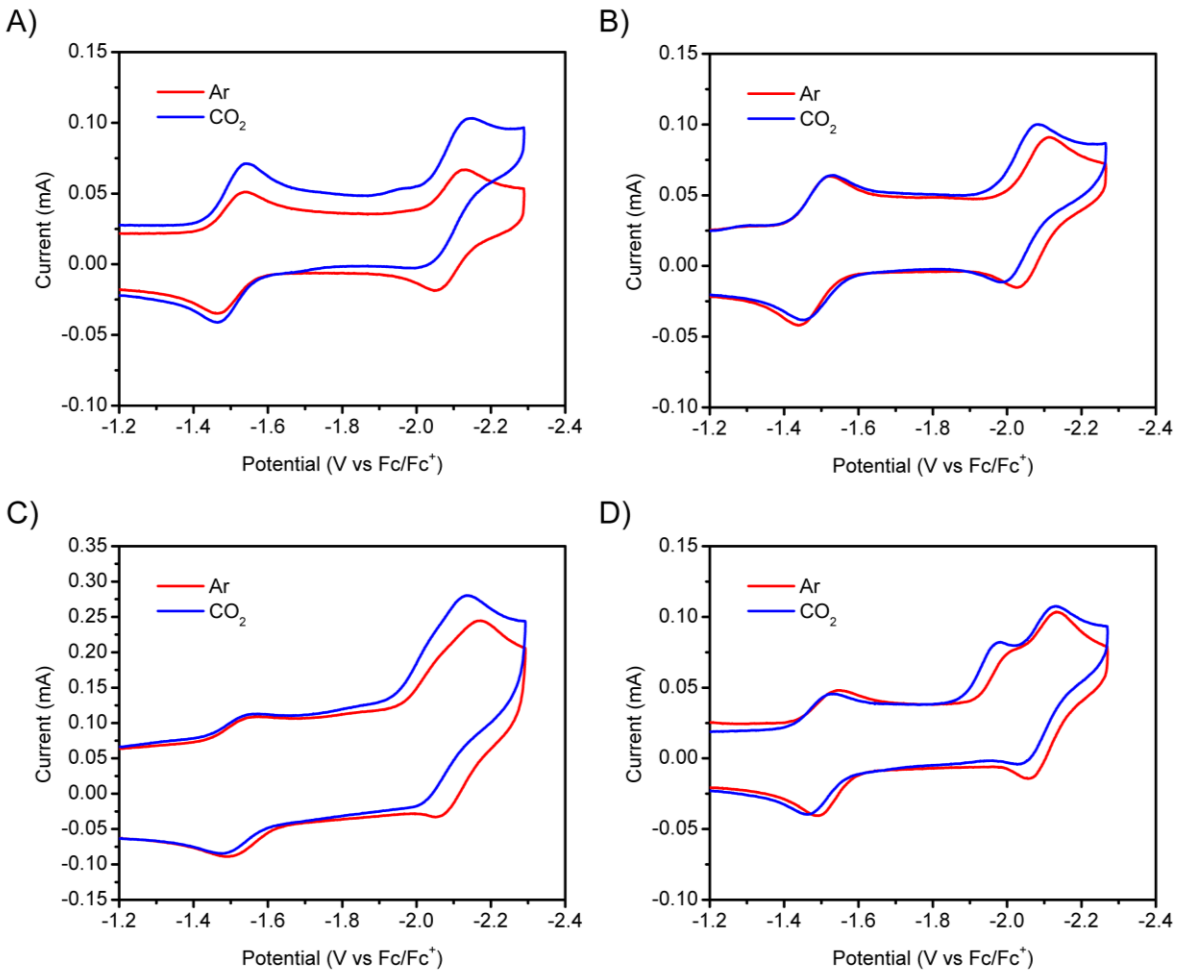

Figure S47. Cyclic voltammograms used to determine CO_2 equilibrium binding constant, K_{CO2}. A) **Fe-TPP** (measured at 2 V/sec), ΔE = 0.011 V. B) **Fe-*ortho*-1-amide** (measured at 2 V/sec), ΔE = 0.041 V. C) **Fe-*ortho*-2-amide** (measured at 10 V/sec), ΔE = 0.038 V. D) **Fe-*para*-2-amide** (measured at 2 V/sec), ΔE = 0.016 V. K_{CO2} for **Fe-*para*-1-amide** was not able to be determined using this method.

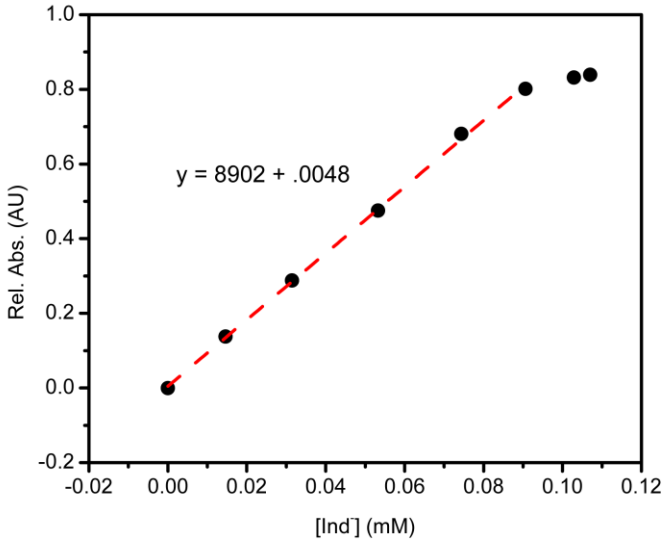

Figure S48. Representative determination of extinction coefficient ε (slope) of 4-chloro-2-nitroaniline anion, Ind^-, by titration of the corresponding aniline into a solution of K-dimsyl base.

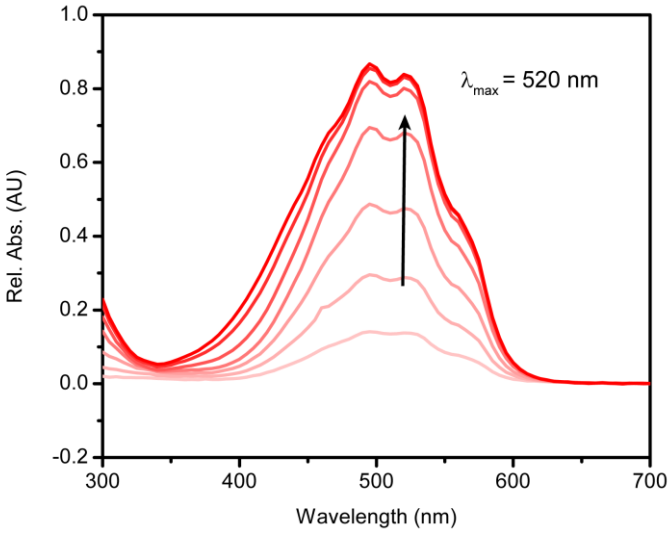

Figure S49. Representative spectral changes observed upon titration of 4-chloro-2-nitroaniline into a solution of K-dimsyl base. Aniline was added in small aliquots until no change in absorbance values at 520 nm was observed, signifying complete consumption of K-dimsyl base.

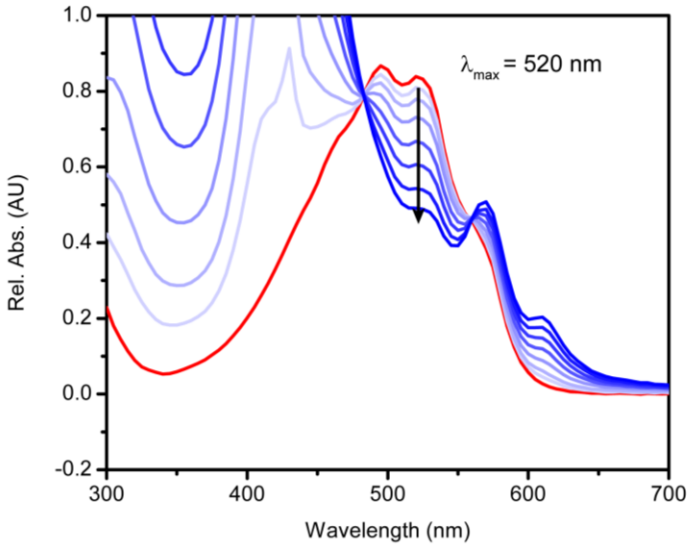

Figure S50. Representative spectral changes observed upon titration of **Fe-*ortho*-2-amide** into the solution of 4-chloro-2-nitroaniline and its anion (from the first phase of the titration experiment). The red trace is identical to that shown in Fig. S37. Note the decrease in absorption at 520 nm as the deprotonated indicator becomes protonated by the pendant amide.

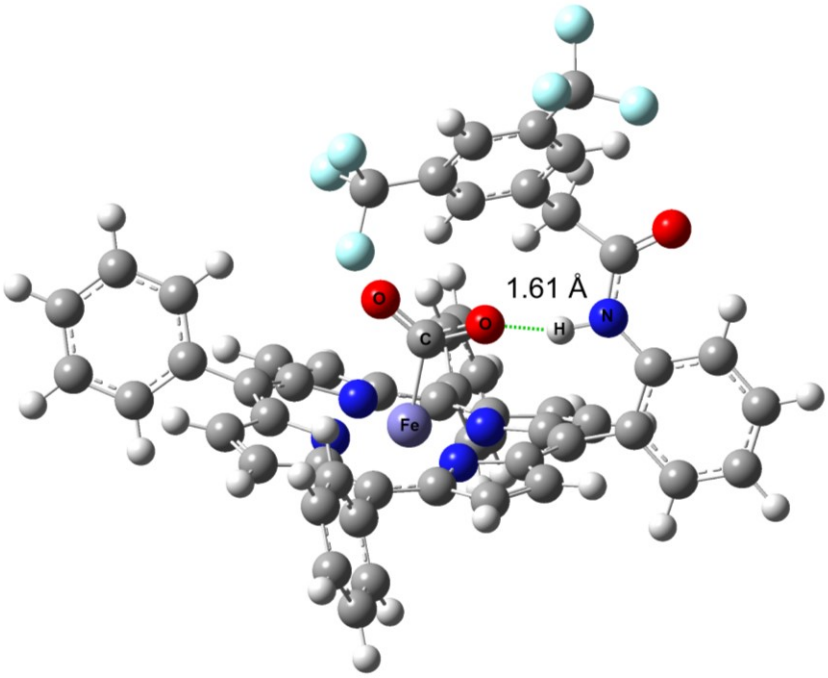

Figure S51. Optimized structure of the Fe^0–CO_2 adduct of **Fe-*ortho*-1-amide**, The hydrogen bond between the amide and bound CO_2 is represented by the green dashed line. Key: **g**ray, carbon; white, hydrogen; red, oxygen; blue, nitrogen; light purple, iron; light blue, fluorine.

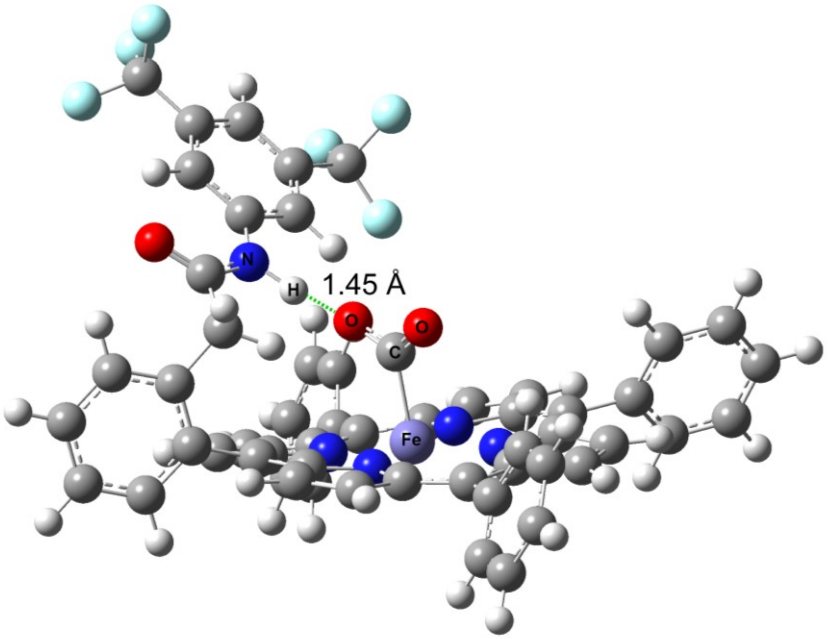

Figure S52. Optimized structure of the Fe^0–CO_2 adduct of **Fe-*ortho*-2-amide**, The hydrogen bond between the amide and bound CO_2 is represented by the green dashed line. Key: gray, carbon; white, hydrogen; red, oxygen; blue, nitrogen; light purple, iron; light blue, fluorine.

UV-Visible Spectra of freebase-, Fe-, and Zn-porphyrins

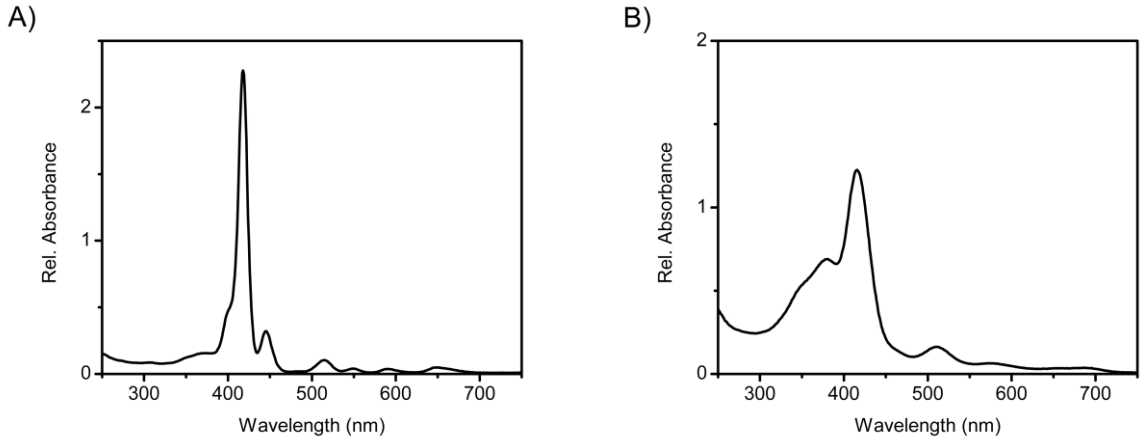

Figure S53. UV-Vis spectra (CH_2Cl_2) of freebase porphyrin ***ortho*-1-amide** (A) and Fe complex **Fe-*ortho*-1-amide** (B).

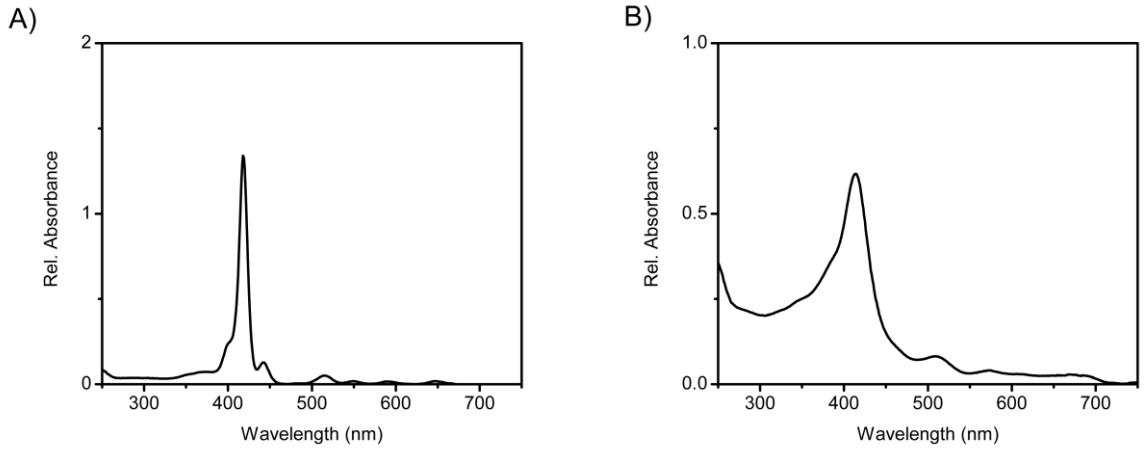

Figure S54. UV-Vis spectra (CH_2Cl_2) of freebase porphyrin ***ortho*-2-amide** (A) and Fe complex **Fe-*ortho*-2-amide** (B).

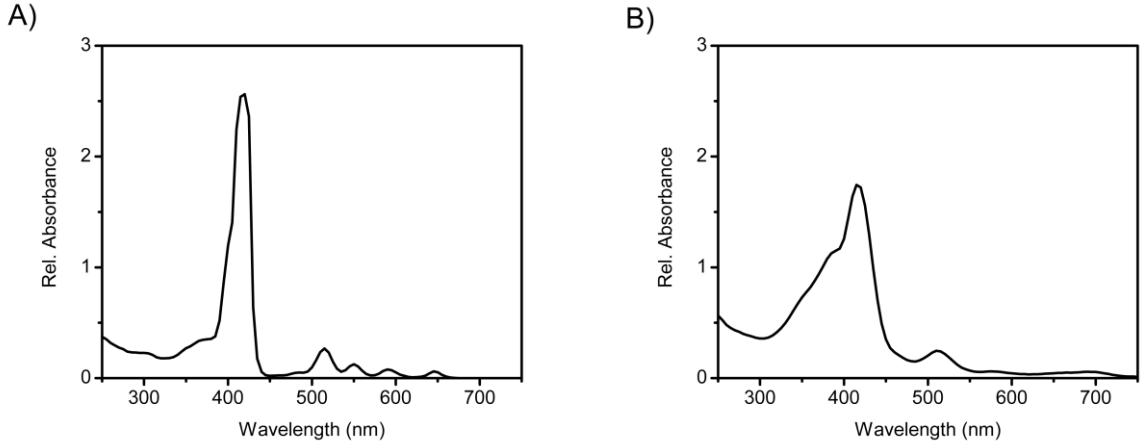

Figure S55. UV-Vis spectra (CH_2Cl_2) of freebase porphyrin ***para*-1-amide** (A) and Fe complex **Fe-*para*-1-amide** (B).

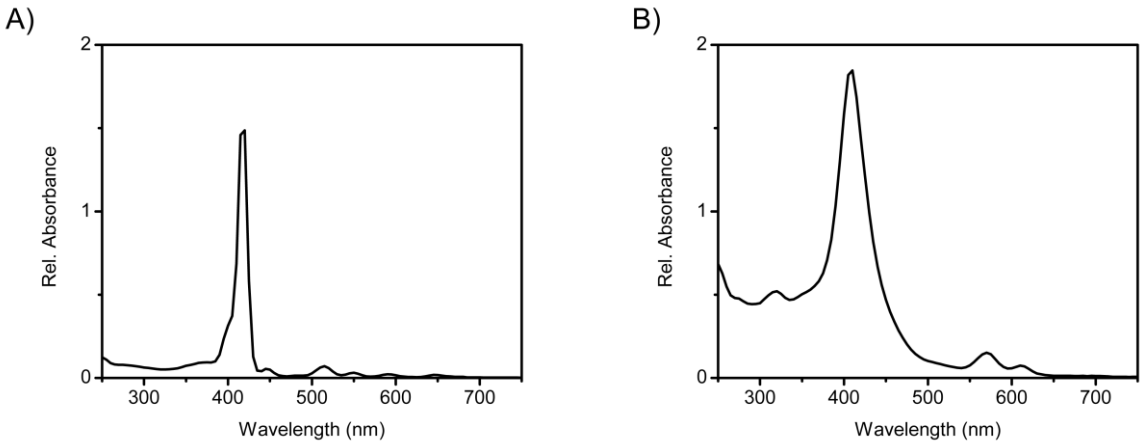

Figure S56. UV-Vis spectra (CH_2Cl_2) of freebase porphyrin ***para*-2-amide** (A) and Fe complex **Fe-*para*-2-amide** (B).

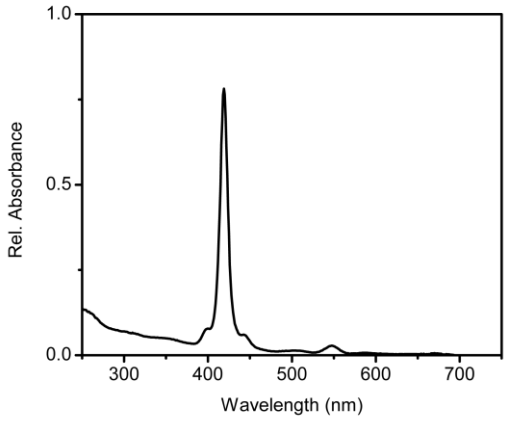

Figure S57. UV-Vis spectra (CH_2Cl_2) of Zn complex **Zn-*ortho*-1-amide**.

Synthetic Procedures:

[3,5-Bis(trifluoromethyl)phenyl]amide (amide). A 50 mL Schlenk flask was charged with 20 mL anhydrous DCM, 3,5-bis(trifluoromethyl)phenylacetic acid (1.00 g, 3.67 mmol), and a catalytic amount of anhydrous DMF (29 µL, 0.37 mmol). Freshly distilled $SOCl_2$ (0.32 mL, 4.41 mmol) was added under a N_2 atmosphere and the solution was stirred at RT for 1.5 h. Solvent was removed under reduced pressure to afford a yellow oil. Anhydrous toluene (5 mL) was added, then removed under reduced pressure to assist in removal of excess $SOCl_2$. The resulting acid chloride was dissolved in anhydrous DCM (20 mL) and 3,5-bis(trifluoromethyl)aniline (0.86 mL, 5.51 mmol) was added, followed by triethylamine (0.61 mL, 4.41 mmol). After reacting overnight at RT, the solvent was removed under reduced pressure. The product was dissolved in EtOAc and washed with water; combined organic fractions were dried over $MgSO_4$ and solvent was removed under reduced pressure. The crude product was purified by column chromatography (starting at 2:1 hexane:DCM and progressing to 1:3 hexane:DCM) on silica, and obtained as a white solid (0.65 g, 37% yield). ^{1}H NMR (500 MHz, CD_3CN) δ 9.02 (br s, 1H), 8.15 (s, 2H), 7.94 (s, 3H), 7.70 (s, 1H), 3.92 (s, 2H). $^{13}C\{^1H\}$ NMR (126 MHz, CD_3CN) δ 169.80, 141.30, 138.77, 132.46 (q, *J* = 33.3 Hz), 131.76 (q, *J* = 32.8 Hz), 131.37 (m), 124.49 (q, *J* = 271.8 Hz), 124.29 (q, *J* = 271.9 Hz), 121.87 (m), 120.12, 117.84 (m), 43.06. ^{19}F NMR (376 MHz, $CDCl_3$) δ -62.57, -62.89. IR (ATR, solid, ν (cm^{-1})): 3264 (w), 3222 (w), 3186 (w), 3096 (w), 1670 (m), 1569 (m), 1469 (m), 1374 (s), 1272 (s), 1171 (s), 1127 (s). ESI-MS calculated for $C_{18}H_8F_{12}NO$ $(M-H)^-$ 482.0, found 482.4; $C_{18}H_9ClF_{12}NO$ $(M+Cl)^-$ 518.0, found 518.4.

5-[2-Nitrophenyl]-10,15,20-triphenyl porphyrin (1). Porphyrin **1** was synthesized according to a modified literature procedure.[9, 10] 2-nitrobenzaldehyde (7.2 g, 47.6 mmol) and benzaldehyde (10.11 g, 95.3 mmol) were added to refluxing propionic acid (400 mL) in a 1 L round bottom flask. Pyrrole (9.9 g, 142.9 mmol) was added dropwise and the solution was heated at reflux for 30 min in the absence of light. Upon cooling to room temperature, methanol (200 mL) was added and the precipitated porphyrins were collected *via* filtration, then washed with water and methanol several times. A solution of the porphyrin mixture in DCM was run through a basic alumina plug to remove oligomers. Porphyrin **1** (R_f = 0.6) was separated from tetraphenylporphyrin (R_f = 0.75) and other nitroporphyrins by column chromatography (2:1 hexane:DCM) on basic alumina, and finally recrystallized from DCM/MeOH (1.7 g, 7% yield). The ^{1}H NMR spectrum agrees well with the literature reports of this compound. ^{1}H NMR (300 MHz, CD_2Cl_2) δ 8.82 – 8.92 (m, 6H), 8.66 – 8.72 (m, 2H), 8.45 (m, 1H), 8.15 – 8.33 (m, 7H), 7.96 – 8.05 (m, 2H), 7.70 – 7.85 (m, 9H), -2.78 (s, 2H).

5-[2-Aminophenyl]-10,15,20-triphenyl porphyrin (2). Porphyrin **2** was synthesized by reduction of **1** according to a modified literature procedure.[9, 10] A solution of **1** (1.39 g, 2.10 mmol) in p-dioxane (300 mL) was sparged with N_2 and $SnCl_2{\cdot}2H_2O$ (5.68 g, 25.20 mmol) was added as a solid. After 10 min, concentrated HCl (480 mL) was added and the solution was heated to reflux for 1 h under N_2 atmosphere in the absence of light. Upon cooling to room temperature, the solution was neutralized to pH 7 with 6 M NaOH and saturated $NaHCO_3$. The biphasic mixture was extracted three times with EtOAc, then the combined organic phase was rinsed with water and brine and dried over $MgSO_4$. Solvent was removed under reduced pressure to afford crude **2**. The product was purified by column chromatography (starting at 1:1 EtOAc:hexane and progressing to 3:1 EtOAc:hexane) on silica, and finally recrystallized from DCM/MeOH (750 mg, 57% yield). The ^{1}H NMR spectrum agrees well with the literature reports of this compound. ^{1}H NMR (300 MHz, CD_2Cl_2) δ 8.81 – 8.96 (m, 8H), 8.16 – 8.30 (m, 6H), 7.86 (d, *J* = 7.5 Hz, 1H), 7.71 – 7.83 (m, 9H), 7.61 (t, *J* = 7.8 Hz, 1H), 7.16 (t, *J* = 7.4 Hz, 1H), 7.14 (d, *J* = 8.0 Hz, 1H), 3.61 (s, 2H), -2.81 (s, 2H). ESI-MS calculated for $C_{44}H_{33}N_5$ $(M+H)^+$ 630.3, found 630.8.

***Ortho*-1-amide.** A 100 mL Schlenk flask was charged with 40 mL anhydrous DCM, 3,5-bis(trifluoromethyl)phenylacetic acid (525 mg, 1.89 mmol), and a catalytic amount of anhydrous DMF (15 µL). Freshly distilled thionyl chloride (167 µL, 2.30 mmol) was added under a N_2 atmosphere and the solution was stirred at RT for 2 h. Solvent was removed under reduced pressure to afford a yellow oil. Anhydrous toluene (5 mL) was added, then removed under reduced pressure to assist in removal of excess $SOCl_2$. The resulting acid chloride was dissolved in anhydrous THF (20 mL) and added dropwise to a solution of porphyrin **2** (115 mg, 0.183 mmol) dissolved in anhydrous THF (25 mL). After reacting overnight at RT in the absence of light, the solvent was removed under reduced pressure to afford crude ***ortho-1*-amide**. The product was purified by column chromatography (starting at 2:1 hexane:DCM and progressing slowly to 1:3 hexane:DCM) on silica (132 mg, 82% yield). ^{1}H NMR (400 MHz, CD_2Cl_2) δ 8.82 – 8.97 (m, 6H), 8.77 (d, *J* = 4.7 Hz, 2H), 8.68 (d, *J* = 8.3 Hz, 1H), 8.14 – 8.28 (m, 6H), 8.01 (d, *J* = 7.0 Hz, 1H), 7.72 – 7.88 (m, 10H), 7.54 (t, *J* = 7.7 Hz, 1H), 7.32 (s, 1H), 7.12 (s, 2H), 7.06 (s, 1H), 2.81 (s, 2H), -2.77 (br s, 2H). ^{13}C{^{1}H} NMR (126 MHz, CD_2Cl_2) δ 167.35, 142.24, 142.04, 138.64, 136.95, 135.41, 135.01, 134.93, 134.89, 134.85, 132.04, 131.21 (q, *J* = 33.1 Hz), 129.80, 129.61, 128.26, 127.20, 127.14, 123.60, 123.24 (q, *J* = 272.3 Hz), 121.62, 121.17, 121.02, 120.84 – 120.94 (m), 112.91, 43.08. ^{19}F NMR (376 MHz, CD_2Cl_2) δ -62.73. Λ_{max} (CH_2Cl_2) 418, 443, 516, 550, 594, 648 nm. ESI-MS calculated for $C_{54}H_{36}F_6N_5O$ $(M+H)^+$ 884.3, found 884.5.

2-Ethoxyindene (**3**)**.** 2-ethyoxyindene was synthesized according to modified literature procedure.[11] 2-Indanone (30 g, 227 mmol) was dissolved in absolute ethanol (175 mL) and degassed with N_2. Triethylorthoformate (53 mL, 318 mmol) was added under inert gas, followed by a 4M solution of HCl in dioxane (1.7 mL, 6.8 mmol). The yellow solution was stirred at room temperature overnight, during which time it turned dark brown. Sodium methoxide (1.44 g, 27 mmol) was added to basify. Solvent was removed by distillation and the residue was distilled at 100˚C (1.4 mmHg) to afford a mixture of of 2,2-diethoxyindane (pale yellow liquid) and 2-ethoxyindene (white crystalline solid at room temperature). To this distillate was added catalytic *p*-toluenesulfonic acid (10 mg). The mixture was heated to 60˚C for 1 hr while distilling away ethanol at 1 atm. The resulting orange oil was purified by Kugelrohr distillation at 135˚C (1.4 mmHg) to afford a white crystalline solid (7.60 g, 21% yield over two steps). The purified product was stored cold under Ar to prevent decomposition. ^{1}H NMR (500 MHz, $CDCl_3$) δ 7.28 (dd, *J* = 7.3, 1.3 Hz, 1H), 7.21 (td, *J* = 7.3, 1.3 Hz, 1H), 7.16 (dd, *J* = 7.3, 1.3 Hz, 1H), 7.04 (td, *J* = 7.3, 1.3 Hz, 1H), 5.68 (s, 1H), 4.02 (q, *J* = 7.1 Hz, 3H), 3.42 (s, 2H), 1.44 (t, *J* = 7.1 Hz, 3H). ^{13}C{^{1}H} NMR (126 MHz, $CDCl_3$) δ 166.77, 145.36, 136.07, 126.69, 123.30, 122.34, 118.88, 99.39, 65.75, 37.94, 14.65. IR (ATR, solid, ν (cm^{-1})): 3070 (w), 3043 (w), 3022 (w), 2977 (m), 2935 (w), 2888 (w), 1735 (m), 1698 (m), 1595 (s), 1578 (s), 1456 (s), 1319 (s), 1150 (s), 1036 (s). EI-GCMS calculated for $C_{11}H_{12}O$ $(M)^+$ 160.09, found 160.10.

2-Formylphenyl acetic acid ethyl ester (**4**)**.** This product was synthesized according to modified literature procedure.[12] A solution of 2-ethoxyindene (1.57 g, 9.81 mmol) in dichloromethane (12 mL) and methanol (50 mL) was cooled to -30˚C. Ozone was bubbled through the cooled solution for 30 min until a faint blue color was apparent. The solution was subsequently sparged with nitrogen for 15 min to remove excess ozone. Triphenylphosphine (10.29 g, 39.23 mmol) was added as a solid. The solution temperature was maintained at -30˚C for 1 hr, then allowed to warm to room temperature slowly and stirred at room temperature overnight. Excess triphenylphosphine was removed by concentrating the solution to approximately 20 mL, then filtering away the white precipitate. This process was repeated several times until a pale yellow oil was obtained. The crude compound was purified by column chromatography (hexane then eventually 3:1 hexane:EtOAc) on silica, with the product eluting as the second spot. Solvent was removed under reduced pressure to afford the product as a white waxy solid (1.73 g, 92% yield). The purified product was stored cold under Ar to prevent decomposition. ^{1}H NMR (300 MHz, $CDCl_3$) δ 10.13 (s, 1H), 7.85 (d, *J* = 7.4 Hz, 1H), 7.67 – 7.40 (m, 2H), 7.30 (d, *J* = 7.3 Hz, 1H), 4.17 (q, *J* = 7.2 Hz, 2H), 4.04 (s,

2H), 1.26 (t, *J* = 7.1 Hz, 3H). $^{13}C\{^{1}H\}$ NMR (126 MHz, $CDCl_3$) δ 193.10, 171.13, 135.76, 134.49, 134.36, 133.86, 132.41, 128.01, 61.09, 39.24, 14.30. IR (ATR, solid, ν (cm^{-1})): 2982 (m), 2935 (w), 2906 (w), 2837 (w), 2748 (m), 1724 (vs), 1692 (vs), 1580 (m), 1412 (m), 1367 (m), 1340 (s), 1214 (s), 1201 (s), 1171 (s), 1028 (s).

5-[2-Phenylacetic acid ethyl ester]-10,15,20-triphenyl porphyrin (5). 5-phenyldipyrromethane (0.97 g, 4.38 mmol), benzaldehyde (0.20 mL, 1.96 mmol), and 2-formylphenylacetic acid ethyl ester (0.53 g, 2.74 mmol) were dissolved in chloroform (250 mL) and sparged with Ar for 15 min. Boron trifluoride etherate (0.16 mL, 1.33 mmol) was added dropwise while stirring, and the reaction proceeded at room temperature in darkness. After 1 hr, 2,3-dichloro-5,6-dicyano-1,4-benzoquinone (DDQ) (0.65 g, 2.85 mmol) was added, and the dark solution was stirred at room temperature for another 1 hr. Solvent was removed under reduced pressure, and the crude porphyrin was purified by column chromatography (starting at 3:1 hexane:DCM and slowly progressing to 1:3 hexane:DCM). The product was obtained as the second spot. A second column using the above conditions was run to remove remaining traces of tetraphenylporphyrin. The product was obtained as a purple solid (102.9 mg, 8 % yield). ^{1}H NMR (500 MHz, $CDCl_3$) δ 8.96 – 8.88 (m, 6H), 8.77 (d, *J* = 4.6 Hz, 2H), 8.33 – 8.23 (m, 6H), 8.16 (d, *J* = 7.5 Hz, 1H), 7.92 – 7.75 (m, 11H), 7.68 (t, *J* = 7.3 1H), 3.62 (q, *J* = 7.2 Hz, 2H), 3.45 (s, 2H), 0.56 (t, *J* = 7.2 Hz, 3H), -2.66 (br s, 2H). $^{13}C\{^{1}H\}$ NMR (126 MHz, $CDCl_3$) δ 171.46, 142.29, 142.14, 141.86, 136.34, 134.70, 134.60, 134.44, 129.73, 128.90, 127.88, 126.84, 126.82, 125.54, 120.58, 120.32, 117.63, 60.36, 39.85, 13.64. Λ_{max} (CH_2Cl_2) 417, 445, 514, 549, 590, 646 nm. ESI-MS calculated for $C_{48}H_{37}N_4O$ $(M+H)^+$ 701.3, found 701.9.

5-[2-Phenylacetic acid]-10,15,20-triphenyl porphyrin (6). Porphyrin **5** (82.5 mg, 0.12 mmol) was dissolved in THF (40 mL). A solution of KOH (0.33 g, 5.88 mmol) in 10 mL water was added, then the reaction was heated to reflux overnight under N_2 in the absence of light. Reaction progress was monitored by the disappearance of the comparatively non-polar methyl ester porphyrin spot by TLC. When complete, the reaction was cooled to room temperature and acidified with 1 M HCl solution, then neutralized by addition of saturated $NaHCO_3$ until the organic phase was pink. The product was extracted into DCM and washed with water, then dried over Na_2SO_4 and solvent was removed under reduced pressure. The crude porphyrin was purified by column chromatography (starting at 1:1 hexane:DCM, then 1:3 hexane:DCM and finally pure DCM) on silica. The product was obtained as the second spot as a purple solid (28 mg, 35% yield). ^{1}H NMR (500 MHz, $CDCl_3$) δ 8.87 – 8.77 (m, 4H), 8.75 (d, *J* = 4.8 Hz, 2H), 8.63 (d, *J* = 4.7 Hz, 2H), 8.23 (d, *J* = 7.2 Hz, 1H), 8.19 (d, *J* = 7.5 Hz, 1H), 8.15 – 8.10 (m, 4H), 8.05 (d, *J* = 7.5 Hz, 1H), 7.84 – 7.68 (m, 4H), 7.66 – 7.50 (m, 8H), 3.37 (s, 2H), -2.79 (br s, 2H). $^{13}C\{^{1}H\}$ NMR (126 MHz, $CDCl_3$) δ 175.36, 142.27, 142.02, 141.93, 135.48, 134.70, 134.61, 134.53, 129.51, 128.86, 127.88, 127.75, 126.81, 126.73, 125.71, 120.60, 120.33, 117.17, 39.06. Λ_{max} (CH_2Cl_2) 418, 444, 514, 549, 590, 647 nm. ESI-MS calculated for $C_{46}H_{33}N_4O_2$ $(M+H)^+$ 673.3, found 673.7.

***Ortho*-2-amide.** Porphyrin **6** (350 mg, 0.52 mmol) was dissolved in anhydrous DCM (60 mL), and freshly distilled $SOCl_2$ (56 µL, 0.78 mmol) was added under N_2, followed by one drop of anhydrous DMF. The dark green solution was stirred for 2 hr at room temperature in the absence of light. The solvent was removed under reduced pressure. Anhydrous toluene (10 mL) was added, then removed under reduced pressure to assist in removal of excess $SOCl_2$. The resulting acid chloride porphyrin was dissolved in anhydrous DCM (60 mL) and 3,5-bis(trifluoromethyl)aniline (0.41 mL, 2.60 mmol) was added. The solution was stirred for 8 hr at room temperature in the absence of light. Next, the reaction solution was poured into saturated $NaHCO_3$ solution (40 mL) to neutralize the protonated porphyrin and extracted with DCM (3x50 mL). The combined organic fractions were washed with water and dried over Na_2SO_4, and solvent was removed under reduced pressure. The product was purified by column chromatography (starting at 1:1 DCM:hexane and progressing to 5:1 DCM:hexane) on silica. The product was obtained as a purple solid

(250 mg, 45% yield). ^{1}H NMR (500 MHz, $CDCl_3$) δ 8.89 (d, *J* = 4.3 Hz, 4H), 8.82 (d, *J* = 4.8 Hz, 2H), 8.71 (d, *J* = 4.7 Hz, 2H), 8.28 (d, *J* = 7.0 Hz, 2H), 8.22 – 8.17 (m, 2H), 8.13 (d, *J* = 6.8 Hz, 2H), 8.01 (d, *J* = 7.4 Hz, 2H), 7.86 – 7.64 (m, 12H), 7.34 (s, 1H), 6.93 (s, 2H), 5.88 (s, 1H), 3.26 (s, 2H), -2.76 (br s, 2H). ^{19}F NMR (376 MHz, $CDCl_3$) δ -62.42. Λ_{max} (CH_2Cl_2) 418, 442, 515, 550, 591, 647 nm. ESI-MS calculated for $C_{54}H_{36}F_6N_5O$ $(M+H)^+$ 884.3, found 884.7.

5-[4-Nitrophenyl]-10,15,20-triphenyl porphyrin (7). Porphyrin **7** was synthesized according to literature procedure.[13] Tetraphenylporphyrin (600 mg, 0.977 mmol) was dissolved in trifluoroacetic acid (40 mL) and stirred under N_2. Sodium nitrite (120 mg, 1.740 mmol) was suspended in trifluoroacetic acid (20 mL) and added to the porphyrin solution over the course of exactly 30 seconds. After 2.5 additional min, the green solution was quenched by pouring into 300 mL cold water and extracted with DCM. The organic layer was neutralized with saturated $NaHCO_3$ solution and rinsed with water, then dried over $MgSO_4$. Solvent was removed under reduced pressure to afford crude **7**. The product was purified by column chromatography (starting at 2:1 hexane:DCM and ending at 1:1 hexane:DCM) on silica (340 mg, 53% yield). The ^{1}H NMR spectrum agrees well with the literature reports of this compound. ^{1}H NMR (400 MHz, $CDCl_3$) δ 8.83 – 8.93 (m, 6H), 8.72 – 8.76 (m, 2H), 8.64 (d, *J* = 8.6 Hz, 2H), 8.41 (d, *J* = 8.6 Hz, 2H), 8.17 – 8.25 (m, 6H), 7.73 – 7.83 (m, 9H), -2.79 (s, 2H).

5-[4-Aminophenyl]-10,15,20-triphenyl porphyrin (8). Porphyrin **7** (375 mg, 0.568 mmol) was dissolved in concentrated HCl (125 mL) and $SnCl_2{\cdot}2H_2O$ (1.537 g, 6.811 mmol) was added as a solid. The solution was heated to 65˚C for 1 h, then poured into 300 mL water and neutralized to pH 8 with ammonium hydroxide. The aqueous phase was extracted with DCM, rinsed with water, and dried over $MgSO_4$. Solvent was removed under reduced pressure to afford crude **8**. The product was purified by column chromatography (starting at 2:1 hexane:DCM and progressing slowly to 3:1 DCM:hexane and finally pure DCM) on silica, followed by recrystallization from DCM/MeOH (199 mg, 46% yield). The ^{1}H NMR spectrum agrees well with the literature reports of this compound. ^{1}H NMR (400 MHz, $CDCl_3$) δ 9.04 – 9.12 (m, 2H), 8.96 – 9.04 (m, 6H), 8.30 – 8.41 (m, 6H), 8.06 (d, *J* = 8.0 Hz, 2H), 7.77 – 7.89 (m, 9H), 6.95 (d, *J* = 7.9 Hz, 2H), 3.79 (br s, 2H), -2.55 (s, 2H). ESI-MS calculated for $C_{44}H_{32}N_5$ $(M+H)^+$ 630.3, found 630.5.

***Para*-1-amide.** A 100 mL Schlenk flask was charged with 40 mL anhydrous DCM, 3,5-bis(trifluoromethyl)phenylacetic acid (341 mg, 1.22 mmol), and a catalytic amount of anhydrous DMF (15 µL). Freshly distilled $SOCl_2$ (108 µL, 1.49 mmol) was added under a N_2 atmosphere and the solution was stirred at RT for 2 h. Solvent was removed under reduced pressure to afford a yellow oil. Anhydrous toluene (5 mL) was added, then removed under reduced pressure to assist in removal of excess $SOCl_2$. The resulting acid chloride was dissolved in anhydrous DCM (20 mL) and added dropwise to a solution of porphyrin **8** (75 mg, 0.119 mmol) dissolved in anhydrous DCM (40 mL). After reacting overnight at RT in the absence of light, the solvent was removed under reduced pressure to afford crude ***para-1*-amide**. The product was purified by column chromatography (starting at 2:1 hexane:DCM and progressing slowly to 1:3 hexane:DCM) on silica (76 mg, 72% yield). ^{1}H NMR (400 MHz, $CDCl_3$) δ 8.88 – 8.85 (m, 9H), 8.23 – 8.20 (m, 9H), 7.76 – 7.71 (m, 12H), 4.05 (s, 2H), -2.80 (br s, 2H). ^{19}F NMR (376 MHz, $CDCl_3$) δ -61.93. Λ_{max} (CH_2Cl_2) 420, 515, 550, 590, 645 nm. ESI-MS calculated for $C_{54}H_{36}F_6N_5O$ $(M+H)^+$ 884.3, found 884.9.

5-[4-Phenylacetic acid methyl ester]-10,15,20-triphenyl porphyrin (9). 5-phenyldipyrromethane (3.92 g, 17.64 mmol), benzaldehyde (0.81 mL, 8.02 mmol), and 4-formylphenylacetic acid methyl ester (2.00 g, 11.22 mmol) were dissolved in chloroform (750 mL) and sparged with Ar for 15 min. Boron trifluoride etherate (0.67 mL, 5.45 mmol) was added dropwise while stirring, and the reaction proceeded at room

temperature in darkness. After 1 hr, 2,3-dichloro-5,6-dicyano-1,4-benzoquinone (DDQ) (3.64 g, 16.04 mmol) was added, and the dark solution was stirred at room temperature for another 1 hr. Solvent was removed under reduced pressure, and the crude porphyrin was purified by column chromatography (starting at 3:1 hexane:DCM and progressing slowly to 1:3 hexane:DCM) on silica and was obtained as a purple solid (1.0 g, 18% yield). ^{1}H NMR (400 MHz, $CDCl_3$) δ 8.88 – 8.85 (m, 8H), 8.24 – 8.17 (m, 8H), 7.77 – 7.72 (m, 9H), 7.68 (d, 2H, *J* = 8.0 Hz) 3.99 (s, 2H), 3.89 (s, 3H), -2.78 (br s, 2H). ESI-MS calculated for $C_{47}H_{34}N_4O_2$ $(M+H)^+$ 687.3, found 687.7.

2-(4-(10,15,20-Triphenylporphyrin-5-yl)phenyl)acetic acid (10). Porphyrin **9** (82.5 mg, 0.12 mmol) was dissolved in THF (40 mL). A solution of KOH (0.33 g, 5.88 mmol) in 10 mL water was added, then the reaction was heated to reflux overnight under N_2 in the absence of light. Reaction progress was monitored by the disappearance of the comparatively non-polar methyl ester porphyrin spot by TLC. When complete, the reaction was cooled to room temperature and acidified with 1 M HCl solution, then neutralized by addition of saturated $NaHCO_3$ until the organic phase was pink. The product was extracted into DCM and washed with water, then dried over Na_2SO_4 and solvent was removed under reduced pressure. The crude porphyrin was purified by column chromatography (starting at 1:1 hexane:DCM, then 1:3 hexane:DCM, then pure DCM, and finally 2% MeOH and DCM) on silica. The product was obtained as the second band as a purple solid (73 mg, 90% yield). ^{1}H NMR (400 MHz, $CDCl_3$) δ 8.92 – 8.89 (m, 8H), 8.27 – 8.25 (m, 8H), 7.80 – 7.75 (m, 11H), 4.09 (s, 2H), -2.74 (br s, 2H). $^{13}C\{^1H\}$ NMR (126 MHz, $CDCl_3$) δ 174.63, 142.04, 141.02, 134.72, 134.54, 133.35, 127.84, 127.74, 126.73, 120.26, 120.23, 119.67, 40.42. Λ_{max} (CH_2Cl_2) 420, 515, 550, 590, 645 nm. ESI-MS calculated for $C_{46}H_{32}N_4O_2$ $(M+H)^+$ 673.3, found 673.7.

***Para*-2-amide.** Porphyrin **10** (400 mg, 0.594 mmol) was dissolved in anhydrous DCM (300 mL), and freshly distilled thionyl chloride (0.144 mL, 1.98 mmol) was added under N_2, followed by one drop of anhydrous DMF. The dark green solution was stirred for 2 hr at room temperature in the absence of light. The solvent was removed under reduced pressure. Anhydrous toluene (5 mL) was added, then removed under reduced pressure to assist in removal of excess $SOCl_2$. The resulting acid chloride porphyrin was dissolved in anhydrous THF (250 mL) and 3,5-bis(trifluoromethyl)aniline (0.464 mL, 2.97 mmol) was added. The solution was stirred for 8 hr at room temperature in the absence of light. Next, the reaction solution was poured into saturated $NaHCO_3$ solution (20 mL) to neutralize the protonated porphyrin and extracted with DCM (3x25 mL). The combined organic fractions were washed with water and dried over Na_2SO_4, and solvent was removed under reduced pressure. The product was purified by column chromatography (starting at 1:1 DCM:hexane and progressing to 5:1 DCM:hexane) on silica. The product was obtained as a purple solid (278 mg, 53% yield). ^{1}H NMR (400 MHz, CD_2Cl_2) δ 8.88 (d, 8H, *J* = 5.7 Hz), 8.28 – 8.20 (m, 10H), 7.80 – 7.75 (m, 12H), 7.70 (s, 1H), 4.10 (s, 12H), -2.84 (br s, 2H).). ^{19}F NMR (376 MHz, CD_2Cl_2) δ -62.51. Λ_{max} (CH_2Cl_2) 420, 515, 545, 590, 645 nm. ESI-MS calculated for $C_{54}H_{36}F_6N_5O$ $(M+H)^+$ 884.3, found 884.6.

***para*-$(CF_3)_4$.** 4-Trifluoromethylbenzaldehyde (7.7 mL, 57.43 mmol) and pyrrole (4.0 mL, 57.43 mmol) were dissolved in 250 mL propionic acid and heated to 110˚C in darkness for 1 h. Water (50 mL) and methanol (250 mL) was added to precipitate the porphyrin product, which was filtered and washed with water and methanol. The crude product was purified by column chromatography (2:1 hexane:DCM) on silica and was isolated as a purple powder (2.11 g, 18% yield). ^{1}H NMR (400 MHz, $CDCl_3$) δ 8.83 (s, 8H), 8.35 (d, *J* = 7.8 Hz, 8H), 8.06 (d, *J* = 7.8 Hz, 8H), -2.84 (s, 2H). ^{19}F NMR (376 MHz, $CDCl_3$) δ -61.27. ESI-MS calculated for $C_{48}H_{27}F_{12}N_4$ $(M+H)^+$ 887.2, found 887.1.

General procedure for synthesis of Fe porphyrins. Metallation of porphyrins was performed in a N_2-filled glovebox or using standard Schlenk techniques and dry solvents. To a solution of the free-base porphyrin (1 eq) in dry THF was added anhydrous $FeBr_2$ (15 eq) as a suspension in dry THF. Distilled lutidine (3 eq) was added and the solution was heated to 65˚C overnight in the absence of light. The resulting solution was opened to air and then neutralized by pouring into 1 M HBr. After extraction into EtOAc and rinsing with copious water, the organic phase was dried over MgSO4 and the solvent was removed under reduced pressure. The crude complex was purified according to the conditions specified below.

[Fe-*ortho*-1-amide]Br. Metallation was performed as described above using 100 mg of ***ortho*-1-amide**. Purification was achieved by column chromatography (5:1 DCM:hexane then progressing to pure DCM and slowly to 2% MeOH in DCM) on silica (94 mg, 82% yield). Λ_{max} (CH_2Cl_2) 380, 417, 514 nm. ESI-MS calculated for $C_{54}H_{33}F_6FeN_5O$ $(M)^+$ 937.2, found 937.3; $C_{55}H_{37}F_6FeN_6O_2$ $(M+MeOH)^+$ 969.2, found 969.4.

[Fe-*ortho*-2-amide]Br. Metallation was performed as described above using 100 mg of ***ortho*-2-amide**. Purification was achieved by column chromatography (1:1 THF:hexane) on silica (59 mg, 51% yield). Λ_{max} (CH_2Cl_2) 383, 414, 510 nm. ESI-MS calculated for $C_{54}H_{33}F_6FeN_5O$ $(M)^+$ 937.2, found 937.7; $C_{55}H_{37}F_6FeN_5O_2$ $(M+MeOH)^+$ 969.2, found 969.7.

[Fe-*para*-1-amide]Br. Metallation was performed as described above using 97 mg of ***para*-1-amide**. Purification was achieved by column chromatography (pure DCM then progressing slowly to 6% MeOH in DCM) on silica (86 mg, 84% yield). Λ_{max} (CH_2Cl_2) 384, 415, 515, 580, and 680 nm. ESI-MS calculated for $C_{54}H_{33}F_6FeN_5O$ $(M+MeOH)^+$ 969.2, found 970.1.

[Fe-*para*-2-amide]Br. Metallation was performed as described above using 140 mg of ***para*-2-amide**. Purification was achieved by column chromatography (pure DCM then progressing slowly to 4% MeOH in DCM) on silica (110 mg, 74% yield). Λ_{max} (CH_2Cl_2) 410, 570, 610 nm. ESI-MS calculated for $C_{54}H_{36}F_6FeN_6O_2$ $(M+MeOH)^+$ 969.2, found 970.4.

Fe-*para*-$(CF_3)_4$. Metallation was performed as described above using 740 mg of ***para*-$(CF_3)_4$**. Purification was achieved by column chromatography (pure DCM then progressing slowly to 2% MeOH in DCM) on silica (480 mg, 61% yield). ESI-MS calculated for $C_{49}H_{28}F_{12}FeN_4O$ $(M+MeOH)^+$ 972.1, found 972.6.

Zn-*ortho*-1-amide. Porphyrin ***ortho*-1-amide** (31 mg, 0.035 mmol) was dissolved in chloroform (6 mL) and sparged with N_2 for 5 min. A solution of $Zn(OAc)_2$ (16 mg, 0.088 mmol) in methanol (1 mL) was added dropwise. The resulting solution was stirred at RT overnight in the absence of light. The organic phase was washed with saturated $NaHCO_3$ three times followed by water three times, then dried over $MgSO_4$. The product was purified by recrystallization *via* vapor diffusion of water into a solution of DMF (29 mg, 87% yield). X-ray quality crystals were grown by slow vapor diffusion of water into a solution of **Zn-*ortho*-1-amide** in DMF. ^{1}H NMR (500 MHz, $CDCl_3$) δ 8.95 – 8.86 (m, 6H), 8.82 (d, *J* = 4.7 Hz, 2H), 8.55 (d, *J* = 8.5 Hz, 1H), 8.26 – 8.04 (m, 6H), 7.94 (d, *J* = 7.4 Hz, 1H), 7.83 – 7.63 (m, 11H), 7.41 (t, *J* = 7.4 Hz, 1H), 7.28 (s, 2H), 7.18 (s, 1H), 7.16 (br s, 1H). $^{13}C\{^1H\}$ NMR (126 MHz, $CDCl_3$) δ 152.55, 150.37, 150.33, 150.26, 150.03, 142.98, 142.84, 140.88, 139.52, 134.82, 134.72 (d, *J* = 4.2 Hz), 134.43, 132.75, 132.08, 132.01, 131.93, 131.71, 131.44, 131.40, 129.25, 127.62, 126.73, 126.61, 126.56, 123.15 (q, *J* = 272.6 Hz), 121.51, 121.47, 121.09, 119.82, 117.46, 114.96 – 114.44 (m). ^{19}F NMR (376 MHz, $CDCl_3$) δ -62.47. Λ_{max} (CH_2Cl_2) 419, 548. ESI-MS calculated for $C_{53}H_{32}F_6N_6OZn$ $(M)^+$ 946.2, found 946.8.

NMR Spectra of Novel Compounds

^{1}H-NMR of [3,5-bis(trifluoromethyl)phenyl]amide in CD_3CN:

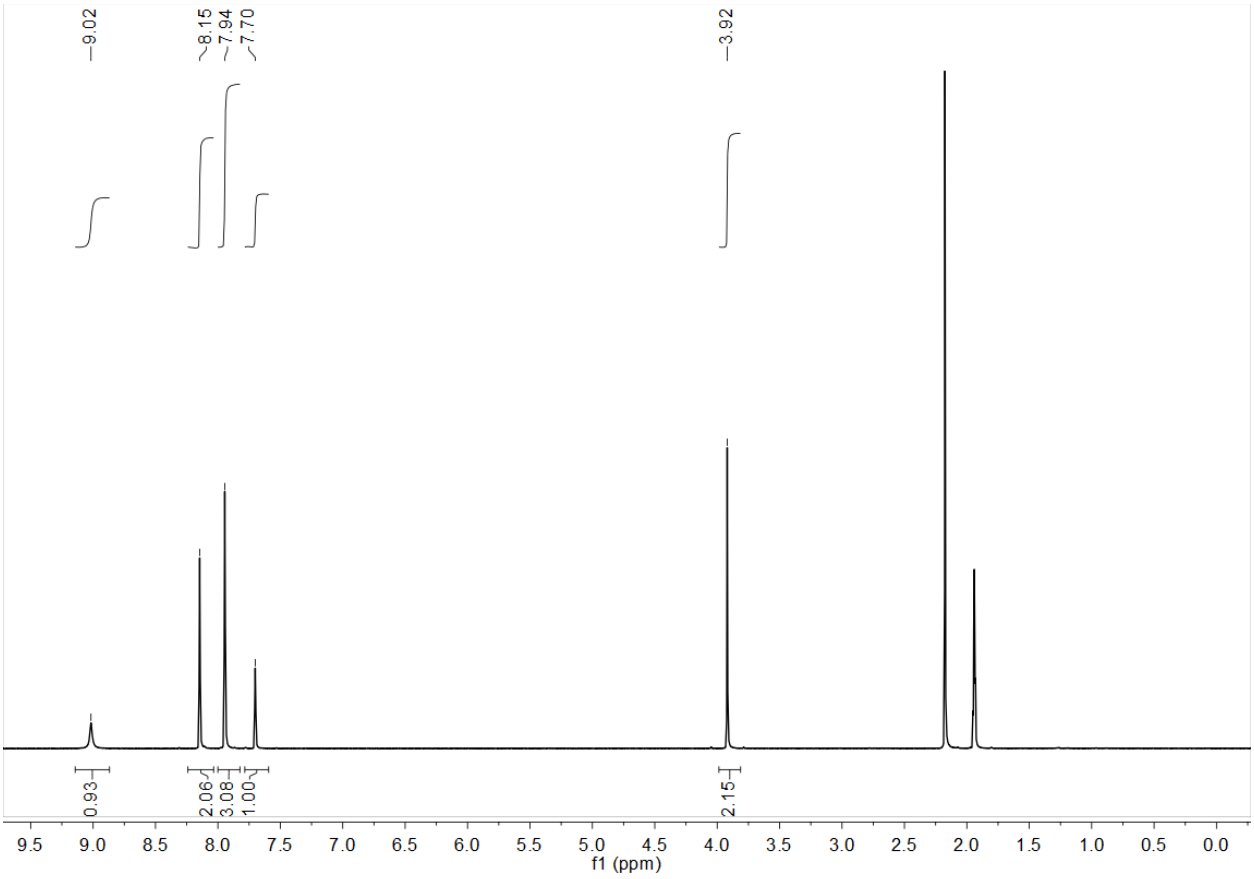

^{13}C-NMR of [3,5-bis(trifluoromethyl)phenyl]amide in CD_3CN:

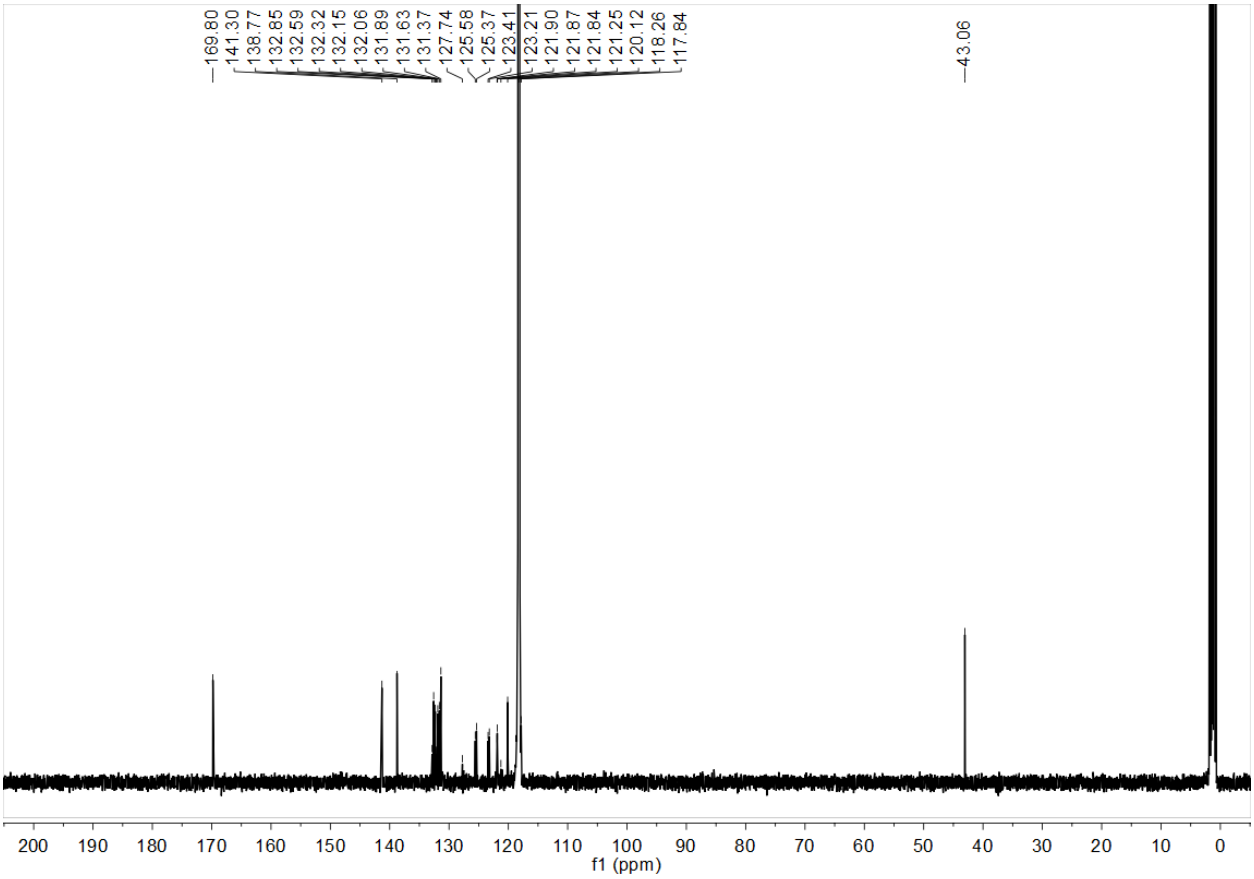

^{19}F-NMR of [3,5-bis(trifluoromethyl)phenyl]amide in CD_3CN:

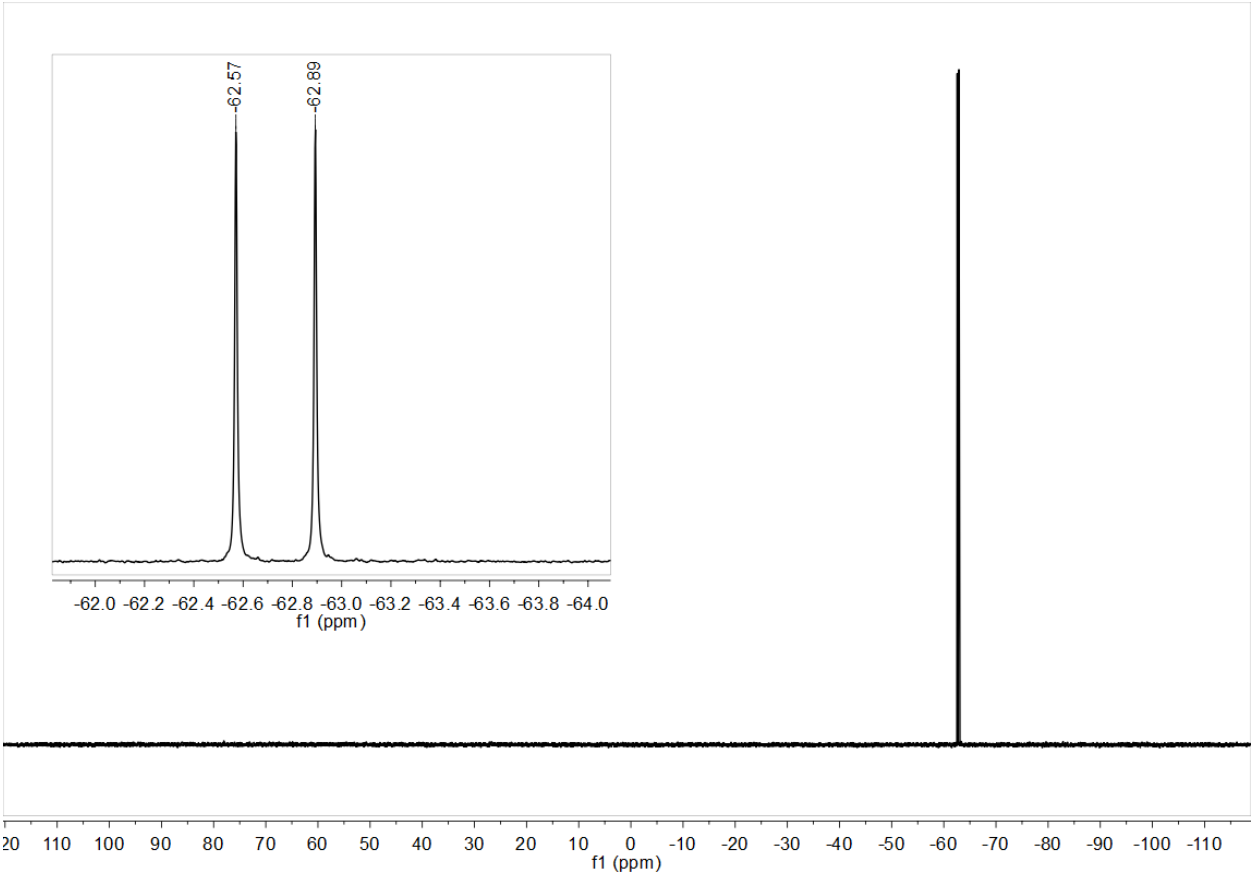

^{1}H-NMR of ***ortho*-1-amide** in CD_2Cl_2:

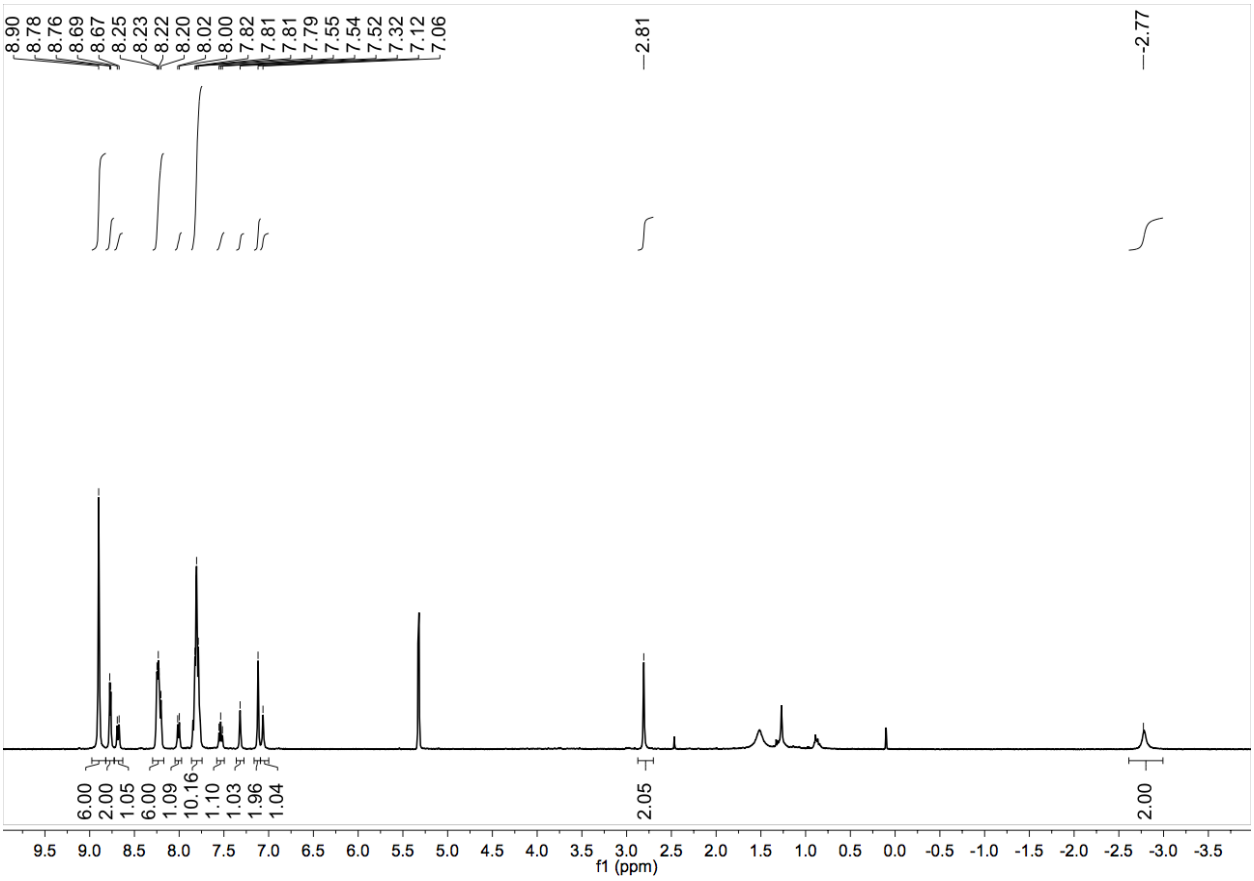

^{13}C-NMR of ***ortho*-1-amide** in CD_2Cl_2:

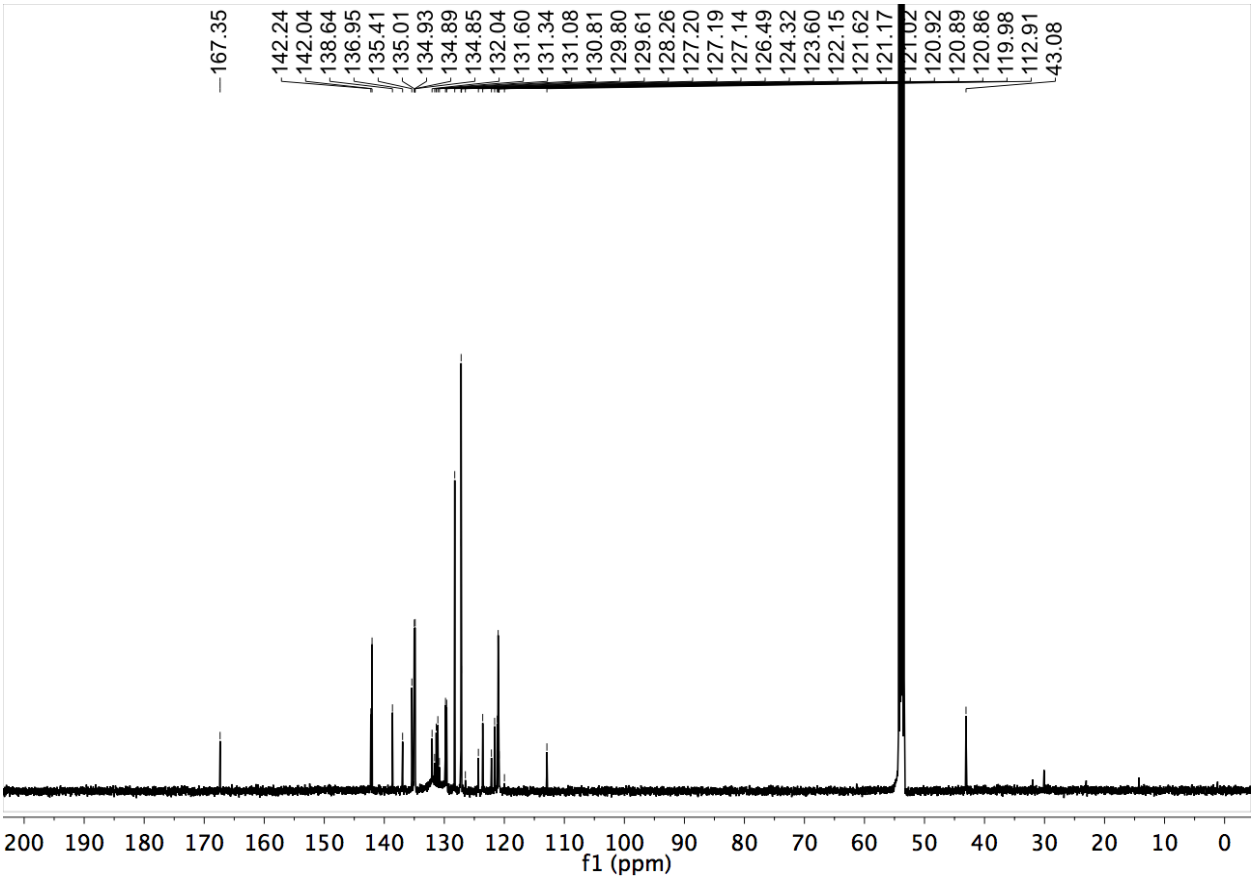

^{19}F-NMR of ***ortho*-1-amide** in CD_2Cl_2:

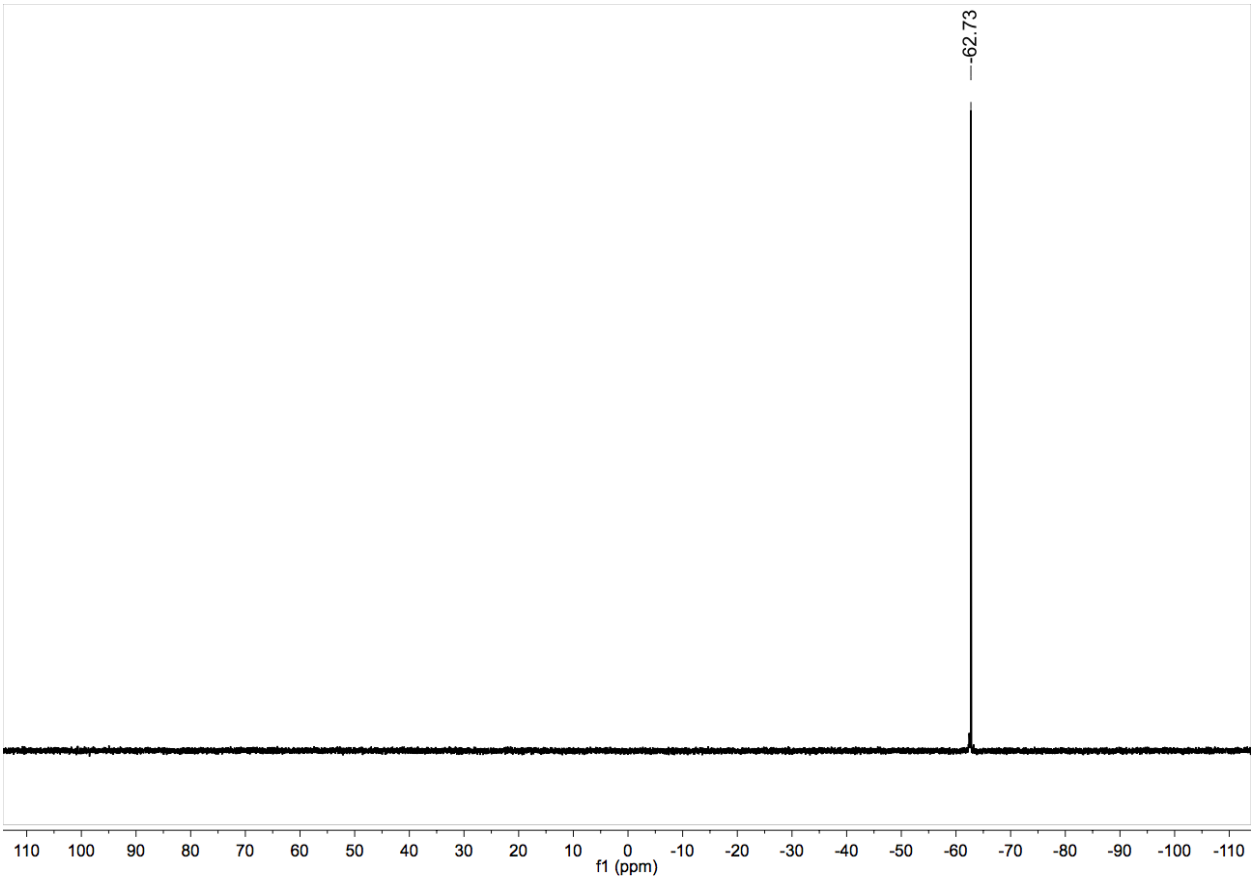

^{1}H-NMR of **2-ethoxyindene** (**3**) in $CDCl_3$:

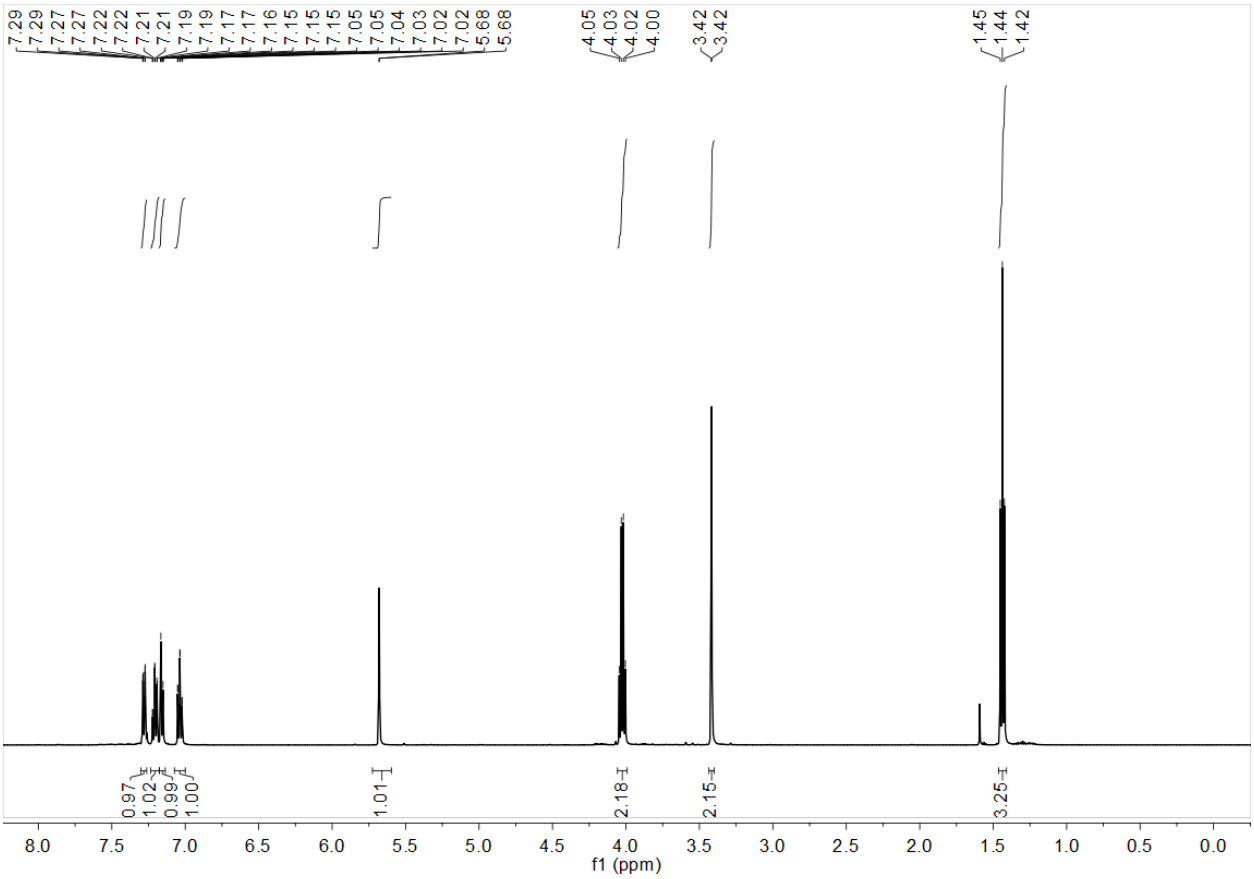

^{13}C-NMR of **2-ethoxyindene** (**3**) in $CDCl_3$:

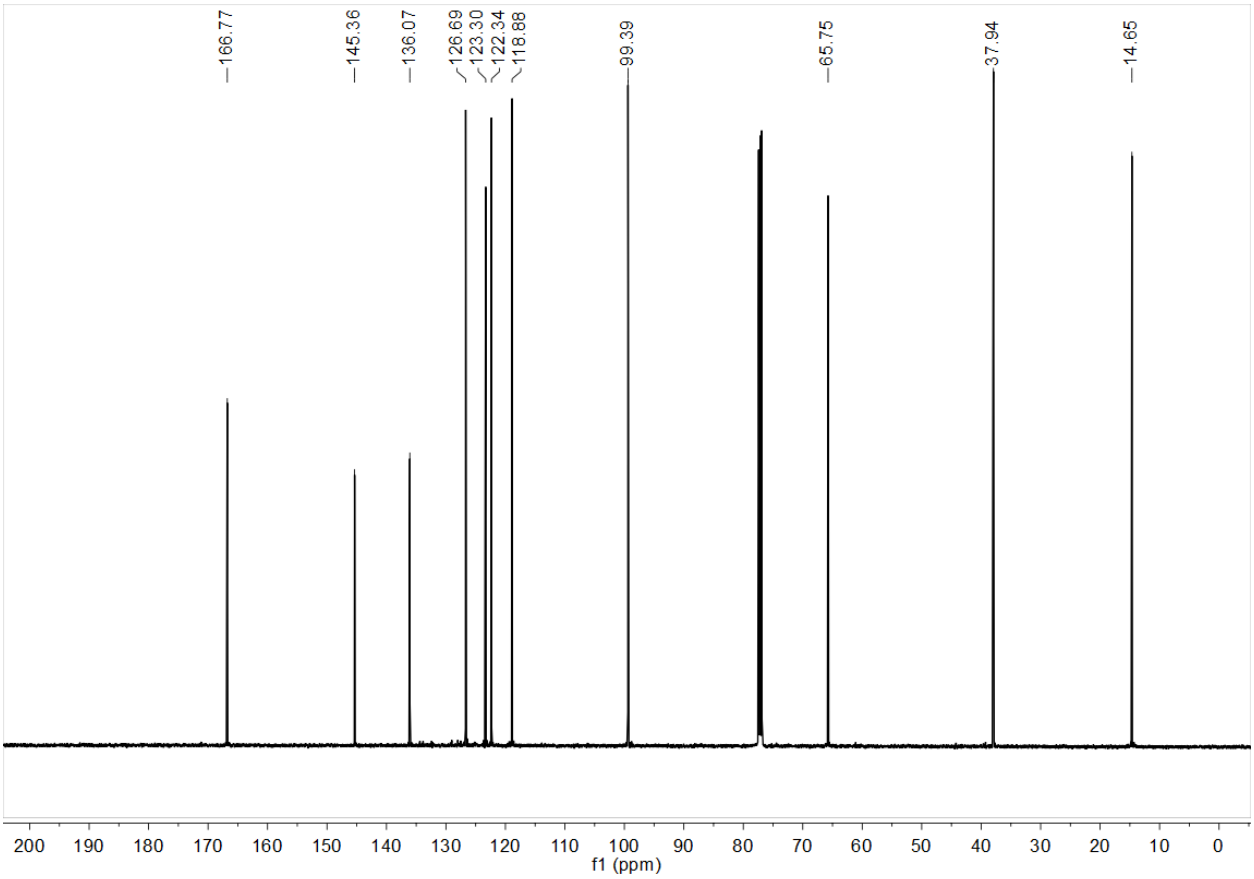

^{1}H-NMR of **2-formylphenylacetic acid ethyl ester** (**4**) in $CDCl_3$:

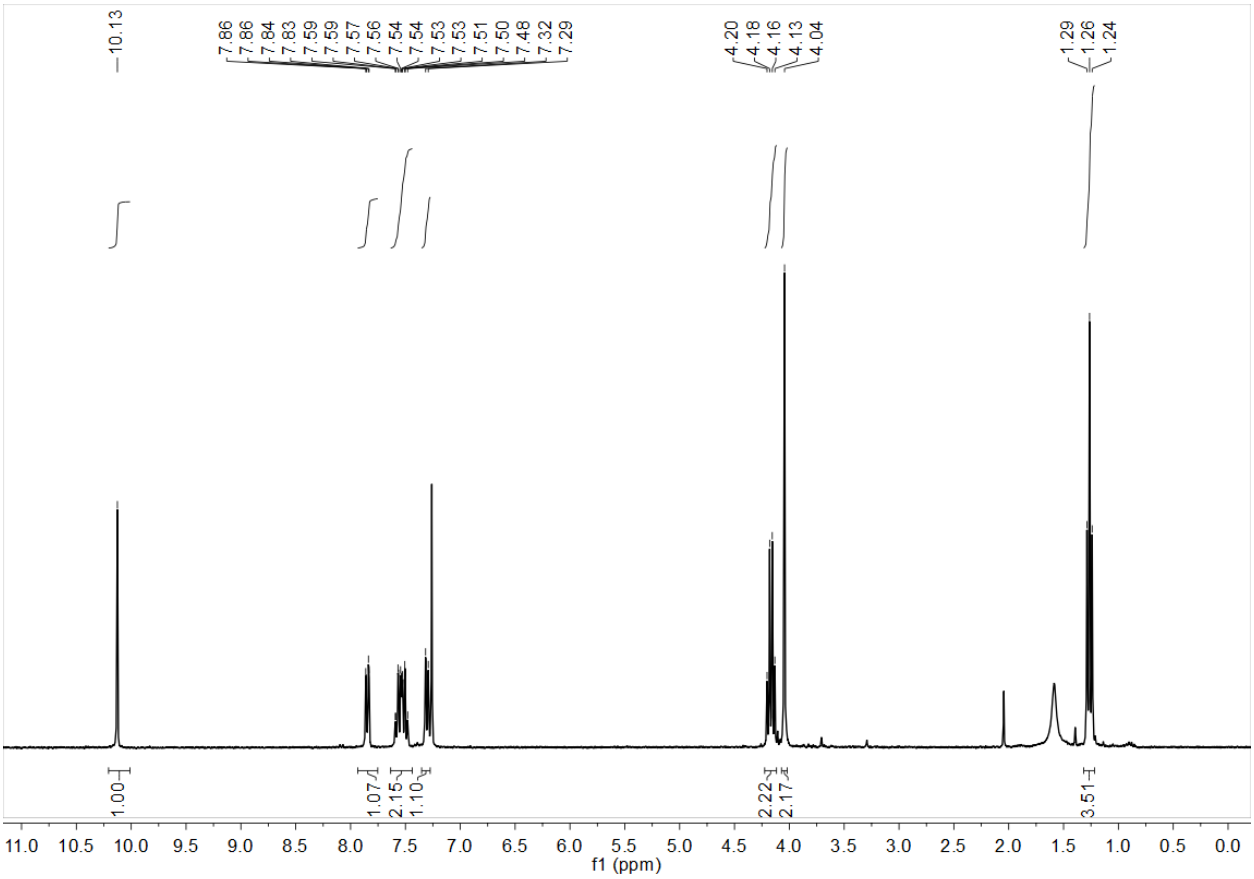

^{13}C-NMR of **2-formylphenylacetic acid ethyl ester** (**4**) in $CDCl_3$:

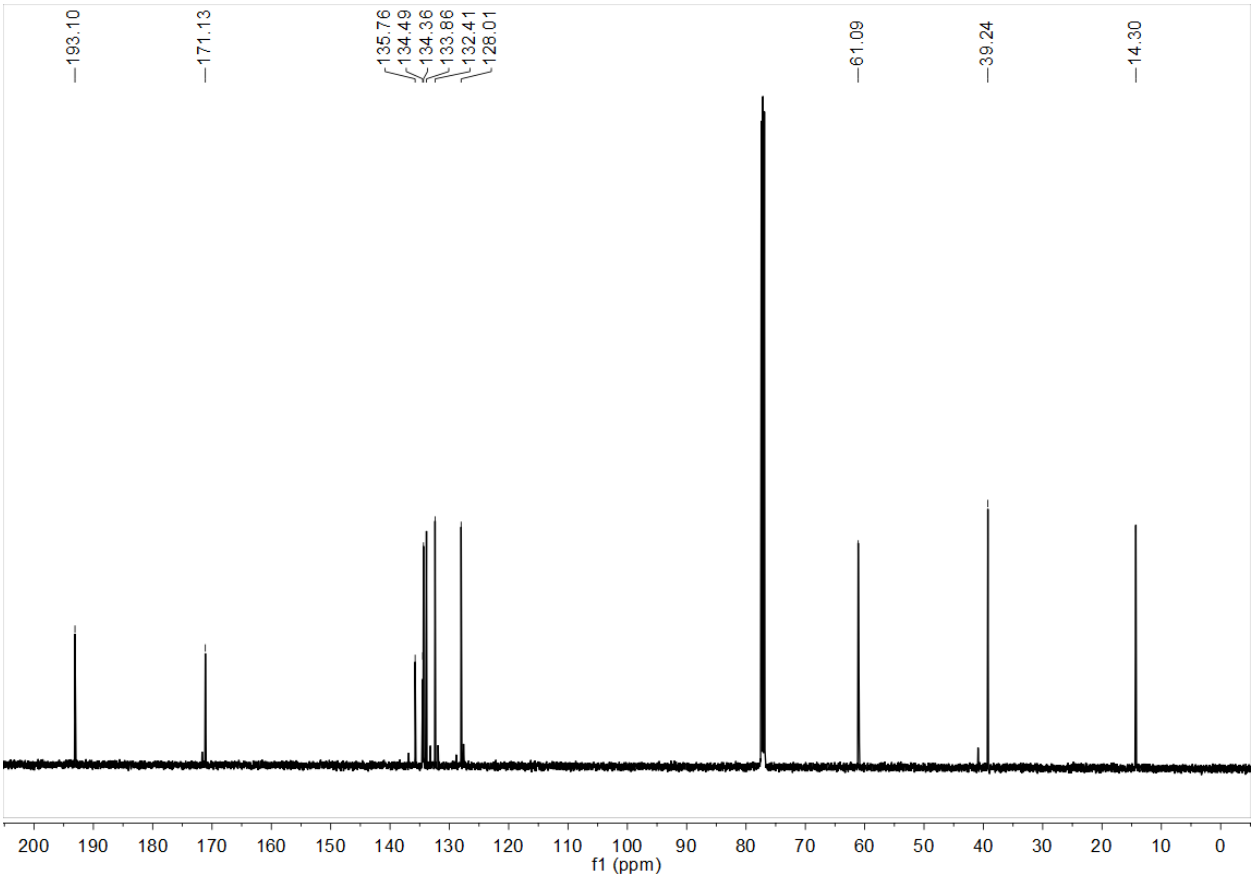

^{1}H-NMR of **5-[phenylacetic acid methyl ester]-10,15,20-triphenyl porphyrin (5)** in $CDCl_3$:

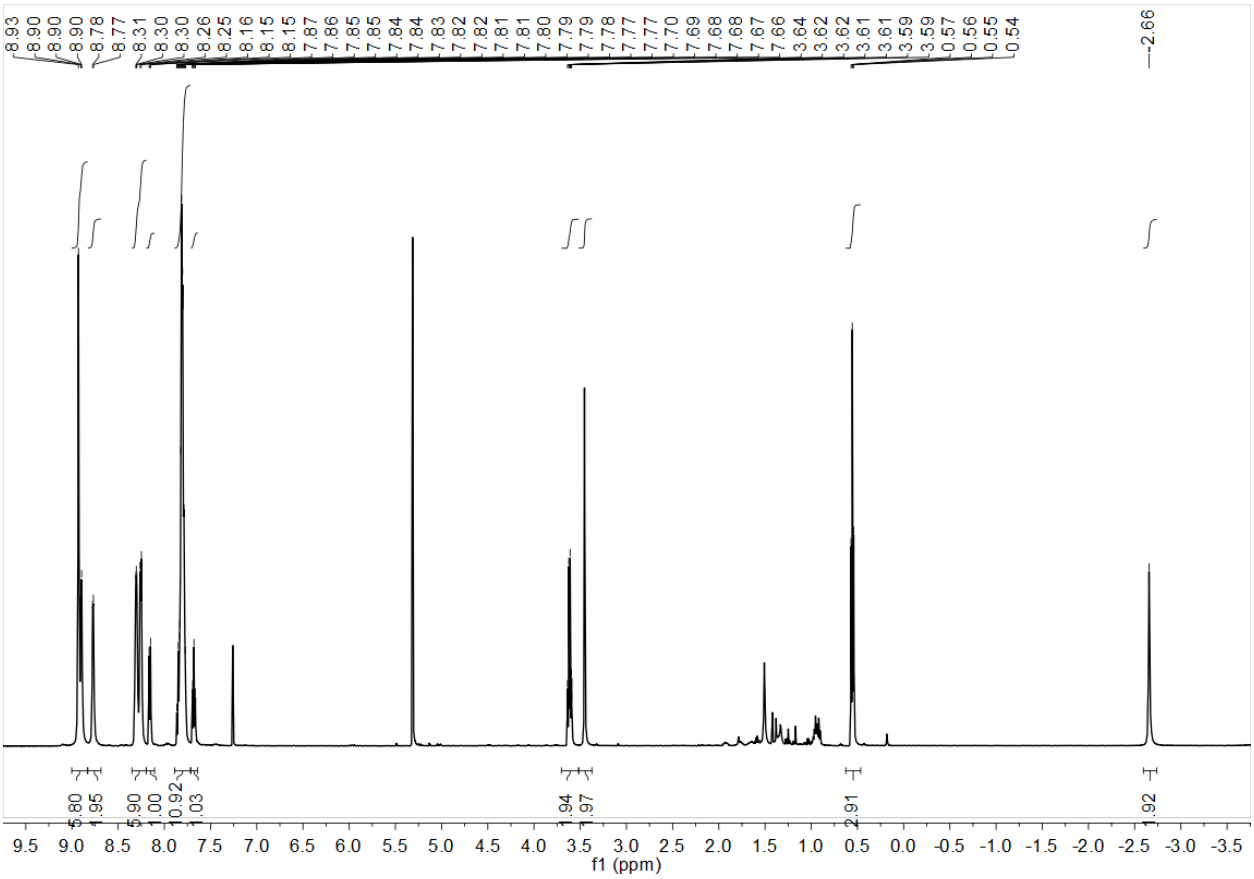

^{13}C-NMR of **5-[phenylacetic acid methyl ester]-10,15,20-triphenyl porphyrin (5)** in $CDCl_3$:

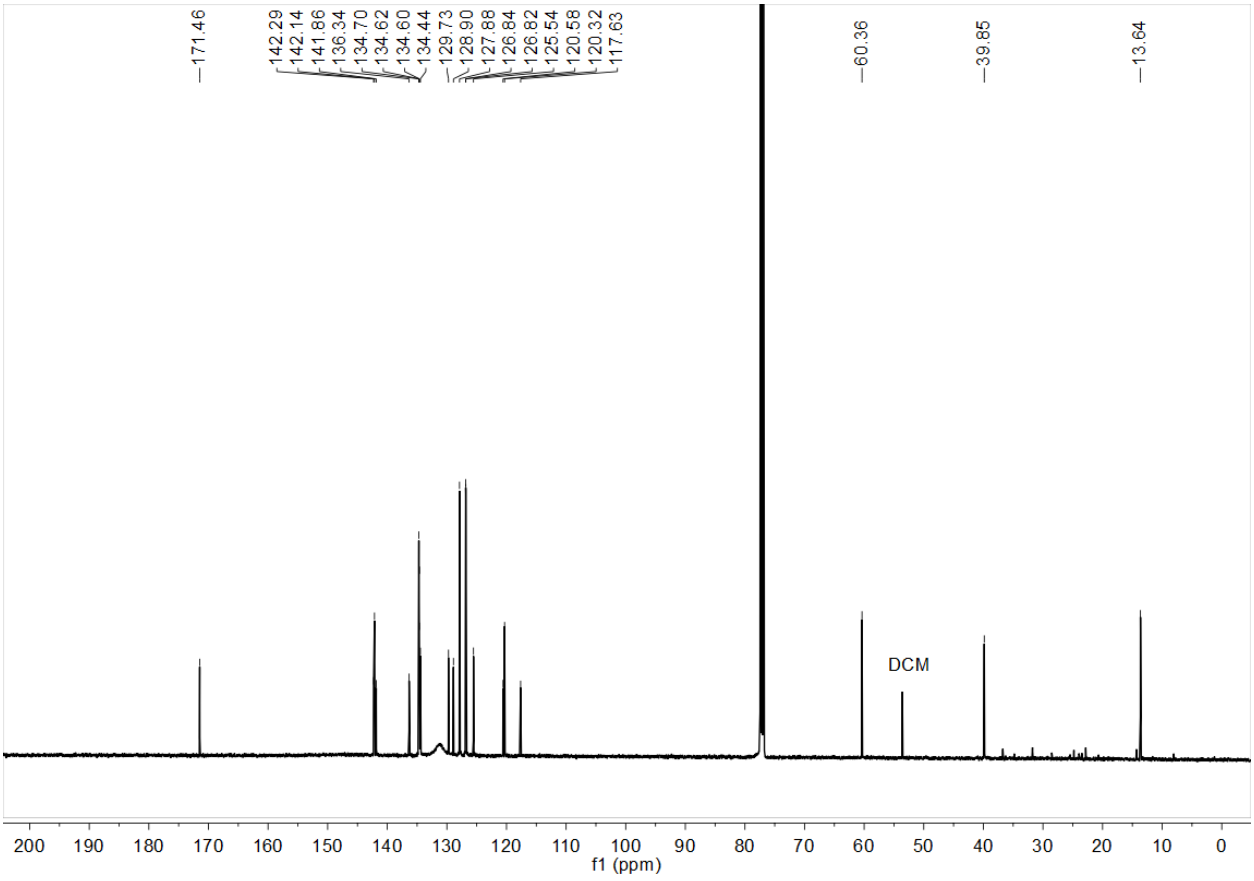

^{1}H-NMR of **5-[phenylacetic acid]-10,15,20-triphenyl porphyrin (6)** in $CDCl_3$:

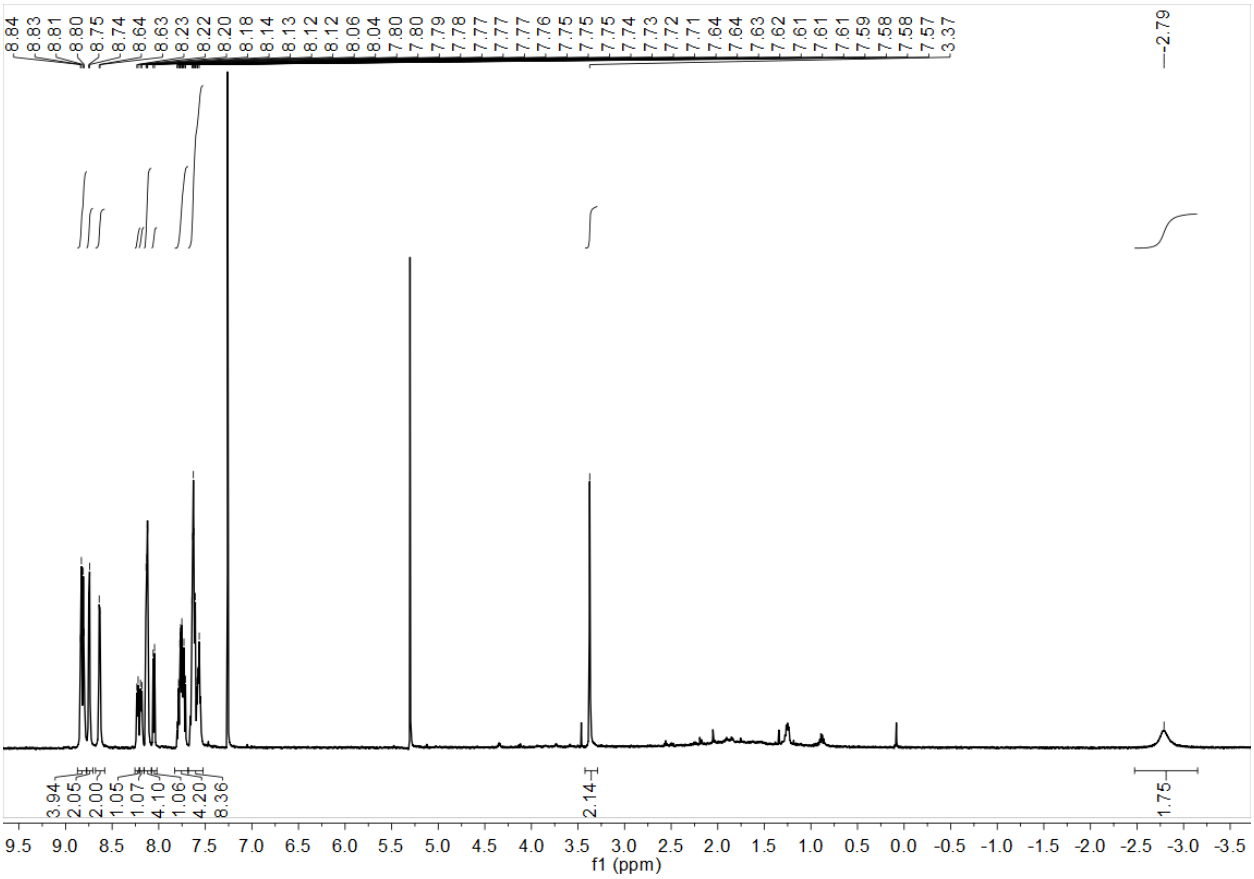

^{13}C-NMR of **5-[phenylacetic acid]-10,15,20-triphenyl porphyrin (6)** in $CDCl_3$:

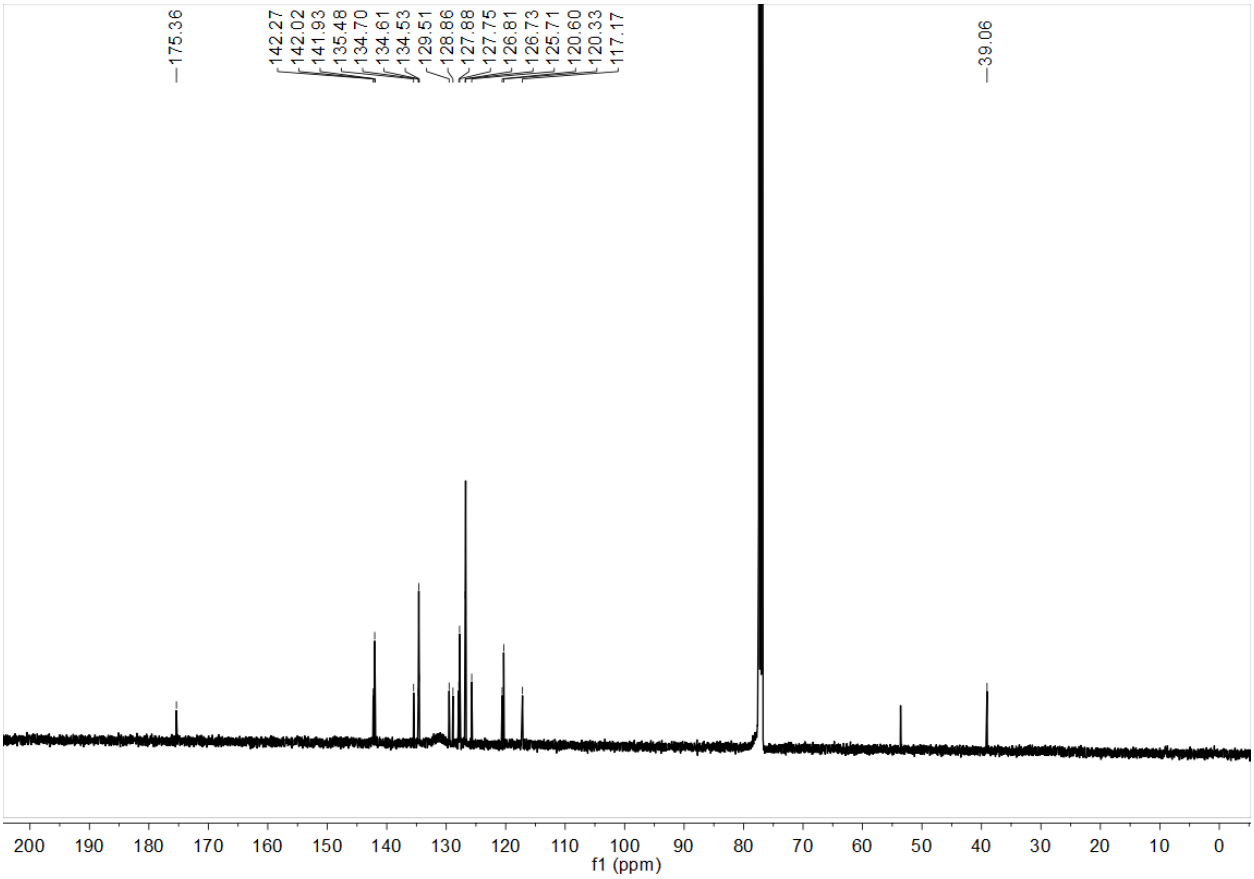

^{1}H-NMR of ***ortho*-2-amide** in $CDCl_3$:

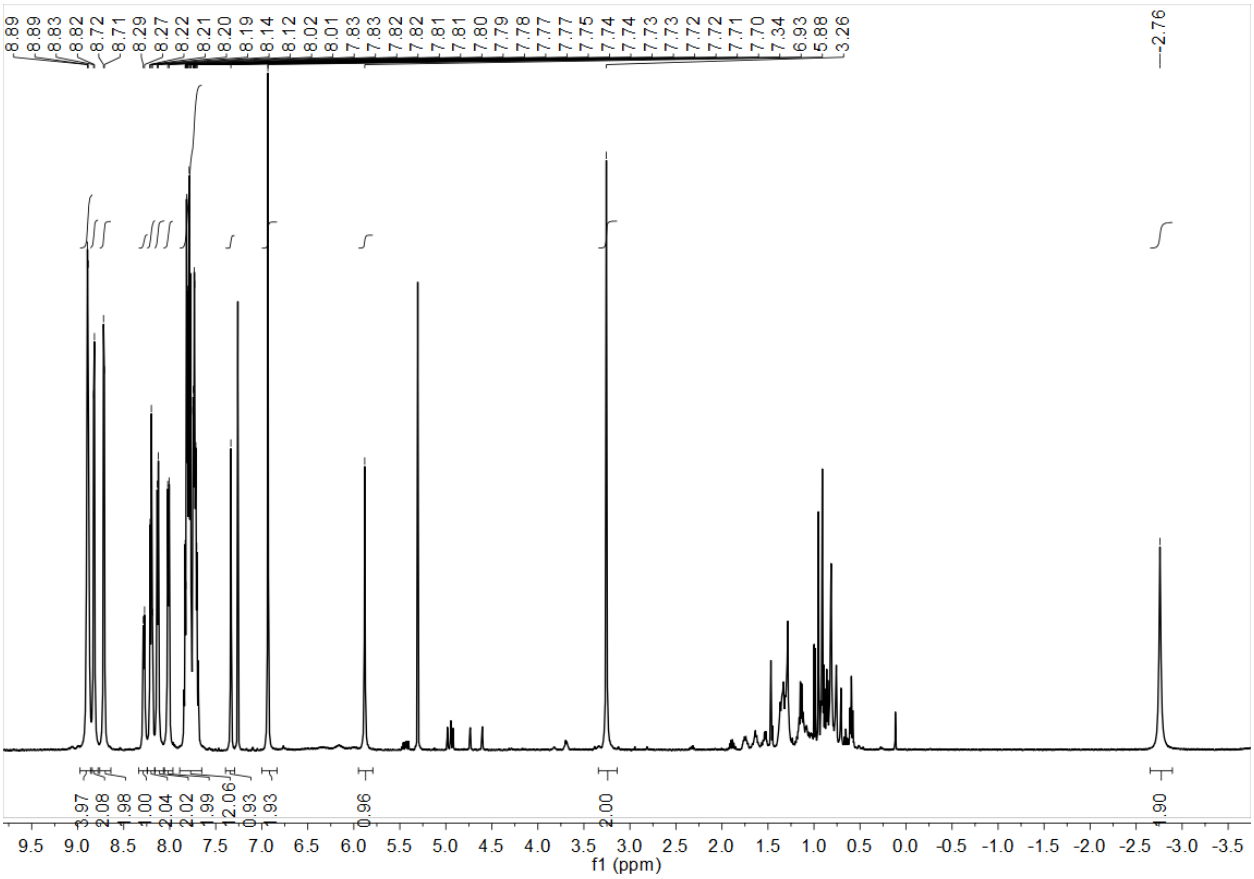

^{19}F-NMR of ***ortho*-2-amide** in $CDCl_3$:

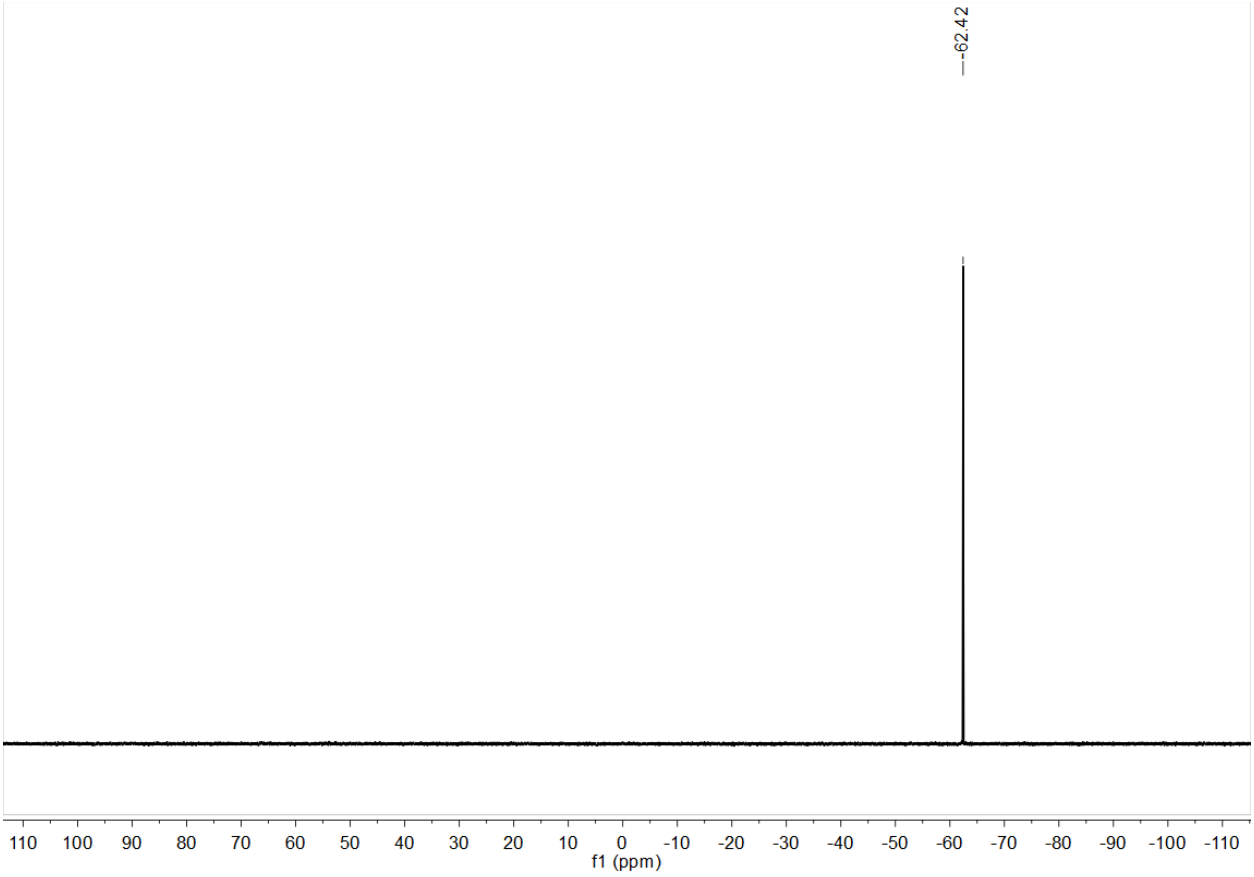

^{1}H-NMR of ***para*-1-amide** in $CDCl_3$:

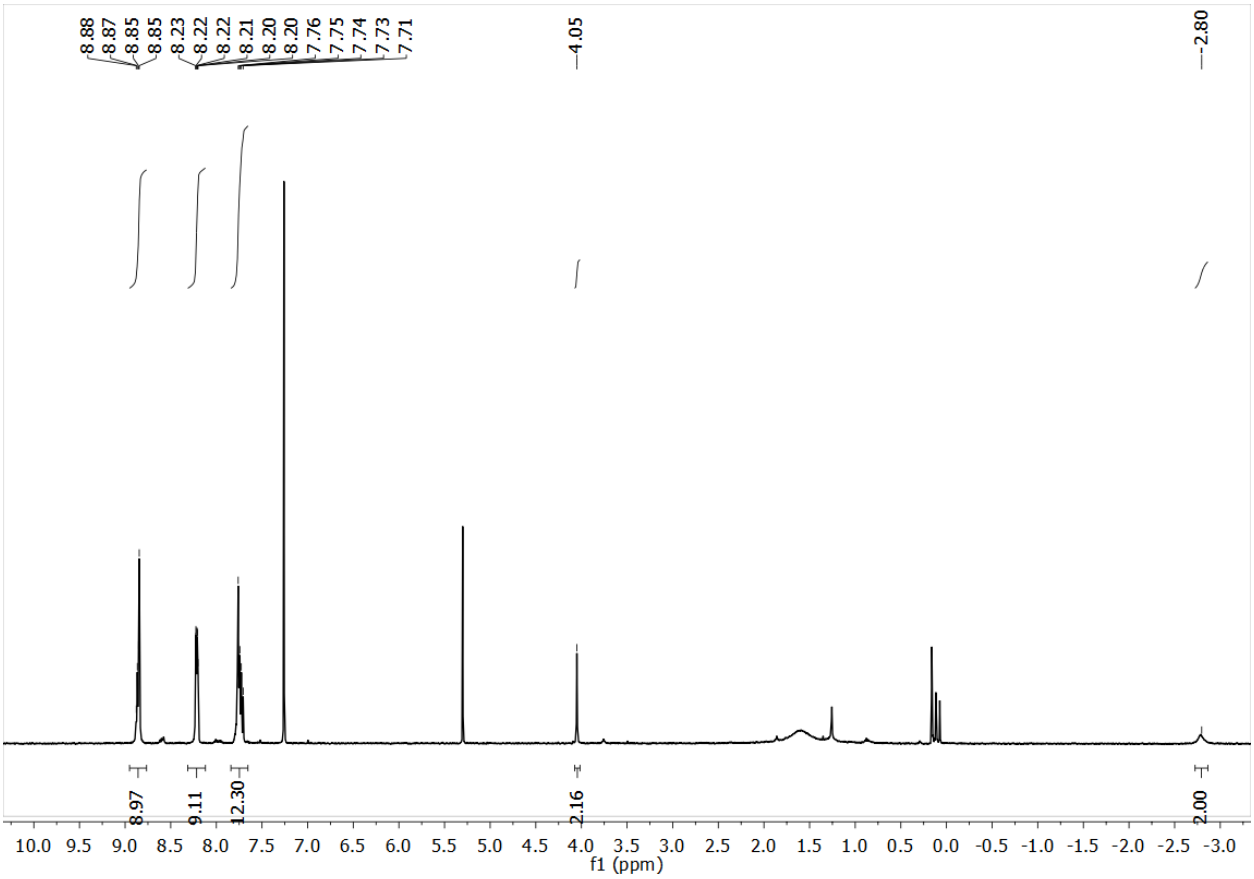

^{19}F-NMR of ***para*-1-amide** in $CDCl_3$:

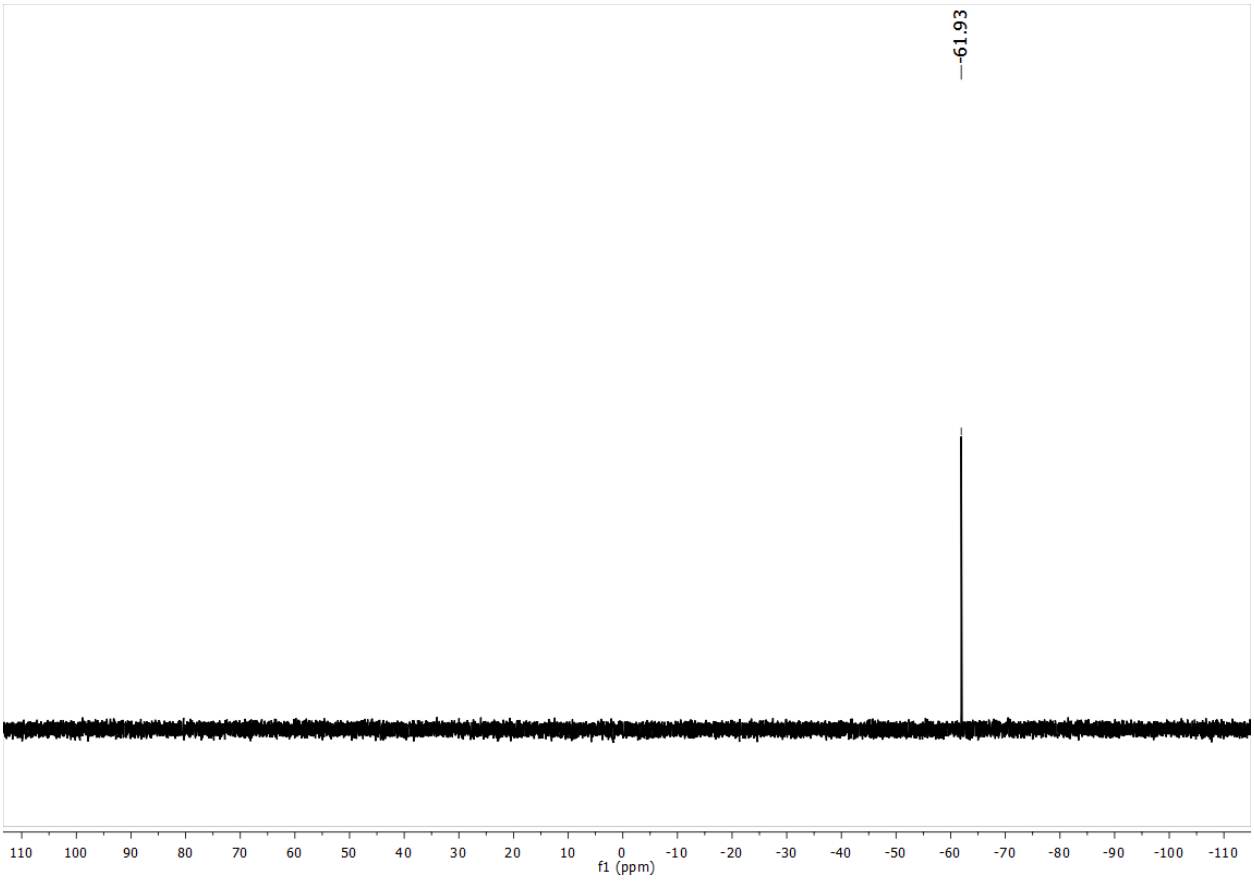

^{1}H-NMR of **Ethyl 2-(4-(10,15,20-triphenylporphyrin-5-yl)phenyl)acetate (9)** in $CDCl_3$:

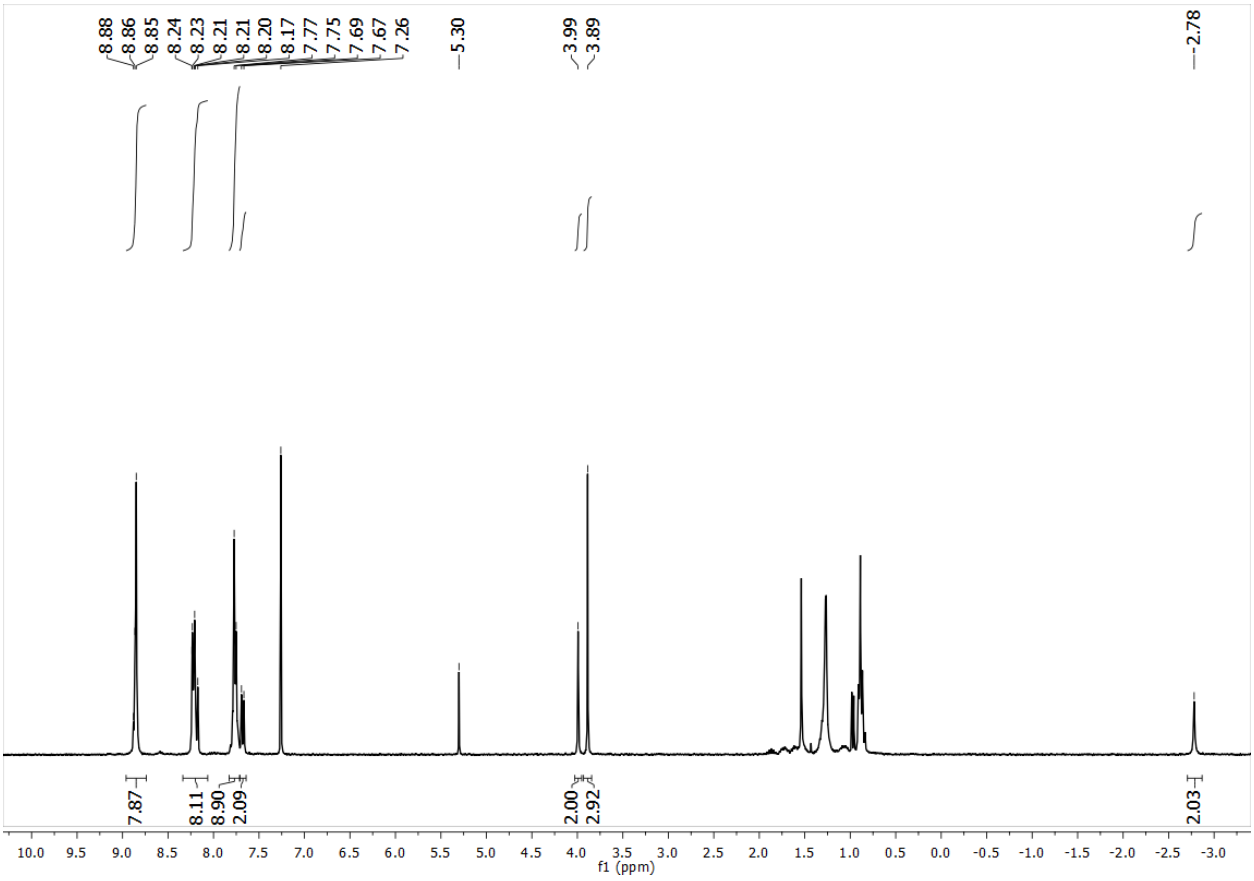

^{1}H-NMR of **2-(4-(10,15,20-Triphenylporphyrin-5-yl)phenyl)acetic acid (10)** in $CDCl_3$:

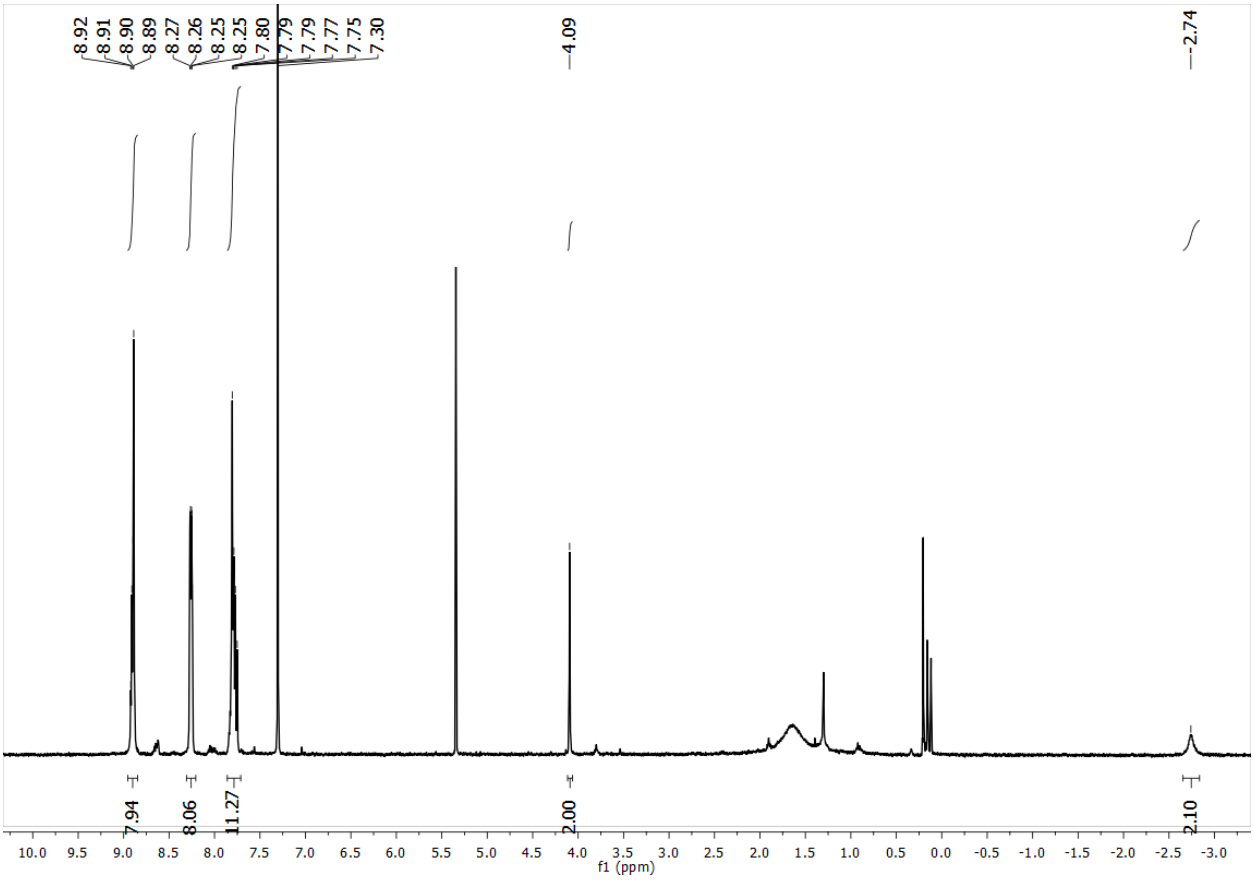

^{13}C-NMR of **2-(4-(10,15,20-Triphenylporphyrin-5-yl)phenyl)acetic acid (10)** in $CDCl_3$:

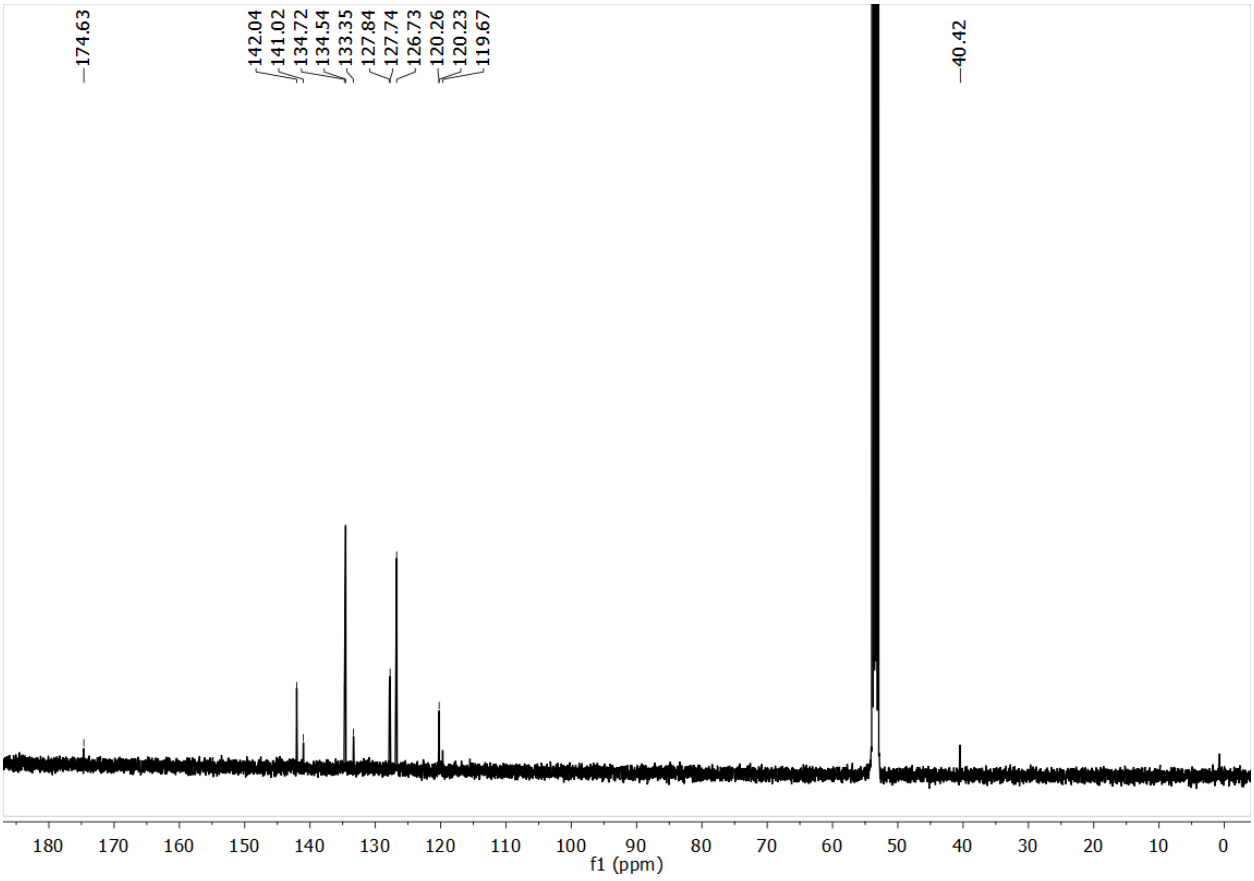

^{1}H-NMR of ***para*-2-amide** CD_2Cl_2:

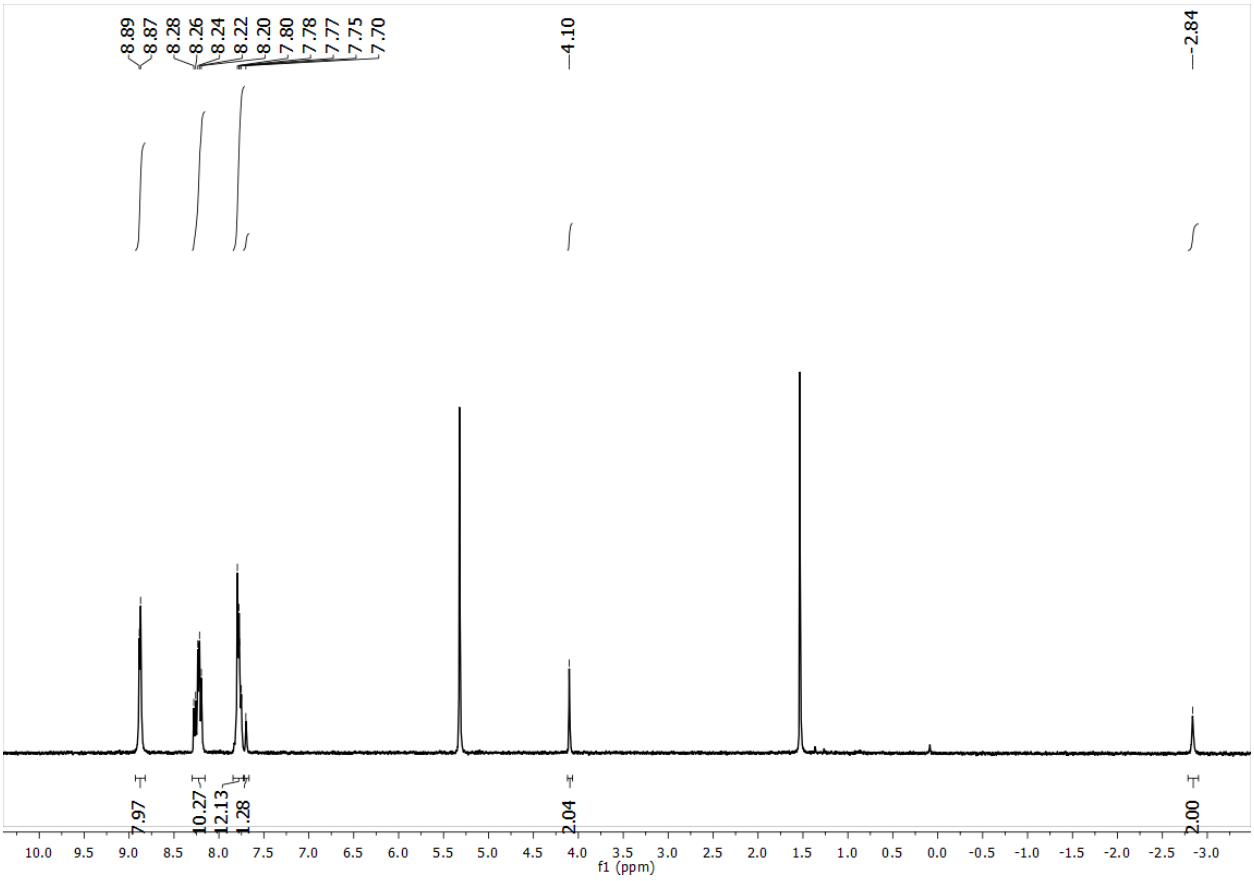

^{19}F-NMR of ***para*-2-amide** CD_2Cl_2:

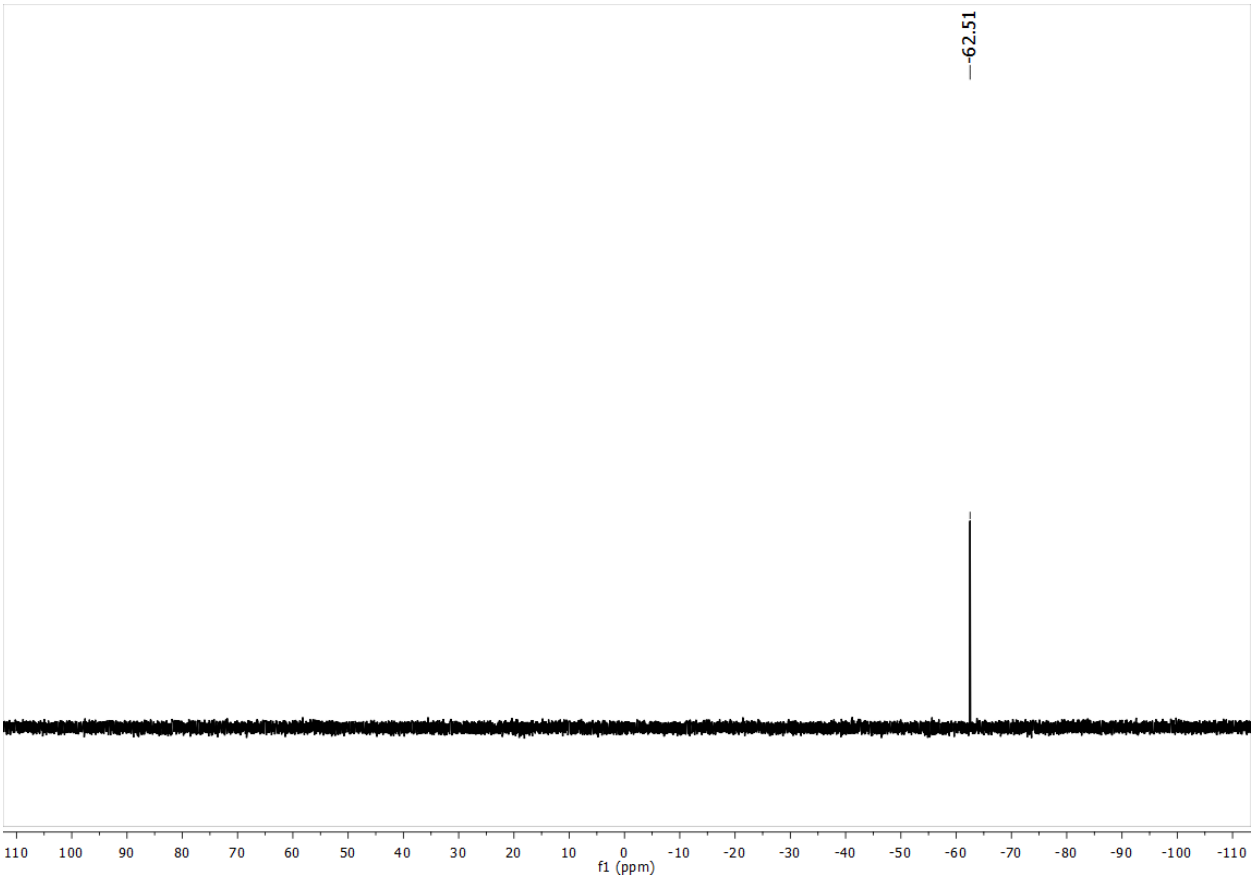

^{1}H-NMR of **Zn-*ortho*-1-amide** in $CDCl_3$:

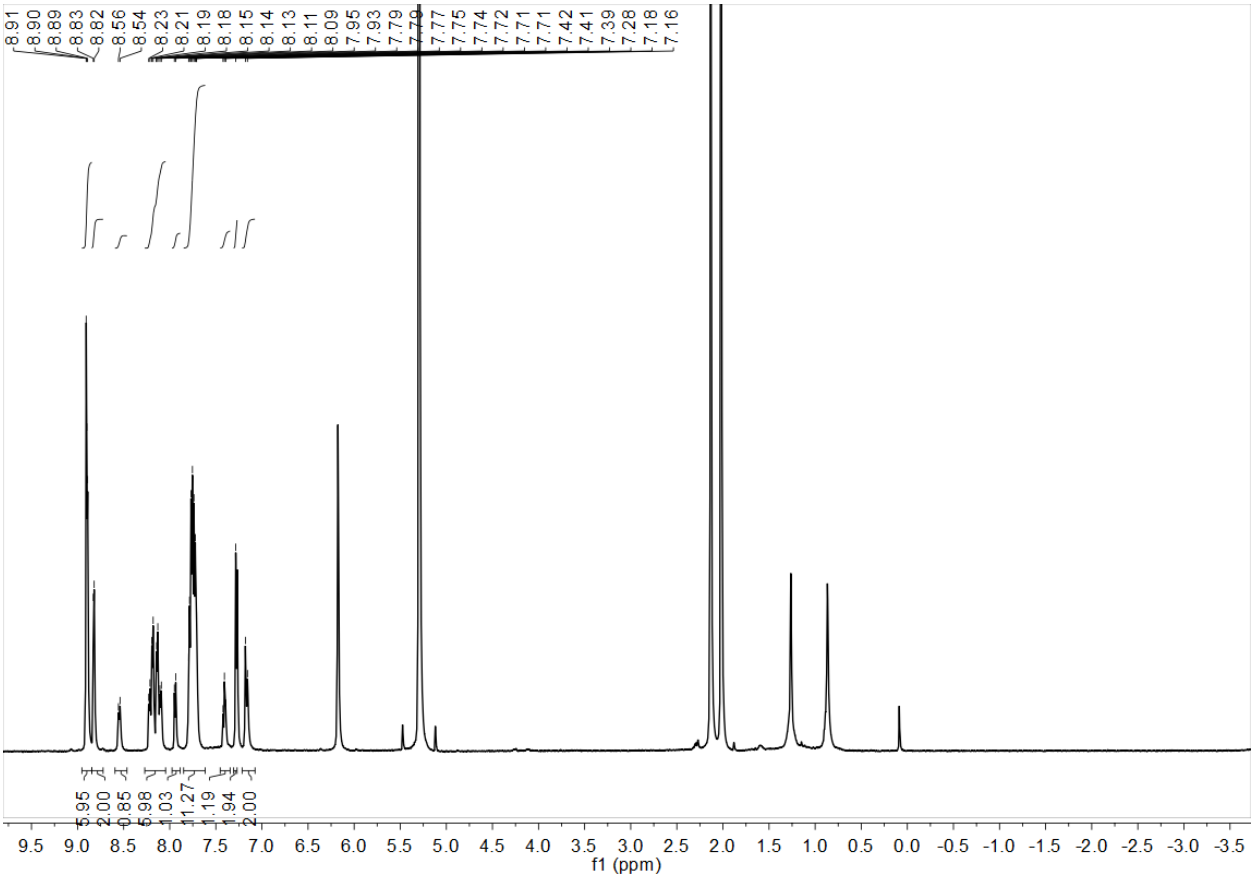

^{13}C-NMR of **Zn-*ortho*-1-amide** in $CDCl_3$:

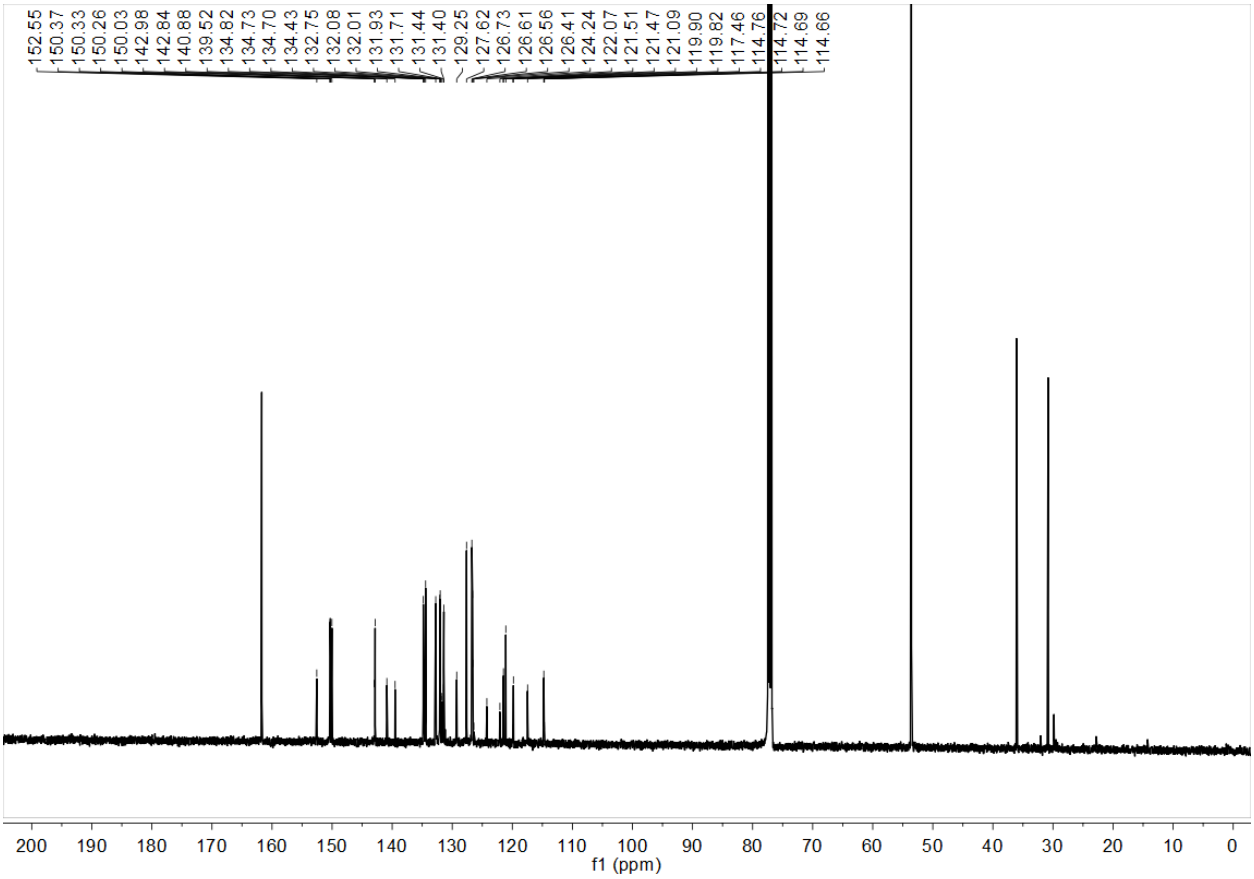

^{19}F-NMR of **Zn-*ortho*-1-amide** in $CDCl_3$:

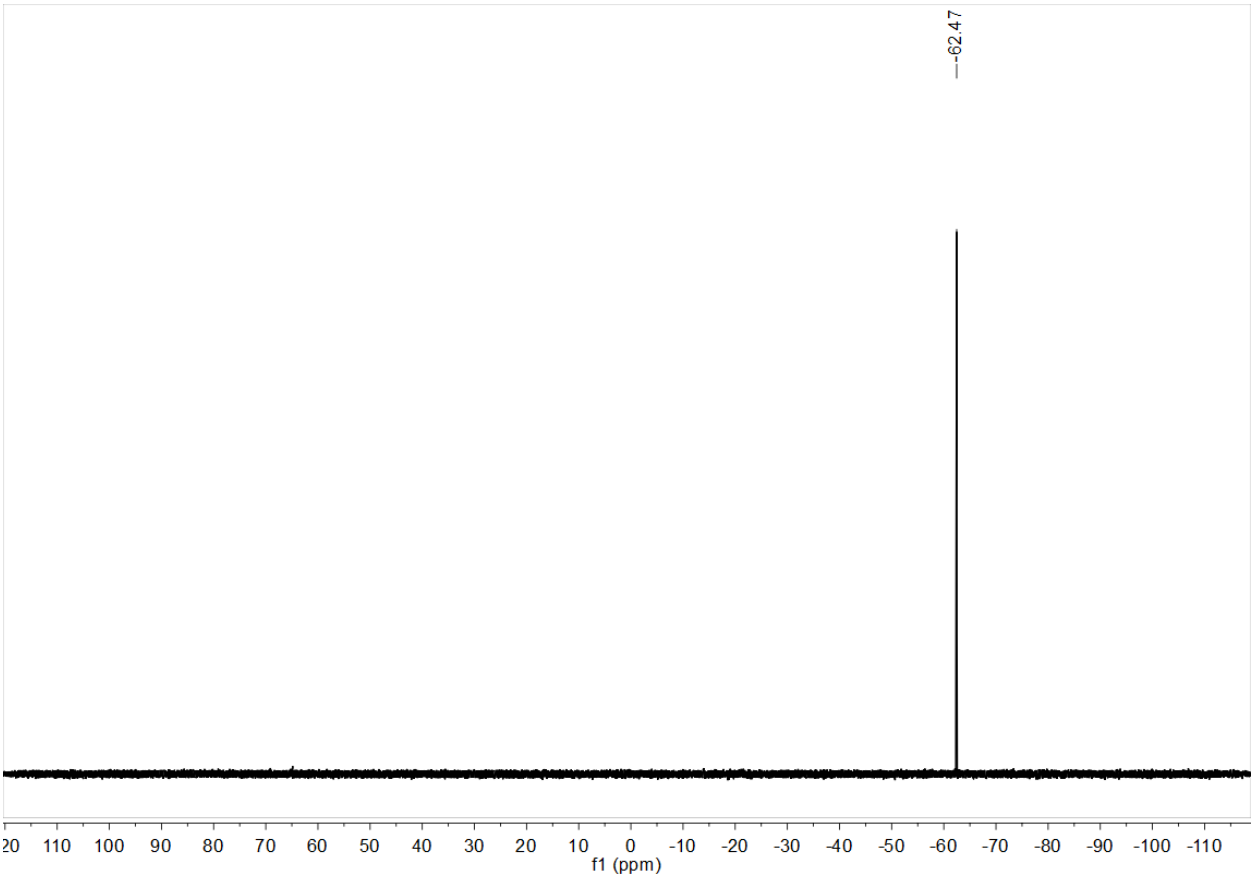

^{1}H-NMR of ***para*-$(CF_3)_4$** in $CDCl_3$:

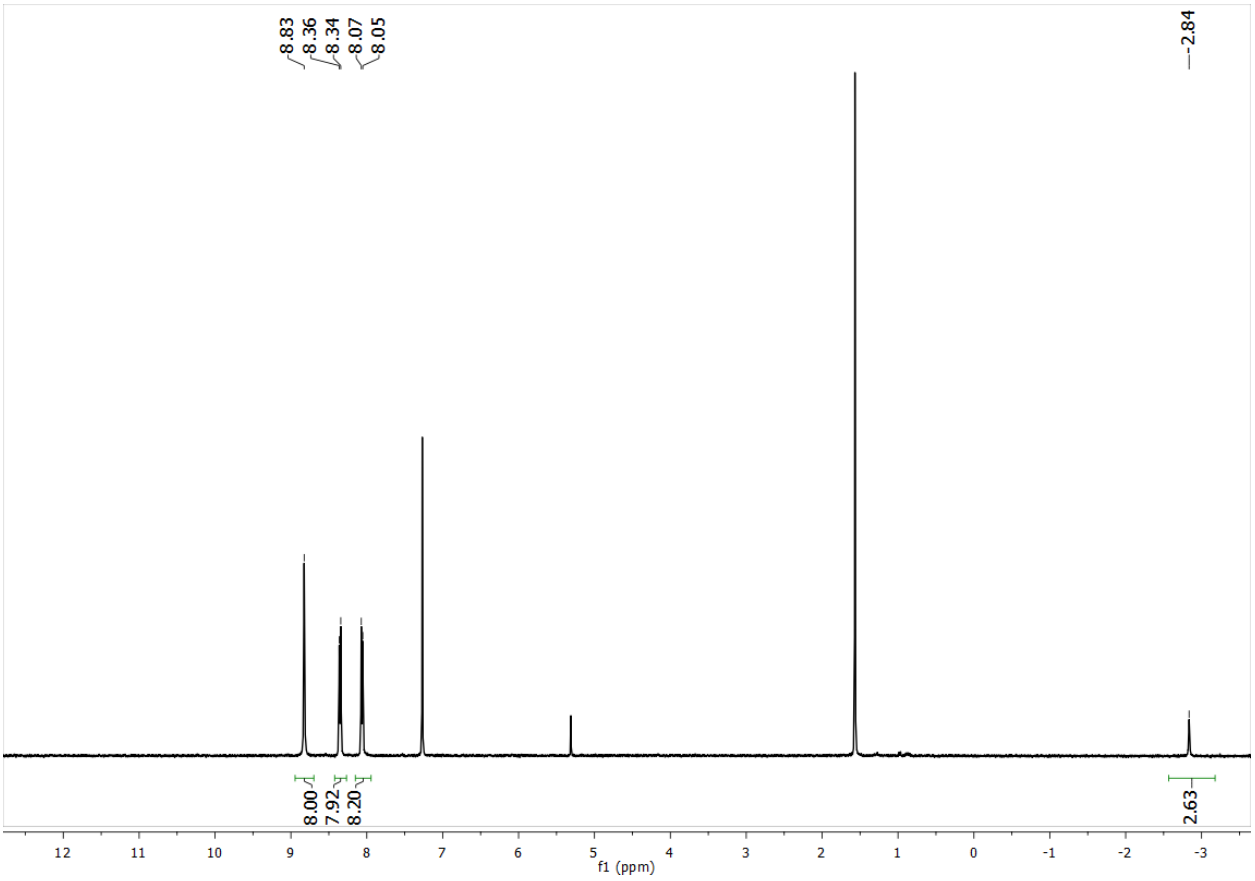

^{19}F-NMR of ***para*-$(CF_3)_4$** in $CDCl_3$:

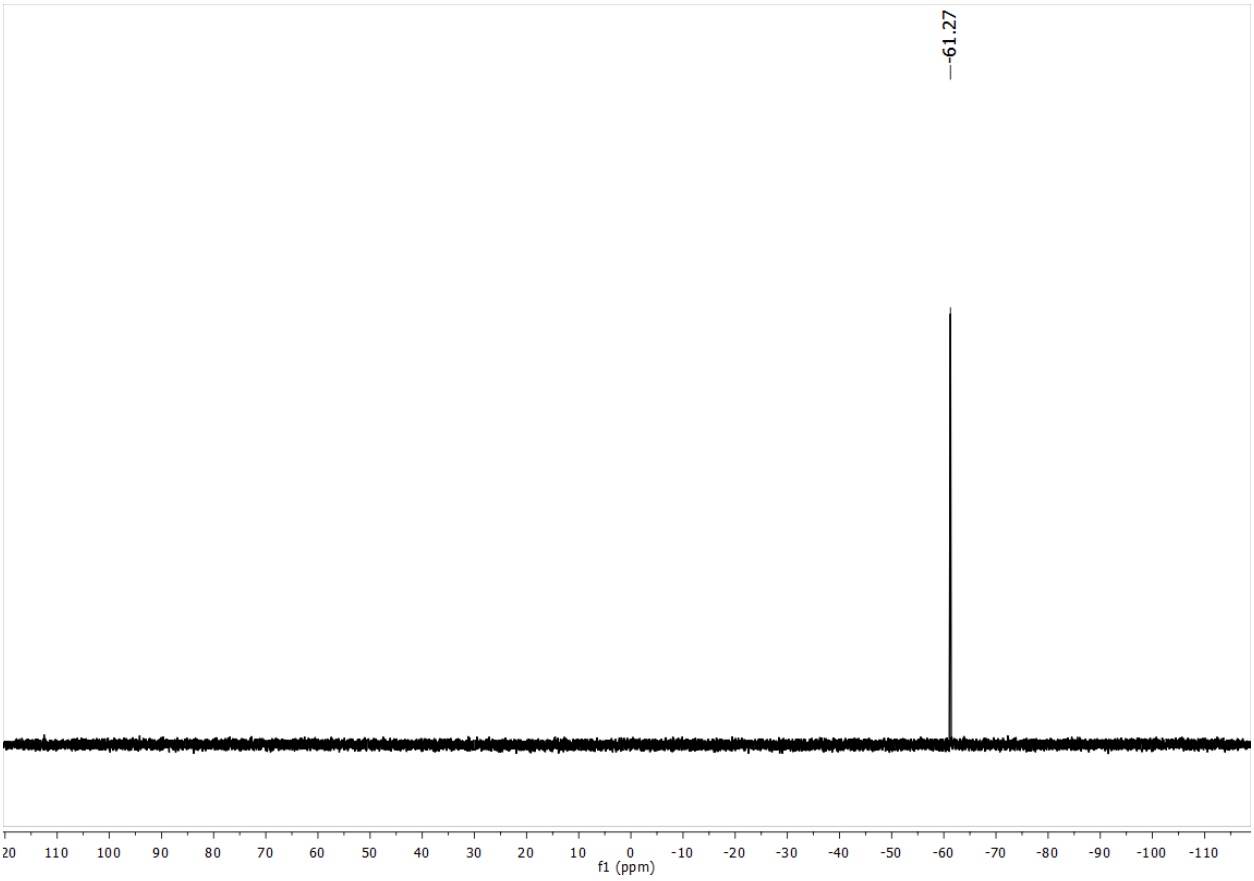

References

1. M. Madadi and R. Rahimi, *Reaction Kinetics, Mechanisms and Catalysis*, 2012, **107**, 215-229.
2. G. M. Sheldrick, *Acta Crystallographica. Section C, Structural Chemistry*, 2015, **71**, 3-8.
3. C. Costentin, S. Drouet, M. Robert and J.-M. Savéant, *J. Am. Chem. Soc.*, 2012, **134**, 11235-11242.
4. C. Costentin, S. Drouet, M. Robert and J.-M. Savéant, *Science*, 2012, **338**, 90-94.
5. R. R. Gagne, J. L. Allison and D. M. Ingle, *Inorg. Chem.*, 1979, **18**, 2767-2774.
6. G. Jakab, C. Tancon, Z. Zhang, K. M. Lippert and P. R. Schreiner, *Org. Lett.*, 2012, **14**, 1724-1727.
7. W. L. F. Amarego, *Purification of Laboratory Chemicals*, Elsevier, 6th edn., 2009.
8. Gaussian 16, Revision A.03, M. J. Frisch, G. W. Trucks, H. B. Schlegel, G. E. Scuseria, M. A. Robb, J. R. Cheeseman, G. Scalmani, V. Barone, G. A. Petersson, H. Nakatsuji, X. Li, M. Caricato, A. V. Marenich, J. Bloino, B. G. Janesko, R. Gomperts, B. Mennucci, H. P. Hratchian, J. V. Ortiz, A. F. Izmaylov, J. L. Sonnenberg, D. Williams-Young, F. Ding, F. Lipparini, F. Egidi, J. Goings, B. Peng, A. Petrone, T. Henderson, D. Ranasinghe, V. G. Zakrzewski, J. Gao, N. Rega, G. Zheng, W. Liang, M. Hada, M. Ehara, K. Toyota, R. Fukuda, J. Hasegawa, M. Ishida, T. Nakajima, Y. Honda, O. Kitao, H. Nakai, T. Vreven, K. Throssell, J. A. Montgomery, Jr., J. E. Peralta, F. Ogliaro, M. J. Bearpark, J. J. Heyd, E. N. Brothers, K. N. Kudin, V. N. Staroverov, T. A. Keith, R. Kobayashi, J. Normand, K. Raghavachari, A. P. Rendell, J. C. Burant, S. S. Iyengar, J. Tomasi, M. Cossi, J. M. Millam, M. Klene, C. Adamo, R. Cammi, J. W. Ochterski, R. L. Martin, K. Morokuma, O. Farkas, J. B. Foresman, and D. J. Fox, Gaussian, Inc., Wallingford CT, 2016.
9. F. Bryden and R. W. Boyle, *Synlett*, 2013, **24**, 1978-1982.
10. J. T. Landrum, D. Grimmett, K. J. Haller, W. R. Scheidt and C. A. Reed, *J. Am. Chem. Soc.*, 1981, **103**, 2640-2650.
11. W. E. Parham and C. D. Wright, *The Journal of Organic Chemistry*, 1957, **22**, 1473-1477.
12. D. A. J. Bleasdale, David W., *J. Chem. Soc., Perkin Trans.*, 1991, **1**, 1683-1692.
13. P. D. Harvey, S. Tasan, C. P. Gros, C. H. Devillers, P. Richard, P. L. Gendre and E. Bodio, *Organometallics*, 2015, **34**, 1218-1227.